NASA Technical Memorandum 86697

Comparison of Calculated and Measured Velocities Near the Tip of a Model Rotor Blade at Transonic Speeds

Michael E. Tauber, F. Kevin Owen, Ronald G. Langhi and Grant E. Palmer

August 1985

National Aeronautics and
Space Administration

NASA Technical Memorandum 86697

Comparison of Calculated and Measured Velocities Near the Tip of a Model Rotor Blade at Transonic Speeds

Michael E. Tauber, NASA Ames Research Center, Moffett Field, California
F. Kevin Owen, Complere, Inc., Palo Alto, California
Ronald G. Langhi, Informatics General Corp, Palo Alto, California
Grant E. Palmer, NASA Ames Research Center, Moffett Field, California

August 1985

National Aeronautics and
Space Administration

Ames Research Center
Moffett Field, California 94035

COMPARISON OF CALCULATED AND MEASURED VELOCITIES NEAR THE TIP OF A MODEL ROTOR BLADE AT TRANSONIC SPEEDS

Michael E. Tauber, F. Kevin Owen,* Ronald G. Langhi,† and Grant E. Palmer

Ames Research Center

SUMMARY

The ability of the ROT22 code to predict accurately the transonic flow field in the crucial region around and beyond the tip of a high-speed rotor blade was assessed. The computations were compared with extensive laser velocimetry measurements made at zero advance ratio and tip Mach numbers of 0.85, 0.88, 0.90, and 0.95. The comparison between theory and experiment was made using 300 scans for the three orthogonal velocity components covering a volume having a height of over one blade chord, a width of nearly two chords, and a length ranging from about 1 to 1.6 chords, depending on the tip speeds. The good agreement between the calculated and measured velocities established the ability of the code to predict the off-blade flow field at high tip speeds. This supplements previous comparisons where surface pressures were shown to be well-predicted on two different tips at advance ratios to 0.45, especially at the critical 90° azimuth blade position. These results demonstrate that the ROT22 code can be used with confidence to predict the important tip region flow field including the occurrence, strength, and location of shock waves causing high drag and noise.

INTRODUCTION

The emphasis on increasing helicopter flight speed has resulted in higher rotor tip Mach numbers. It is essential that these desired performance improvements be achieved with reasonable power requirements and without substantial increases in noise. Since the formation of shock waves in the transonic flow on the advancing blade is the major source of the power requirement and of high-speed noise, the ability to predict this flow field accurately is essential to the design of transonic rotors.

Early high-speed rotor calculations were performed by Caradonna and Isom (refs. 1 and 2) using transonic small disturbance theory. Initially, only steady

*Complere, Inc., Palo Alto, CA.
†Informatics General Corp., Palo Alto, CA.

hovering flight was treated (ref. 1); this was later extended to the unsteady forward flight case (ref. 2). Subsequently, Grant (ref. 3) solved the small disturbance equation more precisely, but assumed quasi-steady flow for a blade in nonlifting forward flight.

Paralleling the development of fixed wing codes, it was also desirable to progress from using small disturbance theory to solving the full potential equation for rotary wings. As a starting point, a widely used full potential fixed wing code, FL022, developed by Jameson and Caughey (ref. 4) was used. FL022 solves the nonconservative, inviscid, full potential equation using exact surface tangency boundary conditions. The rotary wing ROT22 code (refs. 5 and 6) was developed by reformulating FL022 to calculate the flow about a lifting rotor blade in forward flight. Although the full potential equation is solved, the formulation is quasi-steady in that the time derivatives of the perturbation potentials were neglected in the interest of greatly speeding the computation. However, the ROT22 quasi-steady approximation becomes exact in the limit as the advance ratio approaches zero, corresponding to hovering flight.

The present study measured the transonic flow field nonintrusively in the neighborhood of the blade tip and compared the data with computations from the ROT22 transonic rotor flow code. The measurements were made (ref. 7) on a nonlifting, hovering rotor at tip Mach numbers up to 0.95 using a laser velocimeter. Previously, computation/experiment comparisons of surface pressure distributions were made in the neighborhood of rotor tips at advance ratios of 0.4 and 0.45 and gave generally good agreement (ref. 8).

EXPERIMENT

Precise definition of the velocity field surrounding the blade tip is required to calculate transonic noise (refs. 9, 10, and 11). Of the available instrumentation techniques, nonintrusive laser velocimeter measurements provide the only reasonable method to acquire such flow field data and to check the ability of the ROT22 code to predict the velocities off the blade surface. The details of the experiment are described in reference 7 and will be only summarized here.

Test Conditions and Model Configuration

The test was performed in the Ames/Army Aeromechanics Laboratory Hover/Anechoic facility (a large chamber about 10 m per side), with special ducting designed to minimize room circulation. The two-bladed rotor (ref. 12) located in the center of the room was mounted on a tall column containing the drive shaft. The rotor consisted of two cantilever-mounted, manually adjustable blades. The untwisted and untapered blades had NACA 0012 airfoil sections and an aspect ratio of twelve. The rotor radius and chord were 104.5 cm (41.16 in.) and 7.62 cm (3.0 in.), respectively.

The induced velocities were measured at tip Mach numbers of 0.85, 0.88, 0.90, and 0.95 and in a volume one chord (7.62 cm) high and extending from the 95% blade radius location (5.23 cm inboard of the tip) to the sonic circle. The location of the unperturbed sonic circle (ref. 9) is given by

$$S = \frac{1}{M_{TIP}} \tag{1}$$

where S is measured in blade radii from the center of rotation and M_{TIP} is the rotational tip Mach number. The distance of the sonic circle given by equation (1) from the blade tip varied from 7.26 cm at a tip Mach number of 0.85 to 2.17 cm at a Mach number of 0.95.

Most of the velocity measurements were made above the blade; however, a limited number were also measured below the blade to determine the extent of flow asymmetry. The blade was set at a positive collective pitch angle of 1.25° to convect the viscous wake slightly downward and to reduce the turbulence in the plane of rotation. However, the effective angle of incidence in the tip region of the blade was estimated to be less than 0.5°.

Measurement Technique

The general arrangement of the laser velocimeter system used in the present study is shown in figure 1. This fringe mode forward scatter system which utilized the 4880 and 5145 Å lines of an argon-ion laser was specifically designed to measure all three components of induced perturbation velocity by measuring the flow at two different azimuthal positions. By viewing the blade normal to the tip as it swept by, one spectral line measured the induced chordwise velocity component while the other measured the induced vertical velocity component. Translation of both transmitting and receiving optics along the test chamber walls enabled a flow field view normal to the approaching or retreating tip, thus determining the radial and vertical induced velocities. The effective sensing volume was approximately elliptic, 0.2 mm in diameter and 3 mm long, with the axis aligned in the plane of the beams. Bragg cell frequency shifting, which is required for probing directionally intermittent flow fields, was incorporated in both spectral lines. These offsets also enabled the direct measurement of all three velocity components without recourse to ±45° beam orientations with respect to the vertical plane.

Maximum optical system sensitivity is essential for meaningful measurements particularly in large facilities. In these applications solid angle light collection is reduced, raising the possibility that only the velocities of larger particles which may not follow the flow will be observed. Rather than relying entirely on natural aerosols for the light scattering, it was found that the introduction of artificial aerosols of known size distribution greatly enhanced data acquisition rates, particularly in unsteady flows where conditional sampling had to be used. Such aerosols were generated with an ultrasonic nozzle mounted in the facility. The size distribution of the aerosol with a count mean diameter of less than one micron

is shown in figure 2. These aerosols had been found adequate for turbulence studies of shock boundary-layer interactions and vortex flows at transonic and supersonic speeds (ref. 13). The particles were drawn down through the laser velocimeter focal volume by the room air control fans. This produced a sufficient supply of scattering centers for detailed flow field measurements.

Data Acquisition and Reduction

The data acquisition and reduction system consisted primarily of three elements: signal processors, an event synchronizer, and a desk top computer. These elements are shown schematically in figure 3. Conditional sampling techniques were employed to "freeze" the flow field as the rotor swept past the fixed probe volume. To achieve this, a once-per-revolution pulse was used to activate the laser velocimeter electronics each time the rotor approached the probe focal volume. Velocities were then recorded during rotor transit past the focal volume. After the preset time had elapsed, the electronics were inhibited until the next rotor passage.

A schematic of the two-component measurement procedure used in the present test is shown in figure 4. The internal clock of the event synchronizer (multiplexer), which was reset by an external pulse from the rotor drive mechanism, determined the position of the blade relative to the measurement volume. Whenever valid (essentially simultaneous) u and v signals were recieved, the velocity data along with the clock reading (which corresponded to the chordwise position of the measurement volumes) were recorded. From these readings, ensemble averages were generated for the selected chordwise increments along the blade. It must be borne in mind that the measurements were made by collecting data over many blade revolutions since the data rate was insufficient and too inconsistently distributed to obtain enough information at each chordwise location for each blade passage. For this reason, the total number of readings was divided among many incremental blade positions. Some chordwise "windows" would, therefore, be filled before others. However, new readings were accepted and replaced the oldest data until all chordwise locations were filled. This ensured that only the most current data were reduced.

The data contained the information required to calculate the instantaneous velocities. From these determinations, the average velocities, RMS turbulence levels and the cross correlations could all be calculated. Plots of these parameters were displayed on-line as profiles were measured and hard copy was printed as required. All the raw and reduced data were permanently stored on flexible discs.

The orthogonal induced velocity components were measured in an inertial (room-fixed) coordinate system. However, aerodynamic properties of moving bodies are normally calculated in body-fixed coordinates. Therefore, the measured velocity components were transformed into the blade-fixed coordinates of the ROT22 code by using the following expressions:

$$u = v_m + \omega r$$

$$v = v_m \qquad (2)$$

$$w = w_m - \omega x$$

Here u, v, and w are the chordwise, vertical, and radial velocity components, respectively. The subscript m refers to measured values, ω is the blade rotation rate, r the blade radius from the center of rotation, and x the chordwise distance from the leading edge.

The coordinates of the scans were measured with respect to the nonrotating blade. After the data were reduced, it was observed that for the LV scans closest to the blade surface (2.5 mm above the centerline of the airfoil section of the static blade), the beam was obscured by the blade less than predicted. From the scans at y = 2.5 mm, it was determined that the blades were inclined slightly upward in their static positions and that the centrifugal force due to the roughly 3000 rpm rotation rate pulled the blades down about 0.075°. The corresponding vertical tip displacement was about 1.3 mm and this correction was applied to the (nominal) measured y values. Table 1 lists the locations and velocity distributions which were measured at the four tip Mach numbers. At each location, a horizontal velocity component (either u or w) and the vertical one, v, were measured. From 2000 to 8000 measurements were averaged to determine each data point within the velocity distribution; test time limitations thus precluded measuring all three velocity components at each location. Because the LV system had to be moved and realigned when changing horizontal velocity component (u or w) measurements, only u and v, or w and v values were determined at many locations. The greatest difficulty was encountered in measuring v, because light reflecting off the blade surface severely degraded the signal when scanning near the blade. Twelve scans, nine of them v velocity components, were considered unreliable and were eliminated (see Table 1). These twelve cases represented less than 4% of the total of over 300 scans listed in the table.

When measurements were made in the vicinity of the shock, the velocity probability density functions exhibited revolution-to-revolution flow field variations. This unsteadiness of the flow field was noted because data were collected over a large number of rotations. The flow field variability may have been caused by the presence of a transitional boundary layer since the chord Reynolds numbers in the blade tip region were only 1.5 to 1.75 million and no artificial trips were used. In fact, holographic measurements made under very similar test conditions (ref. 14) indicated the presence of lambda shocks and subsequent flow separation. Flow unsteadiness is often associated with shock-induced boundary layer separation (ref. 13) and could be inferred from some of the histograms obtained during the present test. An estimate of the inherent revolution-to-revolution flow field repeatability could be made by comparing the measured and the most likely velocity probability density functions. Such comparisons were made in reference 7 and show that in blade coordinates, the maximum differences in the measured chordwise

TABLE 1.- TEST CONDITIONS

Nominal y*/c	Corrected y/c	M_{TIP} = 0.85									0.88									0.90									0.95								
		$\bar{R}$ = 0.95			1.0			1.176			$\bar{R}$ = 0.95			1.0			1.136			$\bar{R}$ = 0.95			1.0			1.111			$\bar{R}$ = 0.95			1.0			1.053		
		u	v	w	u	v	w	u	v	w	u	v	w	u	v	w	u	v	w	u	v	w	u	v	w	u	v	w	u	v	w	u	v	w	u	v	w
0	0.0170	-	-	-	a	a	a	a	a	-	-	-	-	-	-	-	a	a	a	-	-	-	a	a	-	a	a	a	-	-	-	-	-	-	-	a	a
.033	.051	a	a	-	-	-	-	-	-	-	-	-	-	-	-	-	-	-	-	a	a	-	a	c	-	-	-	-	a	c	-	-	-	-	-	-	-
.067	.084	a	a	-	a	a	a	-	-	-	a	a	a	c	c	-	a	a	-	a	a	a	a	c	-	a	a	-	a	a	a	a	a	a	a	a	a
.10	.117	a	a	-	-	-	-	-	-	-	-	-	-	-	-	-	-	-	-	a	a	-	a	a	-	-	-	-	a	a	-	-	-	-	-	-	-
.133	.151	a	a	a	a	a	a	-	-	-	a	a	a	a	a	a	a	a	-	a	a	a	a	a	c	a	a	a	a	a	a	a	a	a	a	a	a
.167	.184	a	a	a	-	-	-	a	a	-	-	-	-	-	-	-	-	-	-	-	-	-	-	-	-	-	-	-	-	-	-	-	-	-	-	-	-
.20	.217	a	a	a	a	a	a	-	-	-	a	a	a	a	a	a	a	a	-	a	a	c	a	a	a	a	a	-	a	a	a	a	a	a	a	a	a
.233	.251	-	a	a	-	-	-	-	-	-	-	-	-	-	-	-	-	-	-	a	c	-	-	-	-	-	-	-	-	-	-	-	-	-	-	-	-
.25	.267	a	a	-	-	-	-	-	-	-	-	-	-	-	-	-	-	-	-	-	-	-	-	-	-	-	-	-	-	-	-	-	-	-	-	-	-
.267	.284	a	a	a	a	a	a	-	-	-	-	a	a	-	a	a	-	-	-	a	a	a	a	a	a	a	a	a	a	a	a	a	a	a	a	a	-
.30	.317	-	a	a	-	-	-	-	-	-	-	-	-	-	-	-	-	-	-	-	-	-	-	-	-	-	-	-	-	-	-	-	-	-	-	-	-
.333	.351	a	c	a	a	a	-	a	a	-	a	a	a	a	a	a	a	a	-	a	a	a	a	a	a	a	a	-	a	a	a	a	a	a	a	a	a
.40	.417	-	-	-	a	a	-	-	-	-	-	-	-	-	-	-	-	-	-	-	-	-	-	-	-	-	-	-	-	-	-	-	-	-	-	-	-
.50	.517	a	a	a	a	a	-	a	a	-	a	a	a	a	a	a	a	a	a	a	a	a	a	a	a	a	a	a	a	a	a	a	a	-	a	a	a
.667	.684	a	a	-	a	a	-	-	-	-	-	-	-	-	-	-	-	-	-	-	-	-	-	-	-	-	-	-	-	-	-	-	-	-	-	-	-
.833	.851	-	-	-	-	-	-	-	-	-	a	a	-	-	-	-	-	-	-	-	-	-	-	-	-	-	-	-	-	-	-	-	-	-	-	-	-
1.00	1.017	a	a	-	a	a	-	a	a	-	a	a	a	a	a	-	a	a	a	a	a	-	a	a	-	a	a	a	a	a	a	a	a	a	a	a	a
-.033	-.016	-	-	-	a	a	-	-	-	-	-	-	-	-	-	-	-	-	-	-	-	-	a	c	-	-	-	-	-	-	-	-	-	-	-	-	-
-.067	-.050	-	a	a	a	a	a	-	-	-	-	a	a	-	a	a	-	-	-	-	-	-	-	-	-	-	-	-	-	-	-	-	-	-	-	a	a
-.133	-.116	-	-	a	-	a	a	-	-	-	-	a	a	-	a	a	-	-	-	-	-	-	a	a	a	-	-	-	-	-	-	-	-	-	-	-	-
-.20	-.183	-	-	-	-	-	-	-	-	-	-	-	-	-	-	-	-	-	-	-	-	-	a	a	-	-	-	-	-	-	-	-	-	-	-	-	-
-.25	-.233	a	c	-	-	-	-	-	-	-	-	-	-	-	-	-	-	-	-	-	-	-	-	-	-	-	-	-	-	-	-	-	-	-	-	-	-
-.267	-.250	-	-	-		a	a	-	-	-	-	-	-	-	-	-	-	-	-	-	-	-	-	-	-	-	-	-	-	-	-	-	a	a	-	-	-
-.333	-.316	a	c	a	-	-	-	-	-	-	-	-	-	-	-	-	-	-	-	-	-	-	a	a	-	-	-	-	-	-	-	-	-	a	a	-	-	-
-.50	-.483	-	a	a	-	-	-	-	-	-	-	-	-	-	-	-	-	-	-	-	-	-	-	-	-	-	-	-	-	-	-	-	-	a	a	-	-	-
-1.00	-.983	-	-	-	-	-	-	-	-	-	-	-	-	-	-	-	-	-	-	-	-	-	-	-	-	-	-	-	-	-	-	-	-	a	a	-	-	-

-No measurement. [a]Data available. [c]Data obviously questionable.

velocities, u, were less than 10%. The effects on the vertical v and radial w velocities were negligible.

Therefore, the measurements were analyzed in terms of the most likely probability density function profiles which were somewhat sharper with lower RMS levels. Because this approach tended to suppress some of the more realistic viscous effects, the comparison provided a test of the inviscid calculational procedure.

COMPUTATIONS

The ROT22 code described in references 6 and 7 was used to calculate the flow field about the blades. ROT22 solves a quasi-steady approximation to the three-dimensional, full-potential equation in a blade-attached coordinate system. The quasi-steady approximation greatly reduces computation time since the true time-dependent history of the solution need not be computed. A computational grid of 120 cells chordwise, 16 vertically, and 32 spanwise was used. About two-thirds of the spanwise computational planes were on the blade; the remainder were in the inboard cut-out and beyond the blade tip. The code output consisted of the u, v, and w velocity components, nondimensionalized by the rotational tip speed, the pressure coefficient and local Mach number. For the present computation/experiment comparison, special provisions were made for interpolating between computational mesh points for the velocity components along horizontal lines of constant y and between vertical planes. An efficient, fully vectorized version of the code on a CRAY XM-P computer required computation times of 30-40 sec per case.

RESULTS AND DISCUSSION

The flow field over the entire blade was calculated for the four tip Mach numbers of the experiment: 0.85, 0.88, 0.90, and 0.95. Nonlinear spanwise grid spacing was used to enhance resolution in the tip region and to place a computational plane at the 95% radial blade station where one set of measurements was made. The two remaining radial measurement stations, located at the blade tip and idealized sonic cylinder (eq. (1)), were matched by linearly interpolating the computed velocity values. (It was undesirable to place a computational plane at the blade tip since the velocity gradients were very steep at that location.) All computations were made assuming zero collective pitch resulting in no lift since the airfoil section was symmetric. The complexity of even this simplified flow field for the nonlifting blade at zero advance ratio is illustrated in figure 5. Here, calculated contours of constant Mach number were plotted on the blade surface and in the plane of the blade for all four tip Mach numbers. Although the calculations were made for the entire blade, only the tip regions are shown for clarity. Note that for a tip Mach number of 0.90 and higher, the supersonic region on the blade merges with the far field supersonic flow beyond the tip. (The ROT22 calculations were in a blade-attached coordinate system. The flow field is shown as it would

appear to an observer stationed on the blade.) This phenomenon, labeled "delocalization" in reference 9, results when shock waves form on the blade and propagate into the far field, thus producing impulsive noise (ref. 9). Note that ROT22 code predicts the sonic contours beyond the tip. At the tip Mach number of 0.88, the approximate, unperturbed value given by equation (1) matched the computed sonic contour fairly well (fig. 5(b)). However, at the higher tip Mach numbers, the shocks forming on the blade perturbed the flow beyond the tip progressively more strongly and equation (1) provided only a crude approximation for the sonic circle location (fig. 5(c) and 5(d)).

The most recent version of the ROT22 code was used to calculate the flow field about the blade at each of the four tip Mach numbers. To present a clear description of the flow field in the critical tip region of the blade, the orthogonal velocity components are compared at all three spanwise stations at a given height above the centerline of the airfoil at each tip Mach number. However, since measurements were not made of all three velocities and at all three spanwise stations, theory/experiment comparisons are shown only when data were available. Thus blank spaces due to missing figures indicate the absence of experimental data. The theory/experiment comparisons are shown in the following 62 figures (see table 2 for details and figure numbers).

All velocities are shown in a blade-attached coordinate system since that system is used for calculating blade loads. Additionally, the velocities were normalized by the blade tip speed.

As can be seen, the chordwise velocity component u is typically an order of magnitude larger than the vertical component v or the cross-flow velocity w. Therefore, blade pressures and loads are a first order function of u, but depend on v and w only to second order. Thus the generally good agreement between calculations and the experiments enhances confidence in the ability of the ROT22 code to predict flow fields, pressures, and loads under the present conditions.

At some of the stations, the theory/experiment comparisons were affected by difficulties with either measurements or computations. For instance, when measuring the flow very close to the blade surface, the LV beams could be obscured by portions of the blade. This effect can be seen in figures 7, 22, and 40 where there is a lack of data between roughly the 0.1 chord and mid-chord stations.

The steepness of the velocity gradients at the blade tip affected both the measurements and computations. When attempting to measure just outboard of the tip and very close to the blade surface, a very small misalignment could cause the LV beams to be blocked by the tip, resulting in the loss of some data, as in figure 22. A more pervasive problem affected the computations of the velocities, especially the important chordwise component u. The interpolation in the radial direction diffused the shocks in some cases (see figures 10, 40, 44, 52, and 55) and generally degraded the computed values somewhat. Therefore, the agreement with experiment is not quite as good at the blade tip as it is inboard or beyond the tip.

TABLE 2.- FIGURE NUMBERS

Nominal y*/c	Corrected y/c	M_T = 0.85			M_T = 0.88			M_T = 0.90			M_T = 0.95		
		$\overline{R}$			$\overline{R}$			$\overline{R}$			$\overline{R}$		
		0.95	1.00	1.176	0.95	1.00	1.136	0.95	1.00	1.111	0.95	1.00	1.053
0	0.0170	--	6	6	--	--	28	--	39	39	--	--	53
.033	.051	7	--	--	--	--	--	40	40	--	54	--	--
.067	.084	8	8	--	29	--	29	41	41	41	55	55	55
.10	.117	9	--	--	--	--	--	42	42	--	56	--	--
.133	.151	10	10	--	30	30	30	43	43	43	57	57	57
.167	.184	11	--	11	--	--	--	--	--	--	--	--	--
.20	.217	12	12	--	31	31	31	44	44	44	58	58	58
.233	.251	13	--	--	--	--	--	45	--	--	--	--	--
.25	.267	14	--	--	--	--	--	--	--	--	--	--	--
.267	.284	15	15	--	32	32	--	46	46	46	59	59	59
.30	.317	16	--	--	--	--	--	--	--	--	--	--	--
.333	.351	17	17	17	33	33	33	47	47	47	60	60	60
.40	.417	--	18	--	--	--	--	--	--	--	--	--	--
.50	.517	19	19	19	34	34	34	48	48	48	61	61	61
.667	.684	20	20	--	--	--	--	--	--	--	--	--	--
.833	.851	--	--	--	35	--	--	--	--	--	--	--	--
1.00	1.017	21	21	21	36	36	36	49	49	49	62	62	62
-.067	-.050	22	22	--	37	37	--	--	--	--	--	--	63
-.133	-.116	23	23	--	38	38	--	--	50	--	--	--	--
-.20	-.183	--	--	--	--	--	--	--	51	--	--	--	--
-.25	-.233	24	--	--	--	--	--	--	--	--	--	--	--
-.267	-.250	--	25	--	--	--	--	--	--	--	--	64	--
-.333	-.316	26	--	--	--	--	--	--	52	--	--	65	--
-.50	-.483	27	--	--	--	--	--	--	--	--	--	66	--
-1.00	-.983	--	--	--	--	--	--	--	--	--	--	67	--

The impulsive noise due to the delocalization phenomenon is thought to be caused by the propagation of the shock forming on the blade into the far field (ref. 9). Therefore, it was instructive to look at the LV data and the calculations at the sonic circle locations to see when the presence of shock waves was discernible. Note that the u velocity is the component most strongly affected by shock waves and that the shocks were strongest close to the plane of the blade which corresponds to small values of y/c. At the tip Mach numbers of 0.85 and 0.88 where delocalization was absent (figs. 5(a) and 5(b)), no signs of shocks were visible (see figs. 6 and 28, for example). Even for a tip Mach number of 0.90 where delocalization occurred but was not extensive (fig. 5(c)), no distinct shock was discernible at the sonic circle (see fig. 39). However, at the highest tip Mach number of 0.95 which caused extensive delocalization (fig. 5(d)), the shock forming on the blade definitely propagated to the sonic circle region. In fact, the shock was so strong that it was still present one chord above the plane of the blade (fig. 62). Again there was good agreement between the measured and calculated velocities, although the interpolation within the already coarse grid located one chord above the plane of the blade tended to diffuse the computed shock. The large increase in the shock strength which occurred at the tip Mach number of 0.95 lends support to the hypothesis of reference 9 that shock propagation into the far field occurs when strong delocalization is present.

CONCLUSIONS

The ability of the ROT22 code to predict accurately the transonic flow field in the crucial region around and beyond the tip of a high-speed rotor blade was illustrated. This supplements the comparisons of reference 8 where surface pressures were shown to be well predicted on two different tips at advance ratios to 0.45. Especially at the critical 90° azimuthal position, where delocalization was most likely to occur in forward flight, the angle of incidence in the tip region was small (ref. 11) and had little effect on the flow beyond the tip. Therefore, the good agreement between the computed and measured velocities, although for a nonlifting blade, indicates that the ROT22 code can be used with reasonable confidence to predict the important tip region flow field and especially the occurrence, strength, and location of shock waves causing high drag and noise.

REFERENCES

1. Caradonna, F. X.; and Isom, M. P.: Subsonic and Transonic Potential Flow Over Helicopter Rotor Blades. AIAA Journal, vol. 10, no. 12, Dec. 1972.

2. Caradonna, F. X.; and Isom, P. P.: Numerical Calculation of Unsteady Transonic Potential Flow Over Helicopter Rotor Blades. AIAA Journal, vol. 14, no. 4, Apr. 1976.

3. Grant, J.: Calculation of the Supercritical Flow Over the Tip Region of a Non-Lifting Rotor Blade at Arbitrary Azimuth. Royal Aircraft Establishment Technical Report 77180, Dec. 1977.

4. Jameson, A.; and Caughey, D. A.: Numerical Calculation of the Transonic Flow Past a Swept Wing. Courant Institute of Mathematical Sciences, COO-3077-140, New York University, N.Y., Jun. 1977.

5. Arieli, R.; and Tauber, M. E.: Computation of Subsonic and Transonic Flow About Lifting Rotor Blades. Presented at the AIAA Atmospheric Flight Mechanics Conference, Boulder, Colo. AIAA Paper 79-1667, Aug. 1979.

6. Arieli, R.; and Tauber, M. E.: Analysis of the Quasi-Steady Flow About an Isolated Lifting Helicopter Rotor Blade. Joint Institute for Aeronautics and Acoustics TR-24, Stanford University, Aug. 1979.

7. Owen, F. K.; Orngard, G. M.; and McDevitt, T. K.: Laser Velocimeter Measurements of Model Helicopter Rotor Flow Fields. NASA CR-177345, Jul. 1984.

8. Tauber, M. E.; Chang, I. C.; Caughey, D. A.; and Philippe, J. J.: Comparison of Calculated and Measured Pressures on Straight and Swept-Tip Model Rotor Blades, NASA TM-85872, Dec. 1983.

9. Schmitz, F. H., and Yu, Y. H.: Transonic Rotor Noise--Theoretical and Experimental Comparison. Paper No. 22, 6th European Rotorcraft and Powered Lift Aircraft Forum, Bristol, England, Sep. 1980.

10. Huston, R. J. (ed.): Rotorcraft Noise, NASA CP-2234, Jul. 1982.

11. Tauber, M. E.: Computerized Aerodynamic Design of a Transonically "Quiet" Blade. AHS Paper A-84-40-46, May 1984.

12. Caradonna, F. X.; and Tung, C.: Experimental and Analytical Studies of a Model Helicopter Rotor in Hover. Paper No. 25, 6th European Rotorcraft and Powered Lift Aircraft Forum, Bristol, England, Sep. 1980.

13. Owen, F. K.: An Assessment of Flow-Field Simulation and Measurement. AIAA Invited Paper No. 83-1721, AIAA Fluid and Plasmadynamics Conference, Danvers, Mass., Aug. 1983.

14. Kittleson, J. K.: Holographic Interferometry Technique for Measuring Transonic Flow Over a Rotor Blade. 9th European Rotorcraft Forum, Paper No. B, Sep. 13-15, 1983, Stressa, Italy.

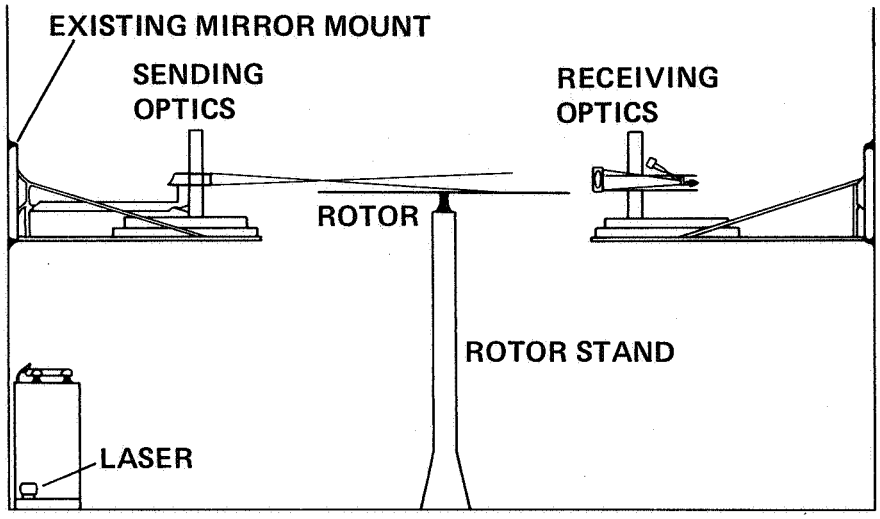

Figure 1.- Test stand and two-color, forward scatter laser velocimeter set-up.

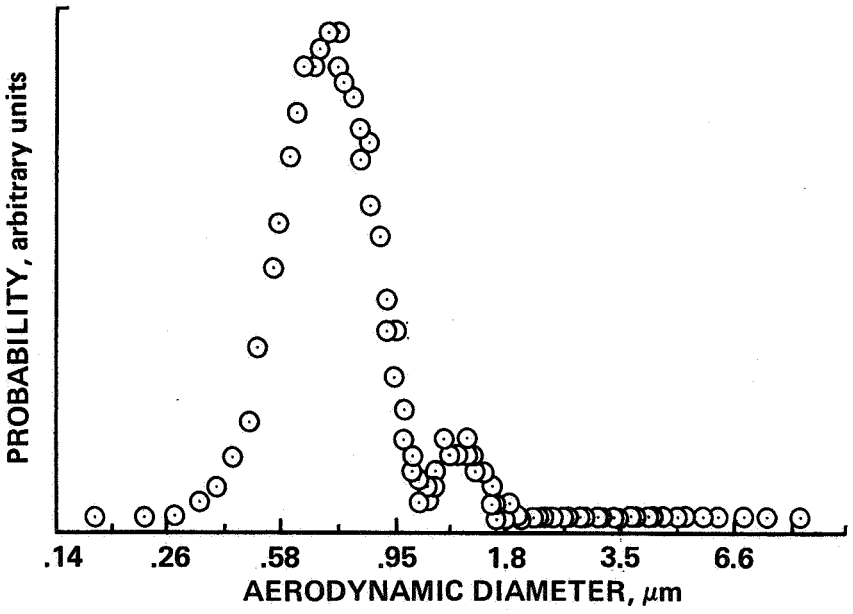

Figure 2.- Seed particle size distribution.

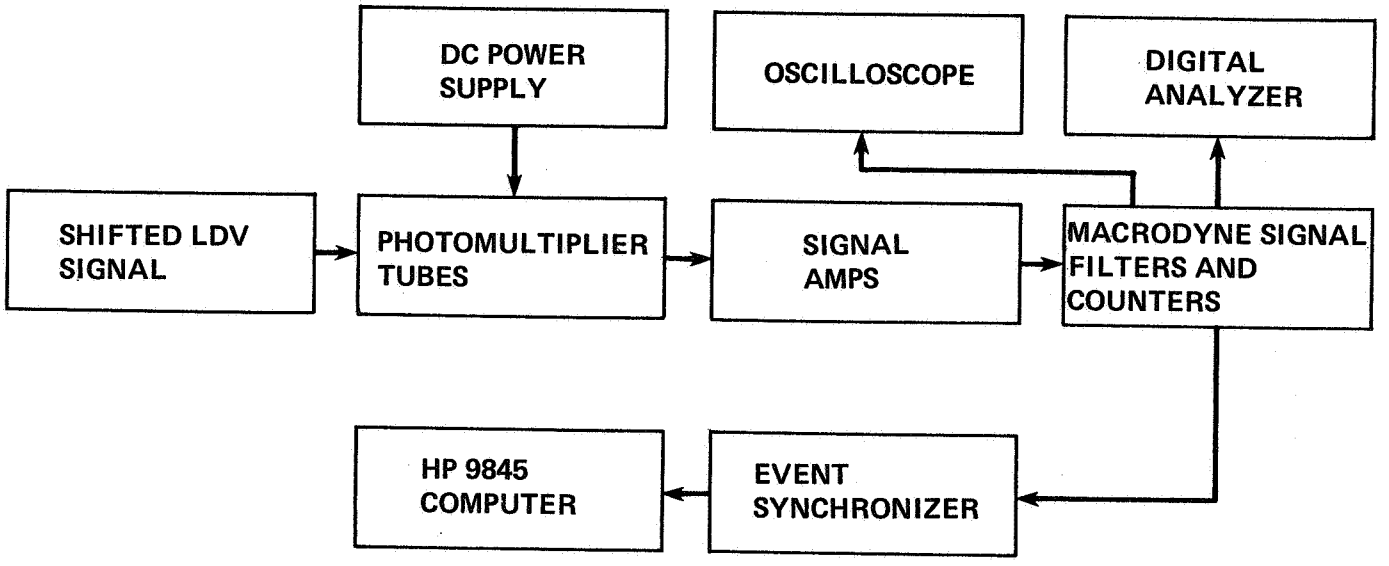

Figure 3.- Data acquisition and reduction system.

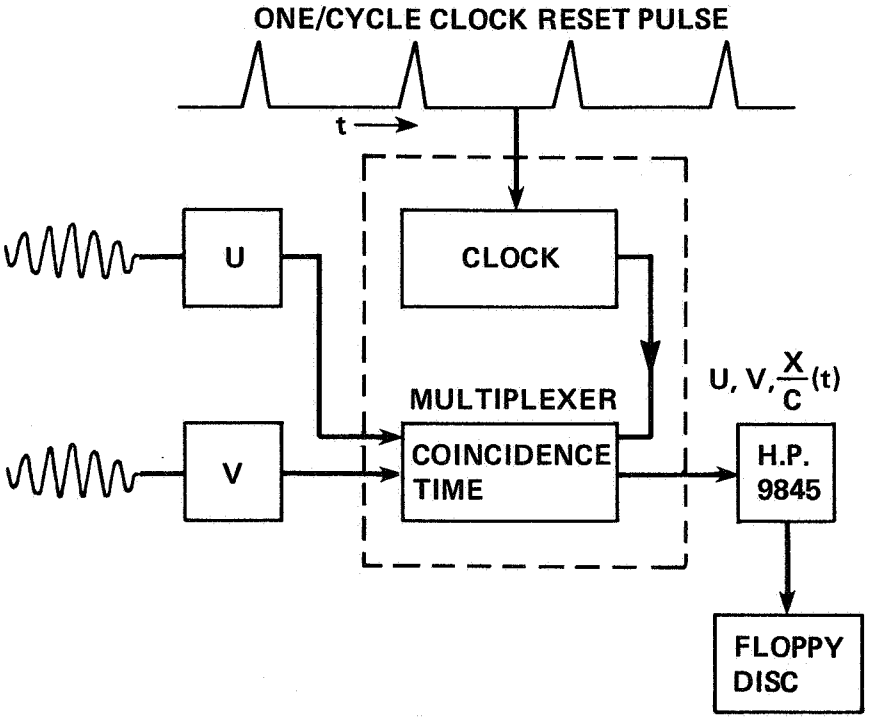

Figure 4.- Conditional sampling data system.

MACH CONTOURS

CONTOUR	MACH NO.	CONTOUR	MACH NO.
1	0.800	7	1.150
2	0.900	8	1.200
3	0.950	9	1.250
4	1.000	10	1.300
5	1.050	11	1.350
6	1.100		

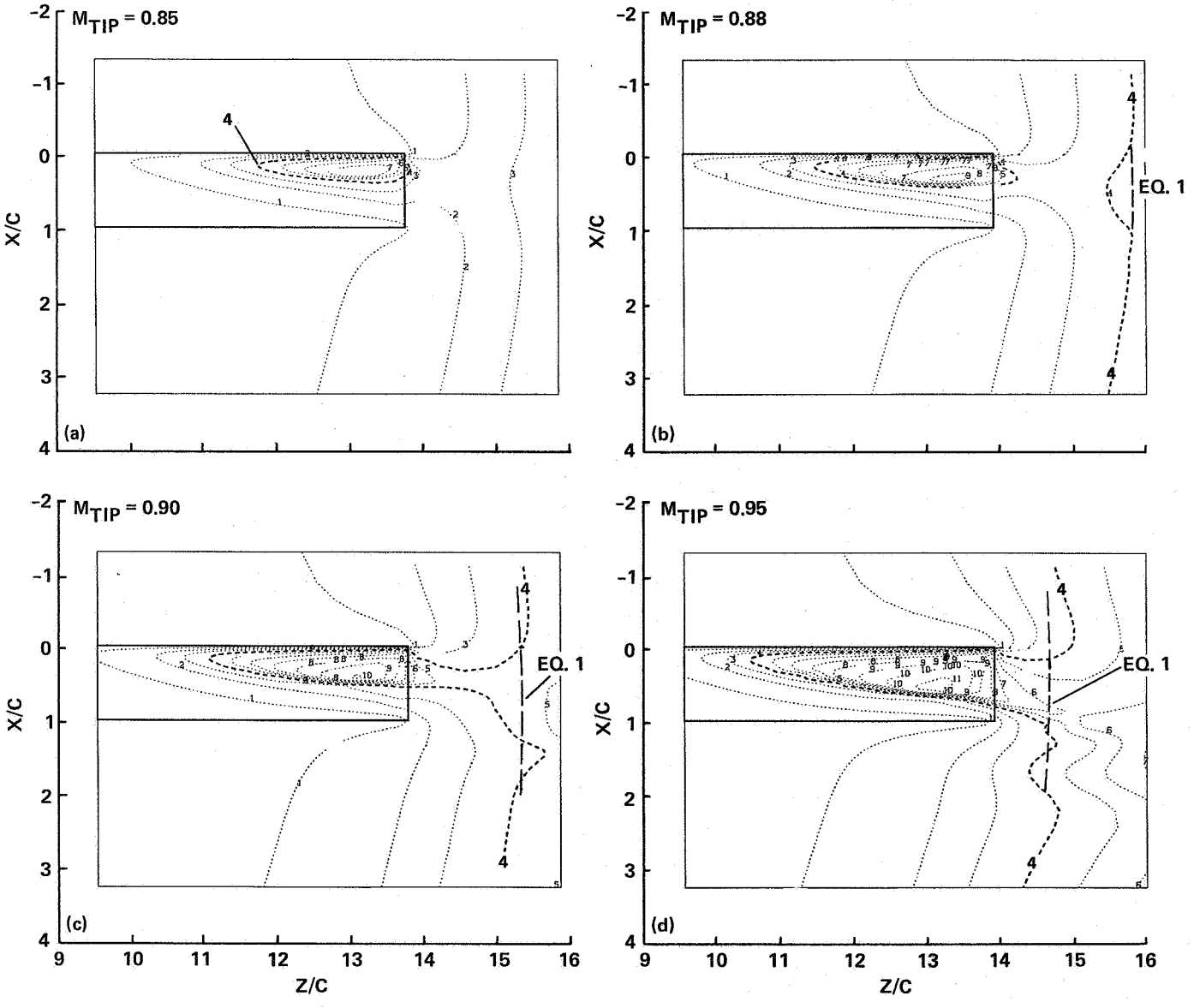

Figure 5.- Mach number contours in tip region. (a) M_{tip} = 0.85; (b) M_{tip} = 0.88; (c) M_{tip} = 0.90; (d) M_{tip} = 0.95.

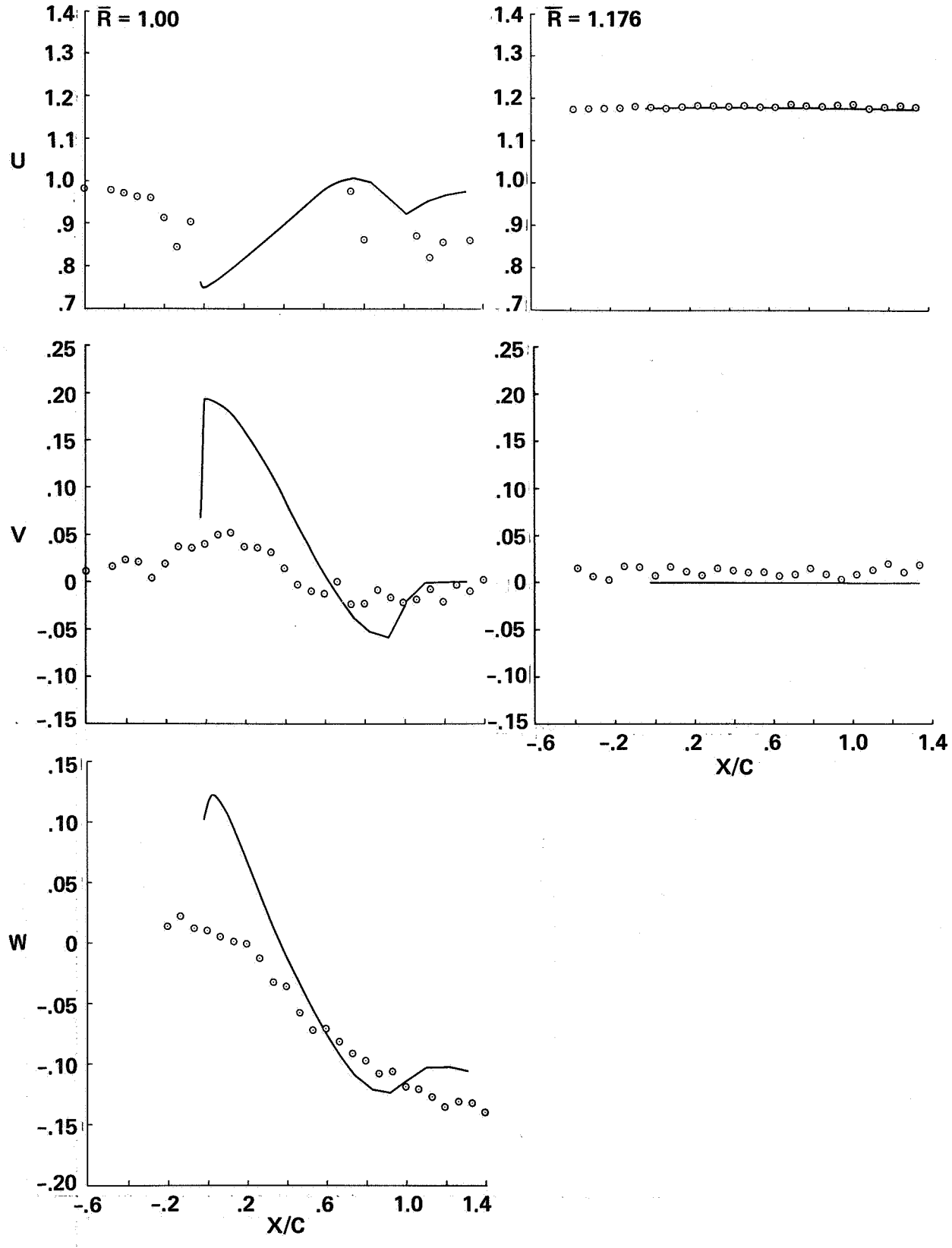

Figure 6.- Computed and measured velocity component comparisons: M_{tip} = 0.85, Y/C = 0.0172.

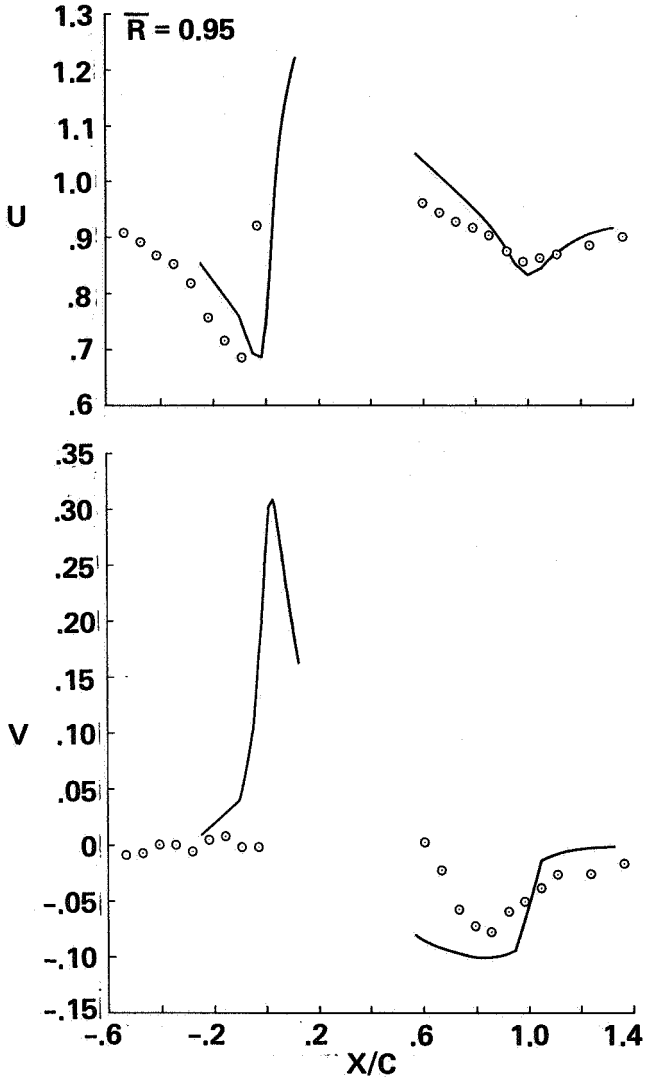

Figure 7.- Computed and measured velocity component comparisons: M_{tip} = 0.85, Y/C = 0.0505.

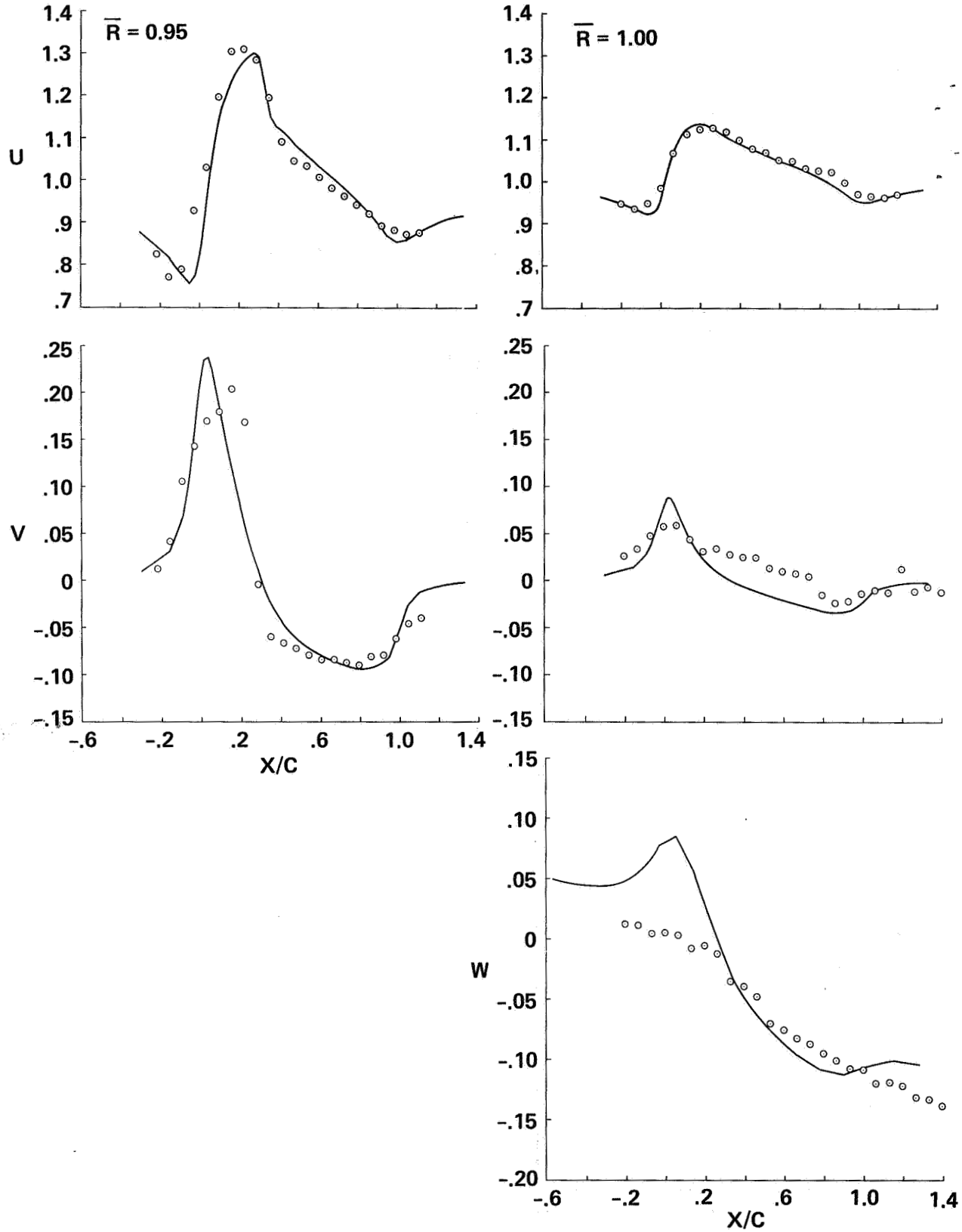

Figure 8.- Computed and measured velocity component comparisons: M_{tip} = 0.85, Y/C = 0.0838.

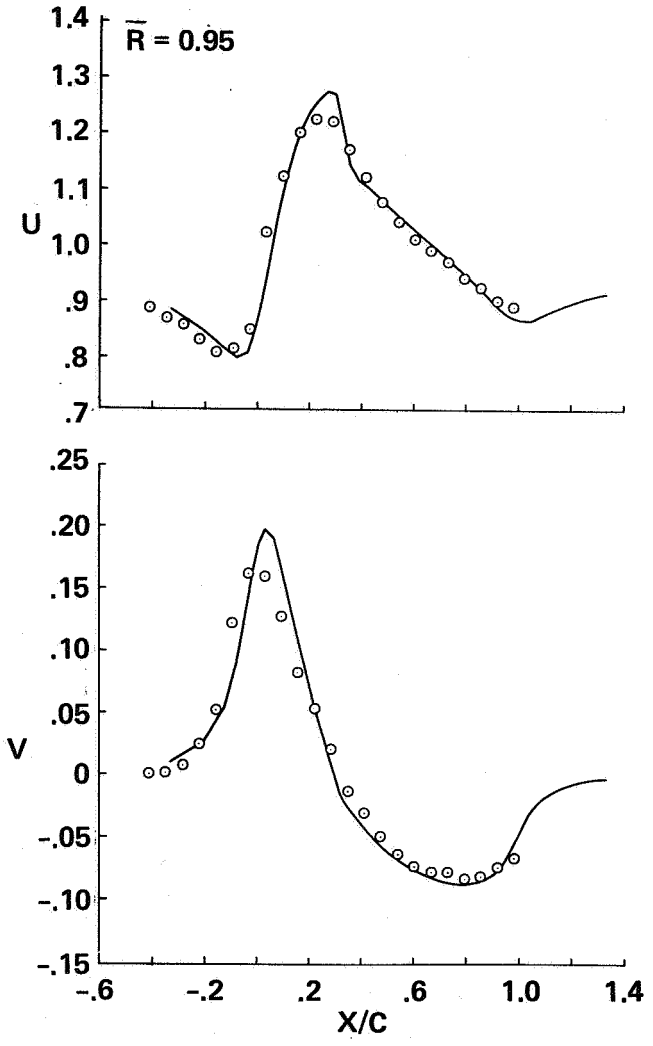

Figure 9.- Computed and measured velocity component comparisons: M_{tip} = 0.85, Y/C = 0.1172.

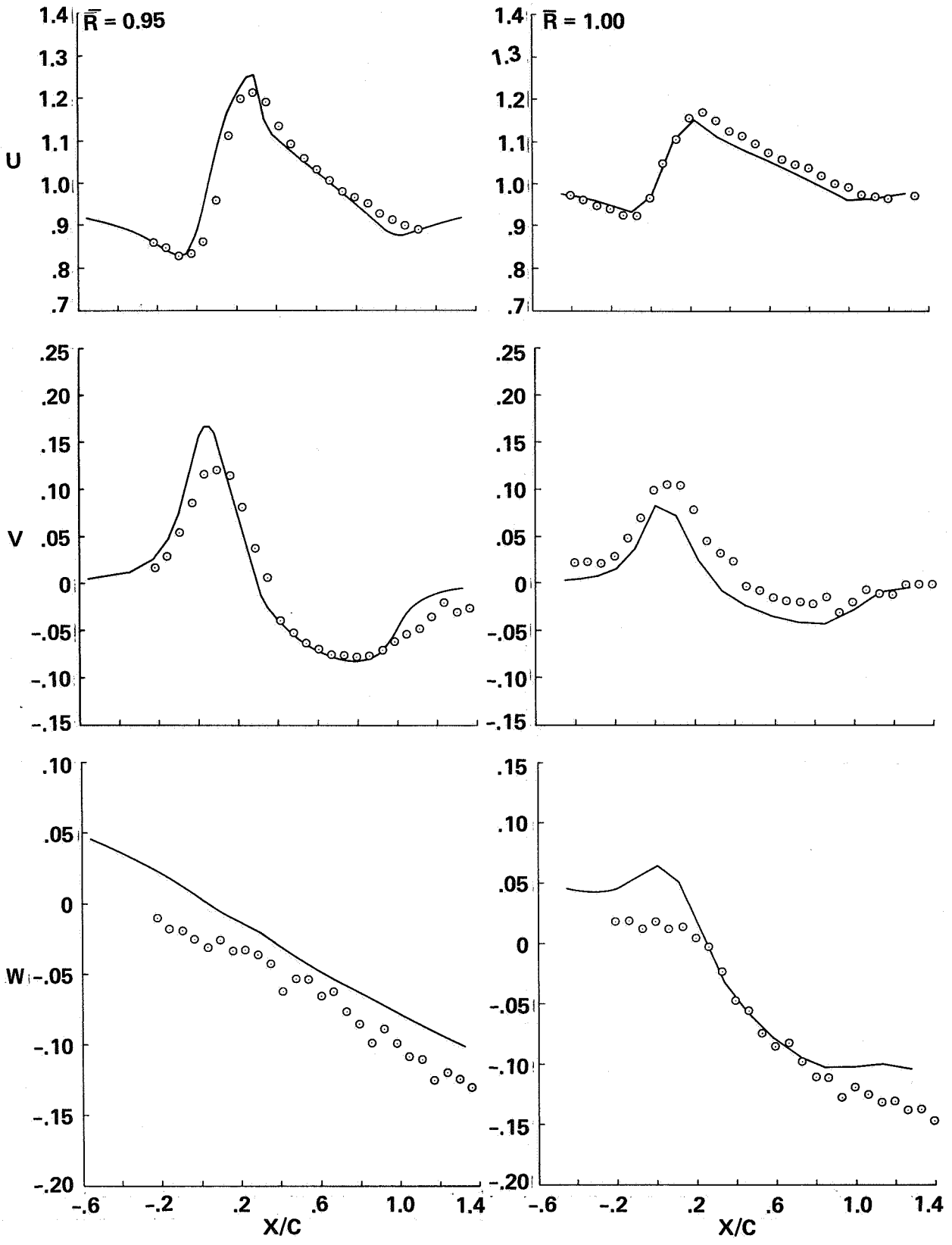

Figure 10.- Computed and measured velocity component comparisons: M_{tip} = 0.85, Y/C = 0.1505.

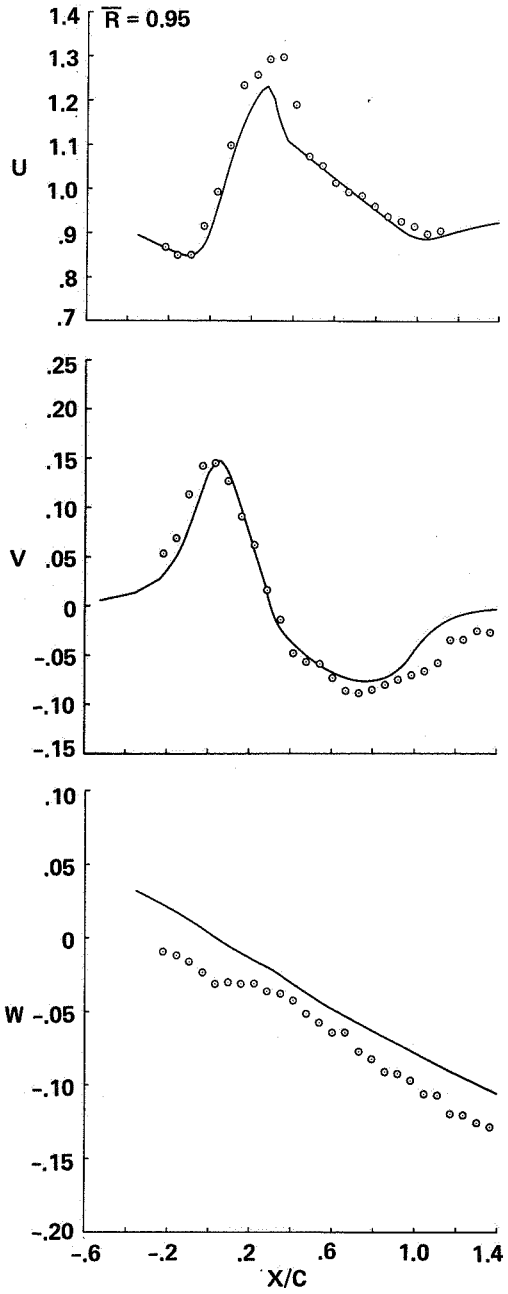

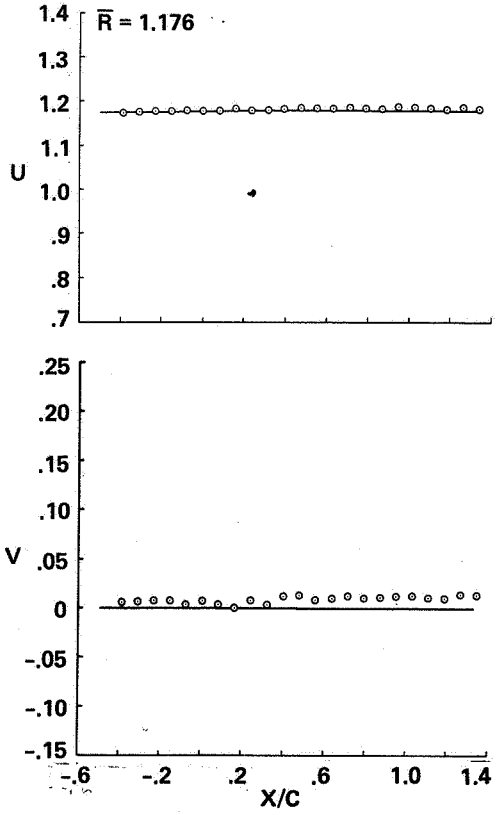

Figure 11.- Computed and measured velocity component comparisons: M_{tip} = 0.85, Y/C = 0.1838.

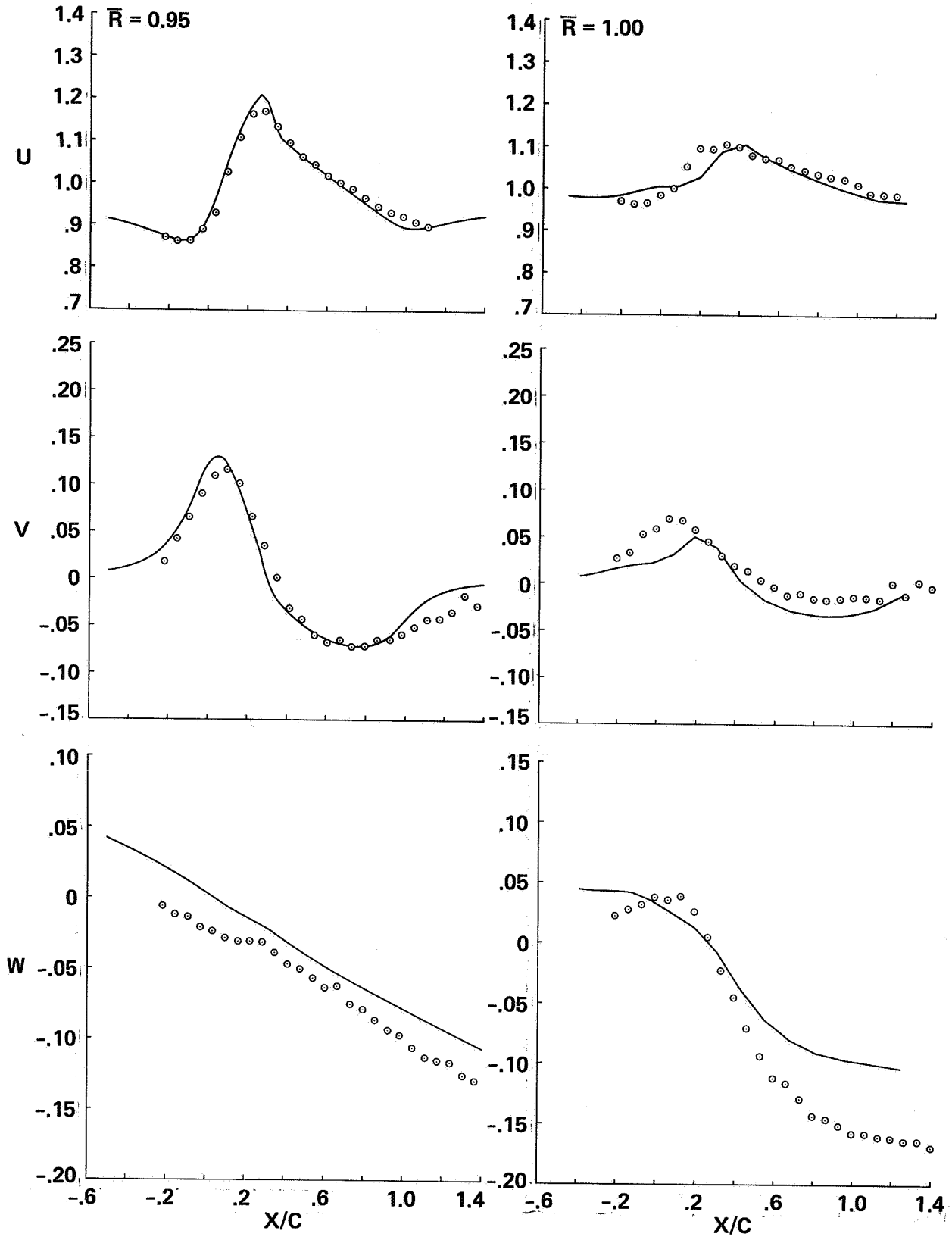

Figure 12.- Computed and measured velocity component comparisons: M_{tip} = 0.85, Y/C = 0.2172.

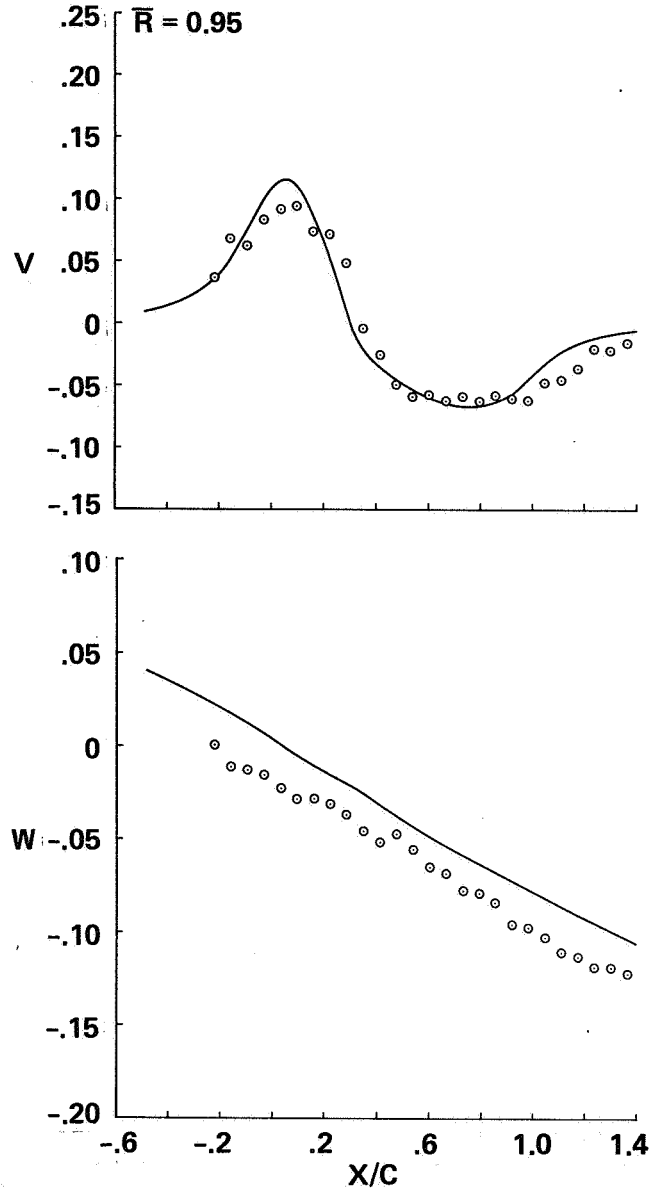

Figure 13.- Computed and measured velocity component comparisons: M_{tip} = 0.85, Y/C = 0.2505.

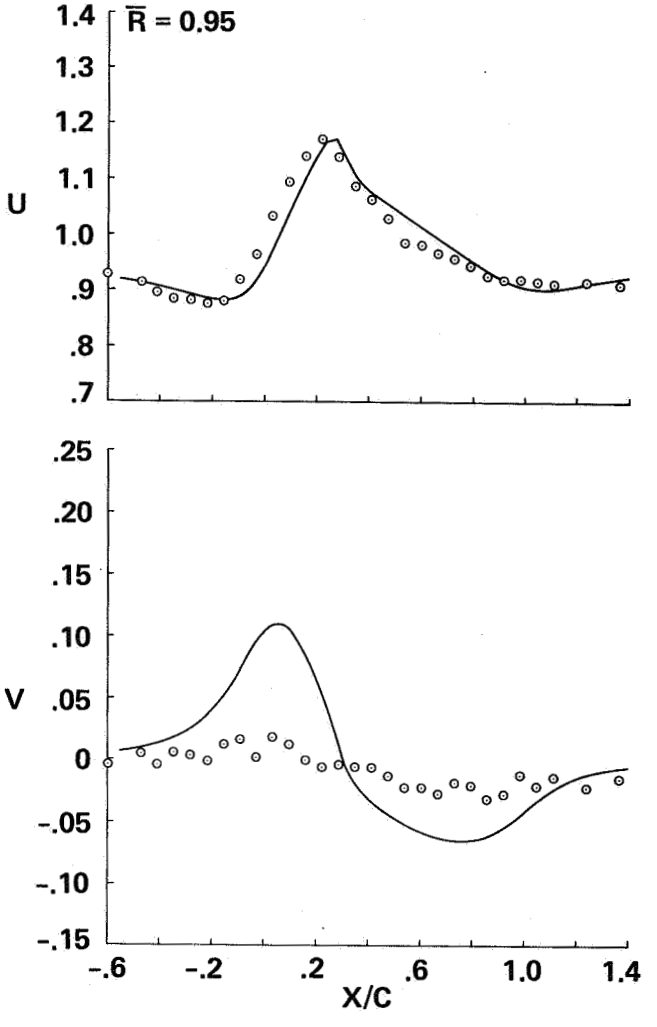

Figure 14.- Computed and measured velocity component comparisons: M_{tip} = 0.85, Y/C = 0.2672.

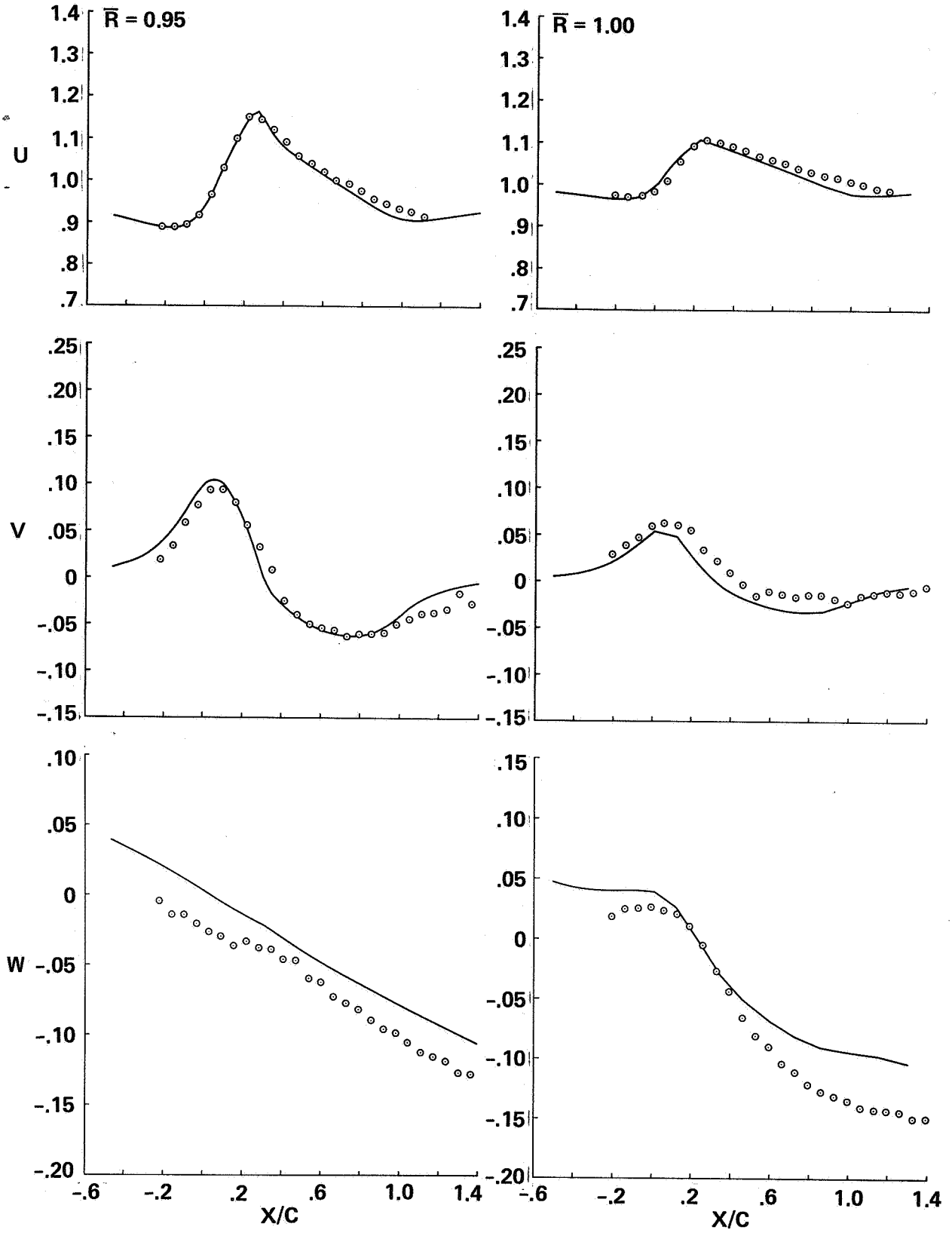

Figure 15.- Computed and measured velocity component comparisons: M_{tip} = 0.85, Y/C = 0.2838.

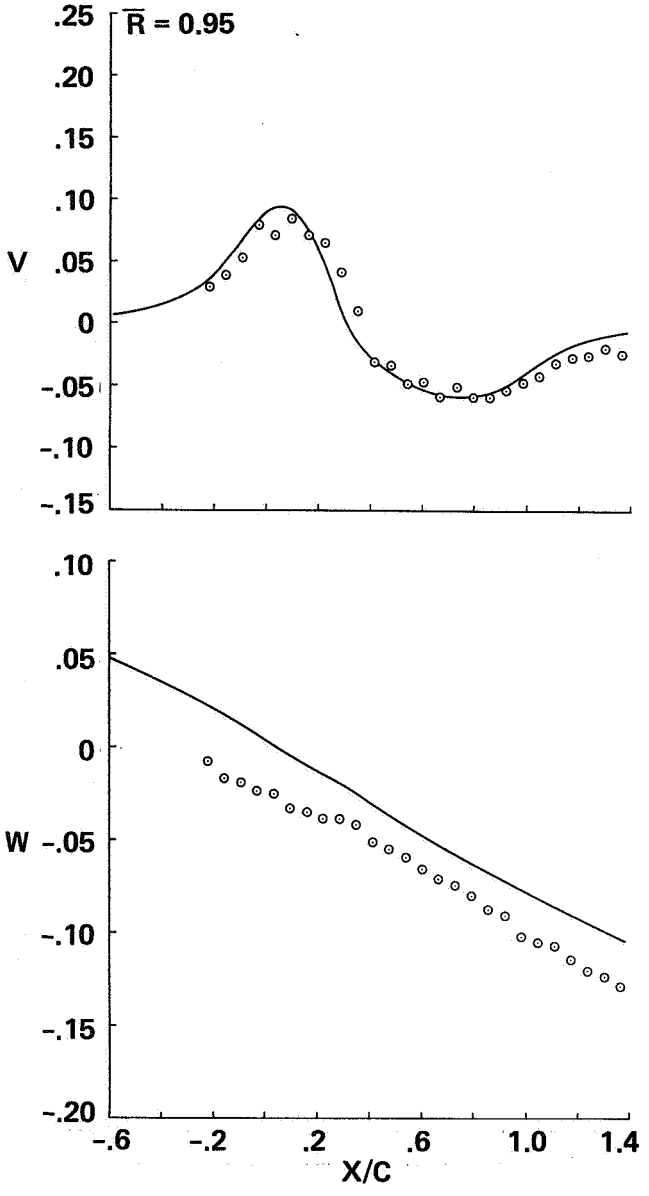

Figure 16.- Computed and measured velocity component comparisons: M_{tip} = 0.85, Y/C = 0.3172.

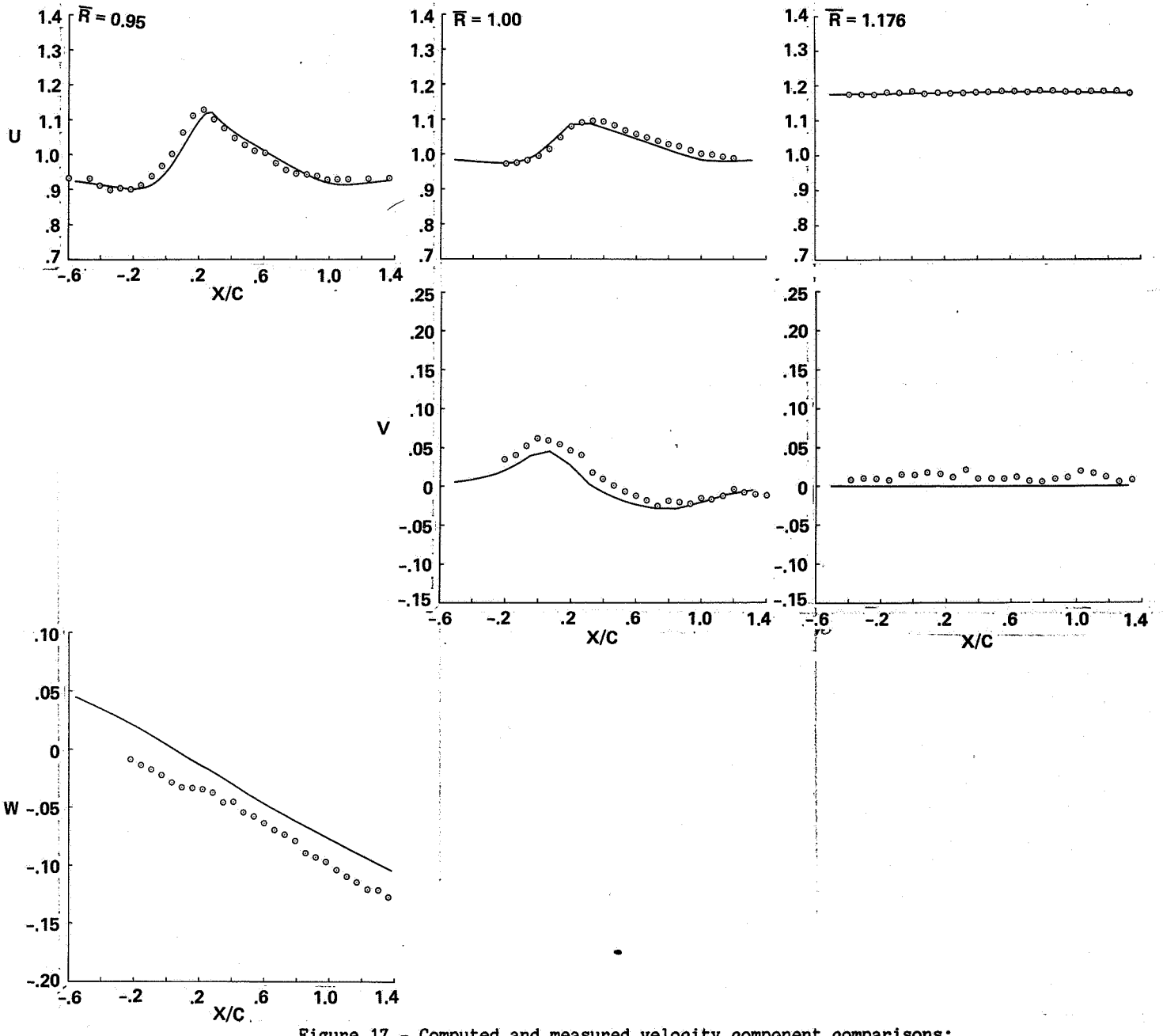

Figure 17.- Computed and measured velocity component comparisons: M_{tip} = 0.85, Y/C = 0.3505.

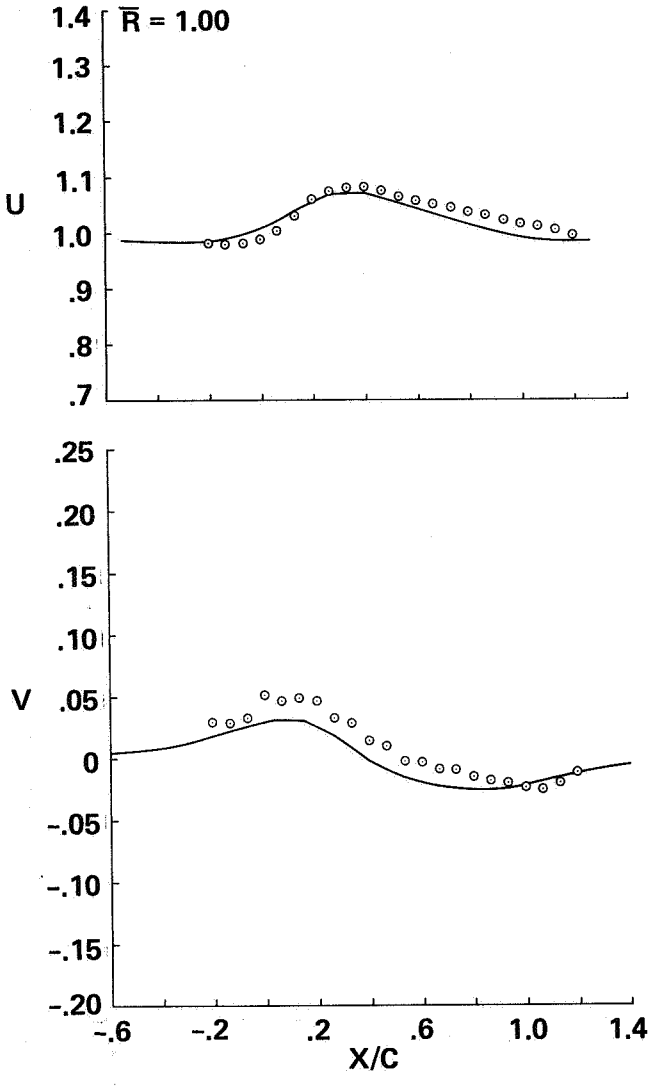

Figure 18.- Computed and measured velocity component comparisons: M_{tip} = 0.85, Y/C = 0.4172.

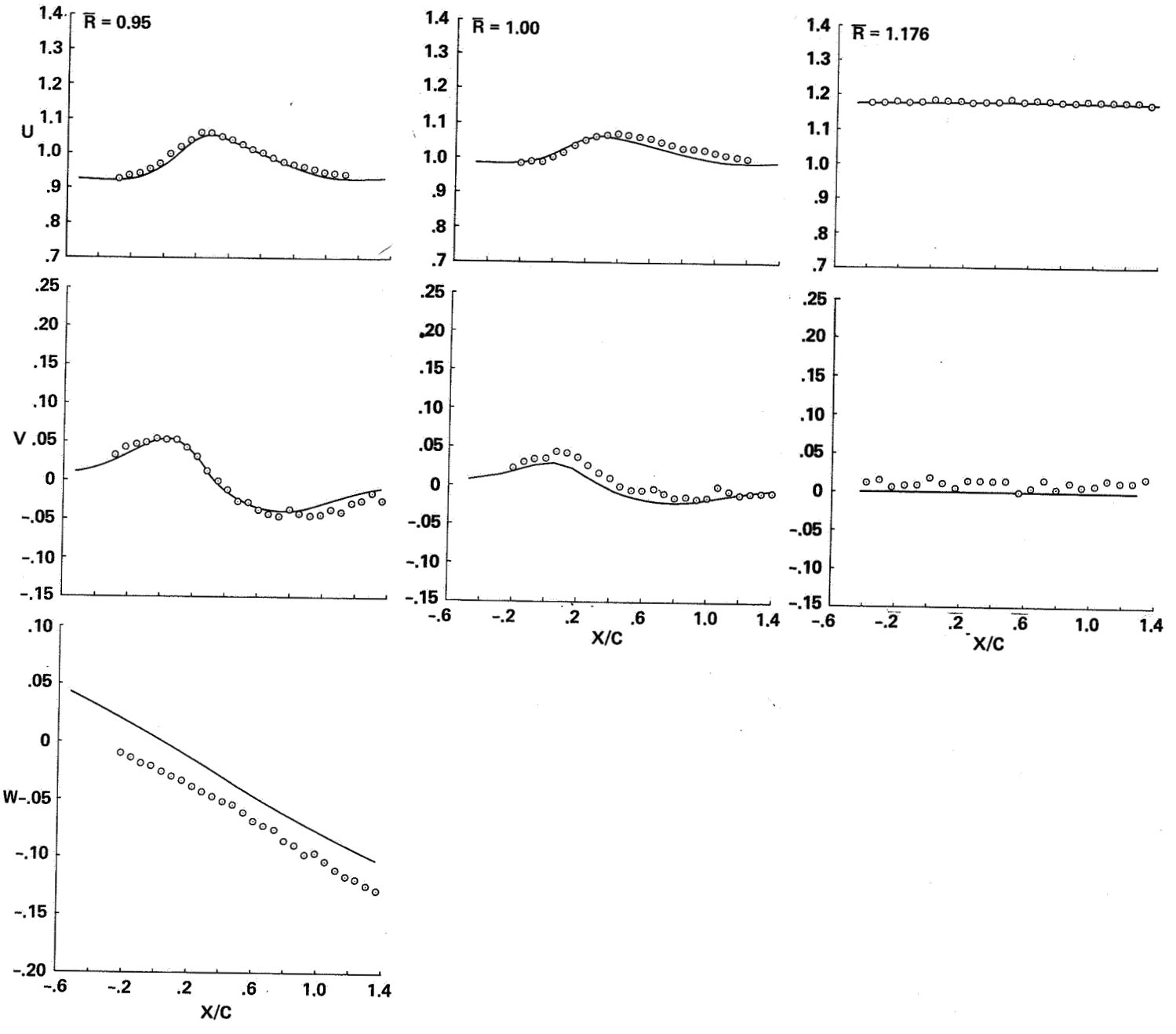

Figure 19.- Computed and measured velocity component comparisons:
M_{tip} = 0.85, Y/C = 0.5172.

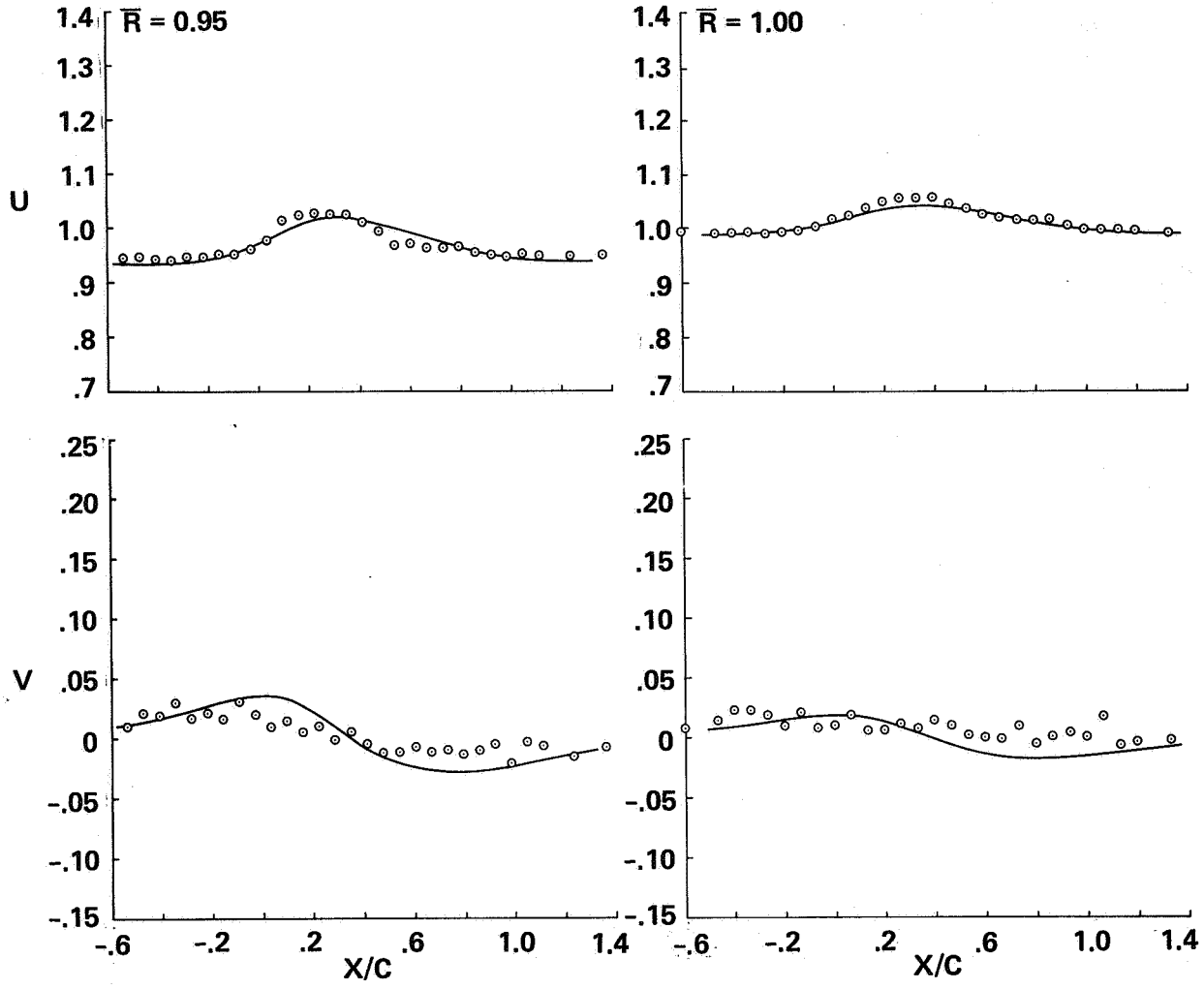

Figure 20.- Computed and measured velocity component comparisons: M_{tip} = 0.85, Y/C = 0.6838.

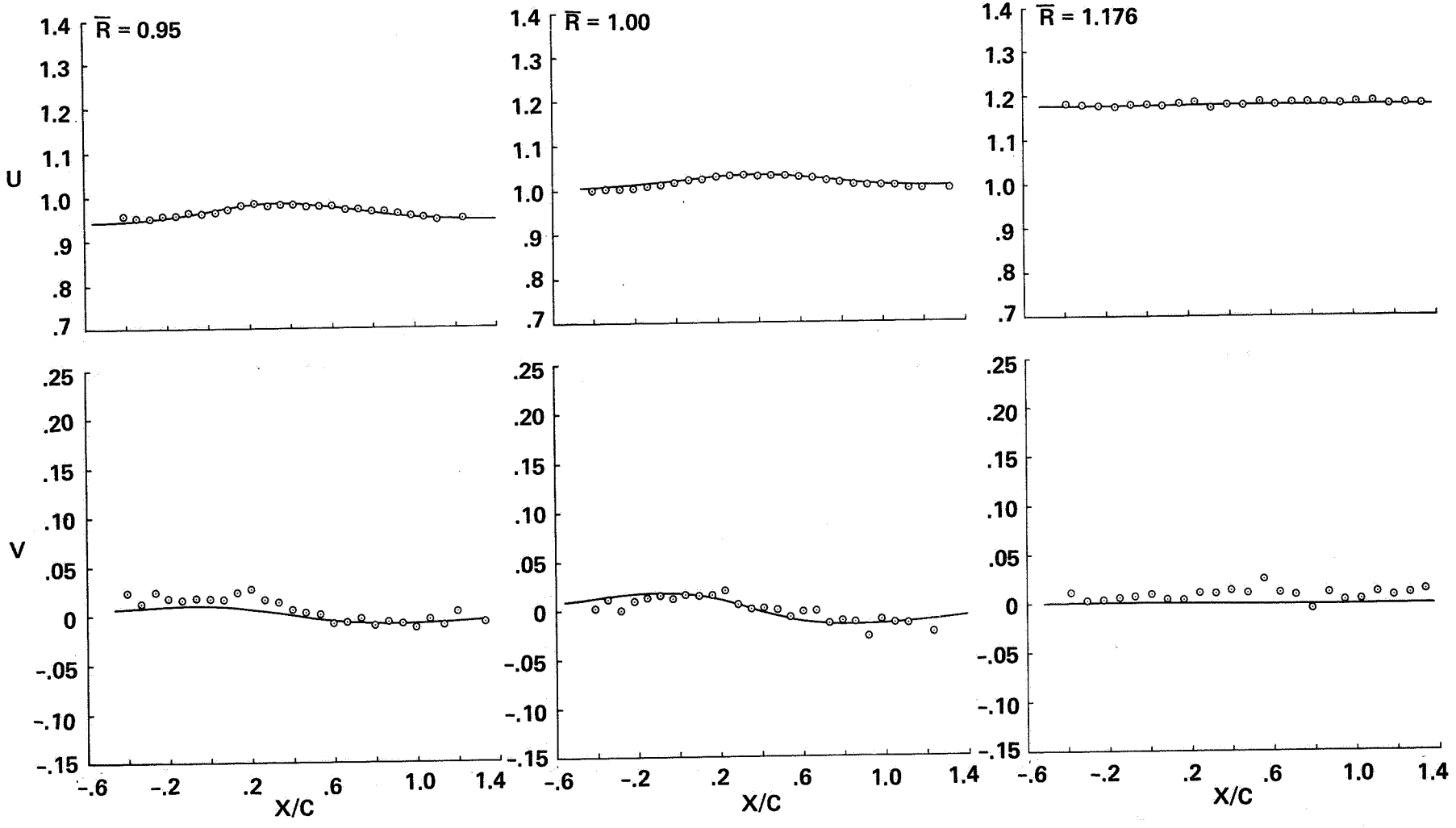

Figure 21.- Computed and measured velocity component comparisons:
M_{tip} = 0.85, Y/C = 1.0172.

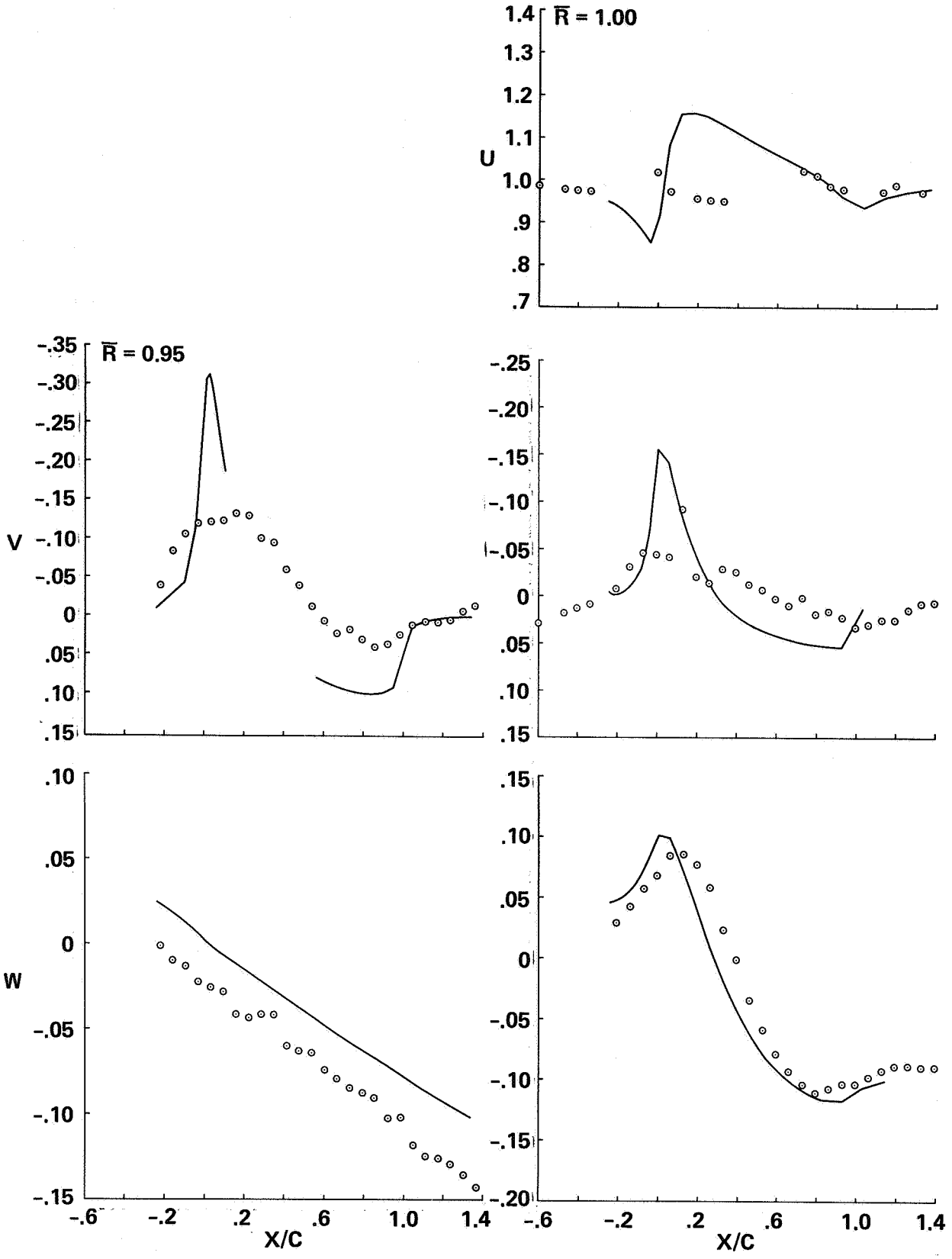

Figure 22.- Computed and measured velocity component comparisons: M_{tip} = 0.85, Y/C = -0.0495.

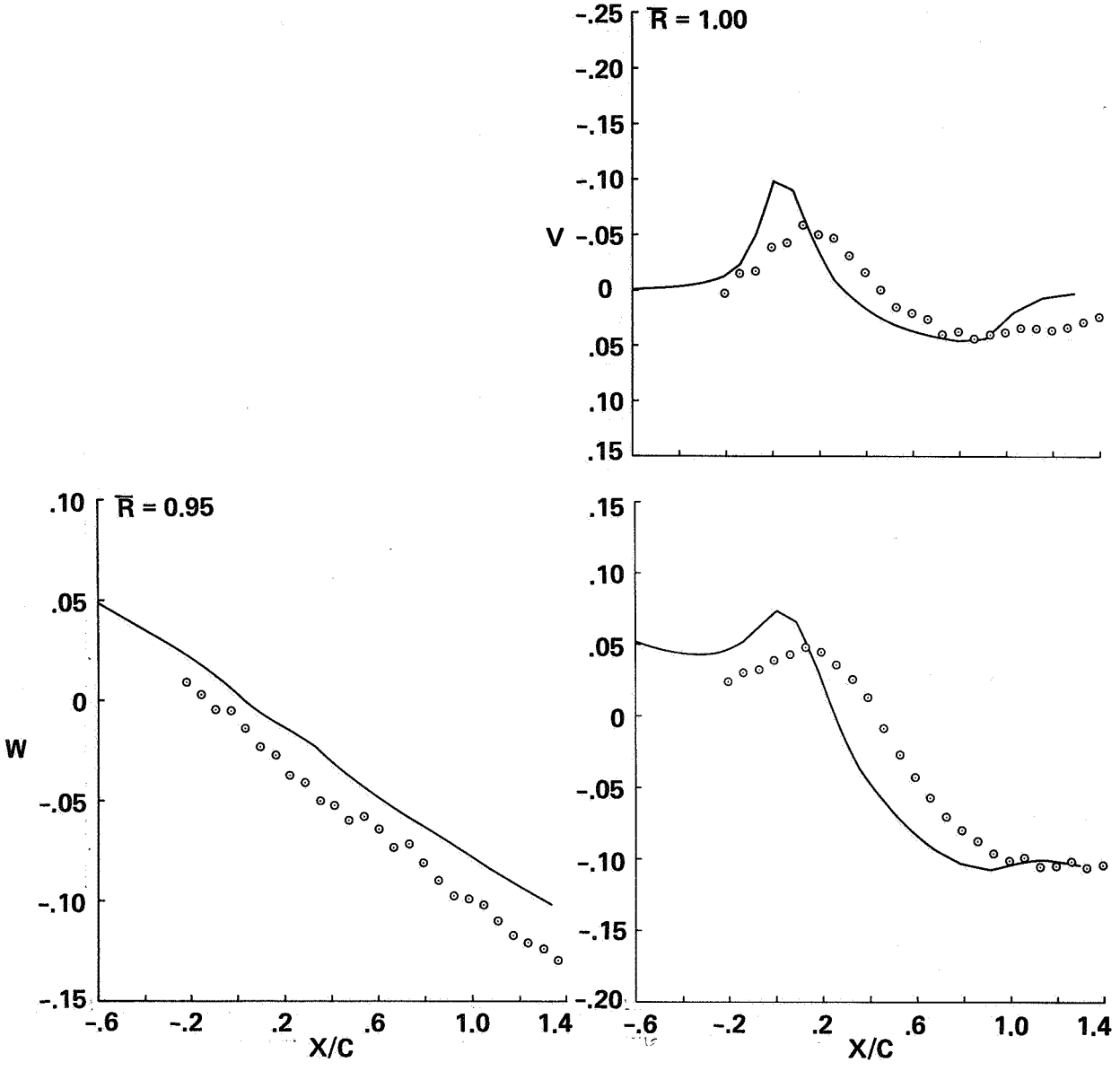

Figure 23.- Computed and measured velocity component comparisons: M_{tip} = 0.85, Y/C = -0.1162.

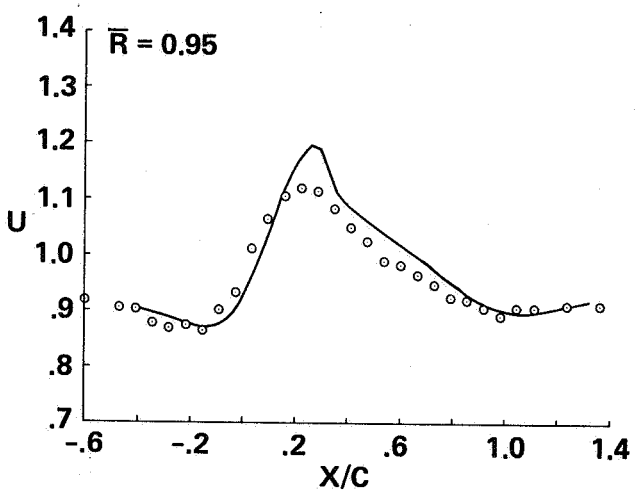

Figure 24.- Computed and measured velocity component comparisons: M_{tip} = 0.85, Y/C = -0.2328.

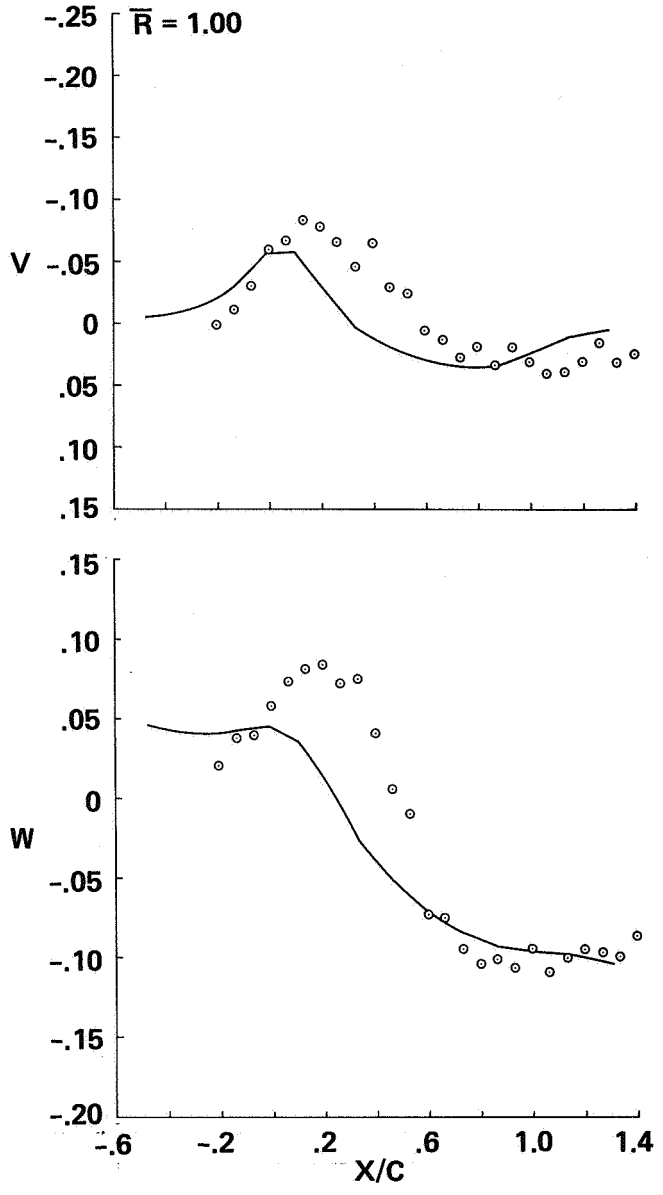

Figure 25.- Computed and measured velocity component comparisons: M_{tip} = 0.85, Y/C = -0.2495.

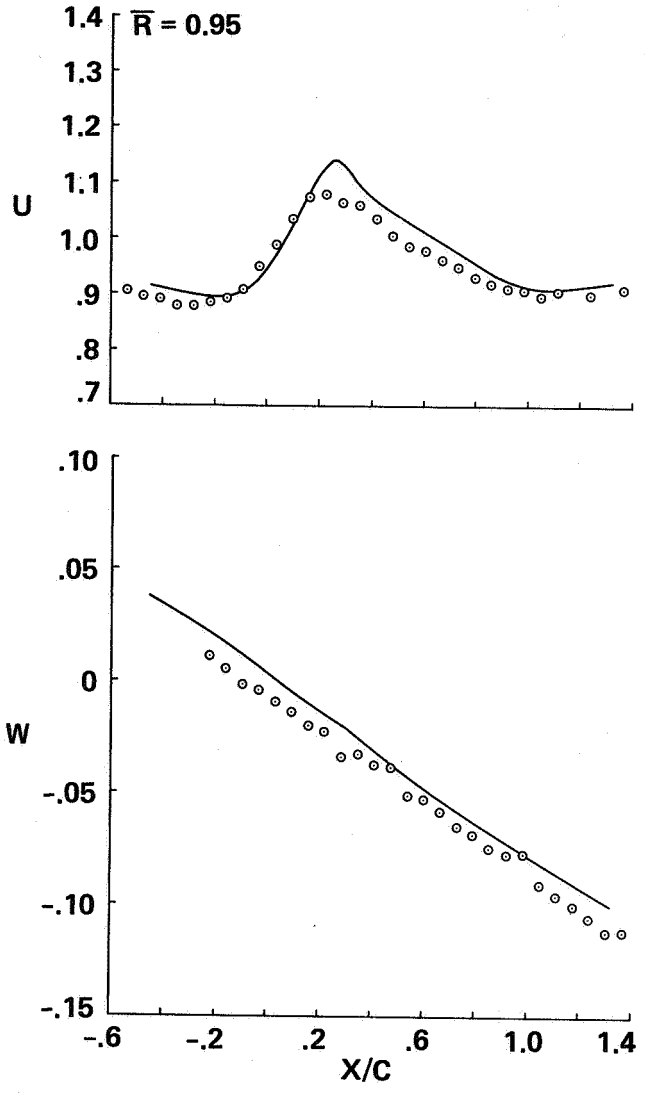

Figure 26.- Computed and measured velocity component comparisons: M_{tip} = 0.85, Y/C = -0.3162.

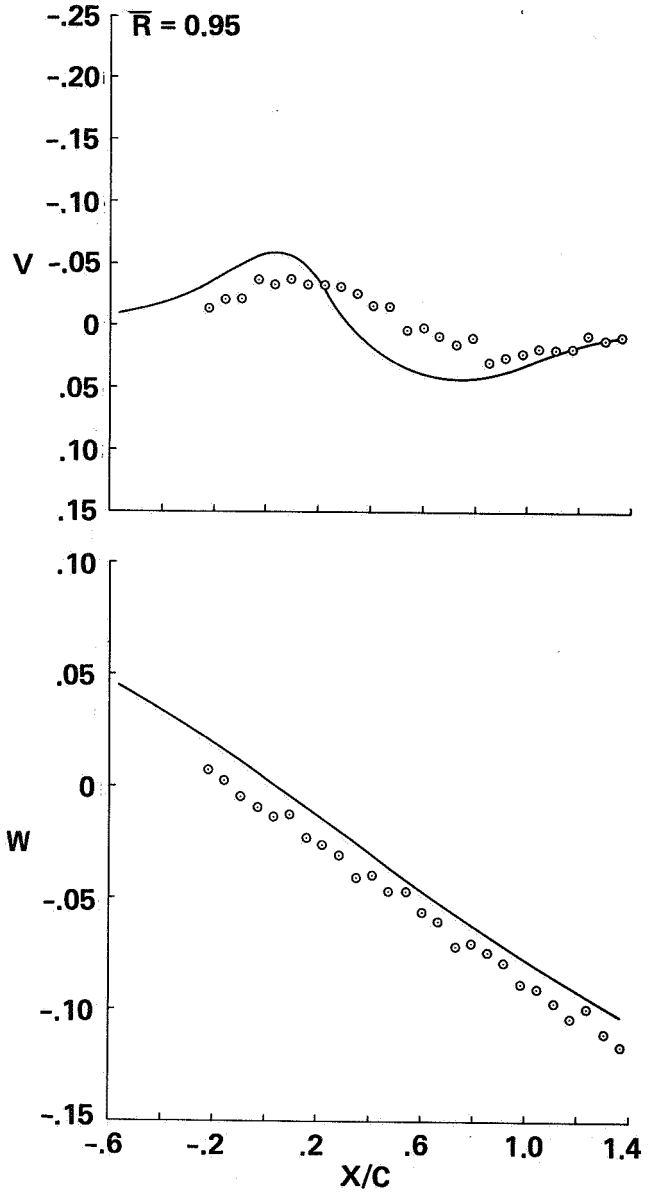

Figure 27.- Computed and measured velocity component comparisons: M_{tip} = 0.85, Y/C = -0.4828.

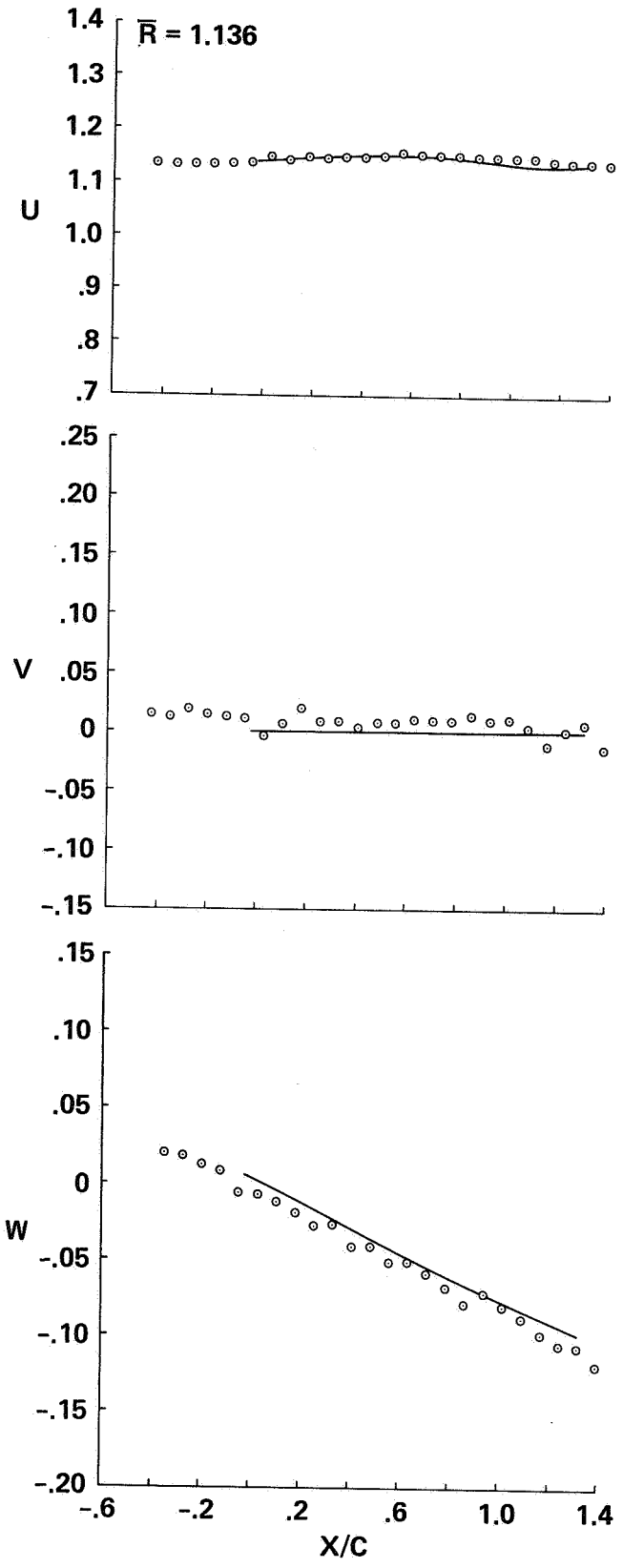

Figure 28.- Computed and measured velocity component comparisons: M_{tip} = 0.88, Y/C = 0.0172.

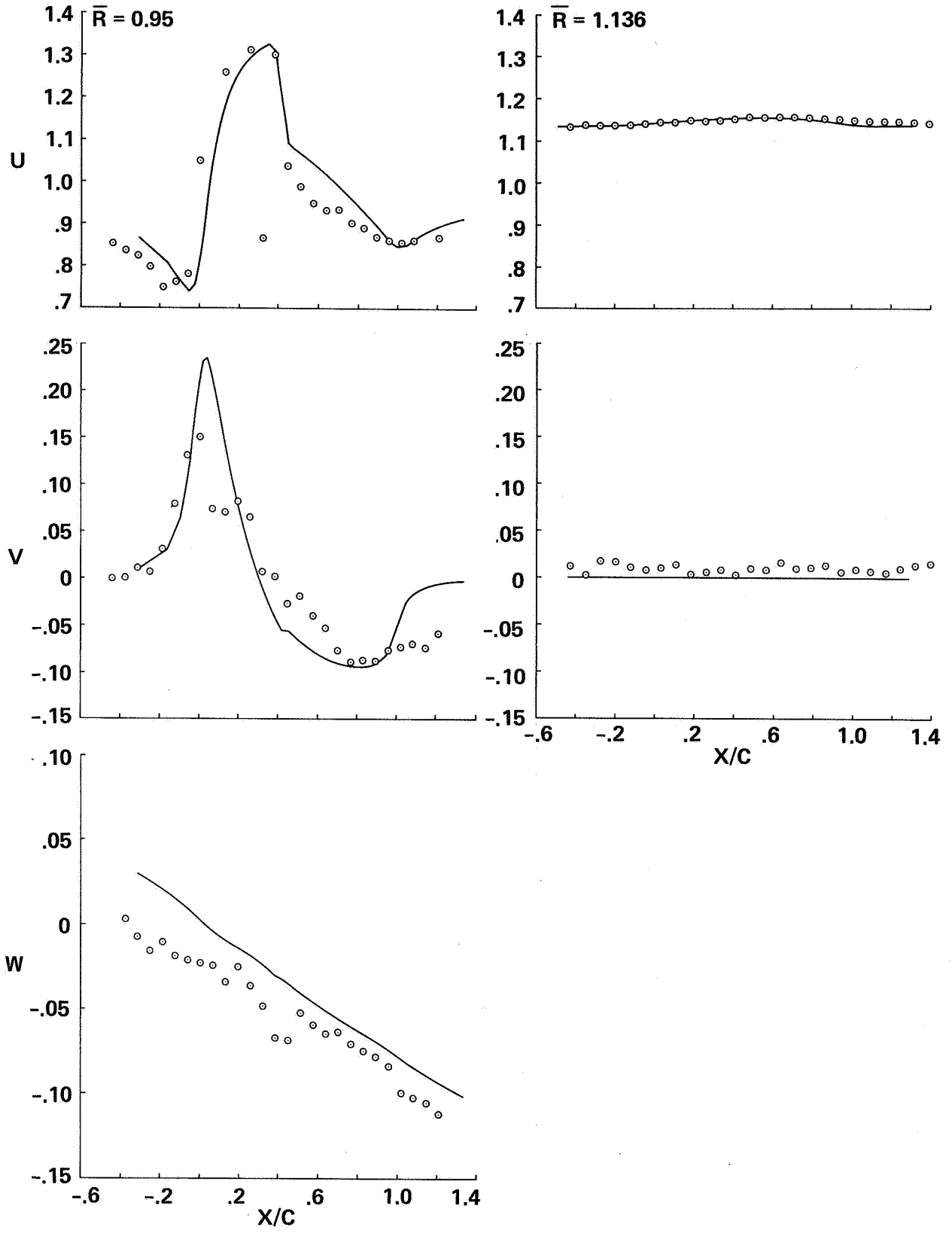

Figure 29.- Computed and measured velocity component comparisons: M_{tip} = 0.88, Y/C = 0.0838.

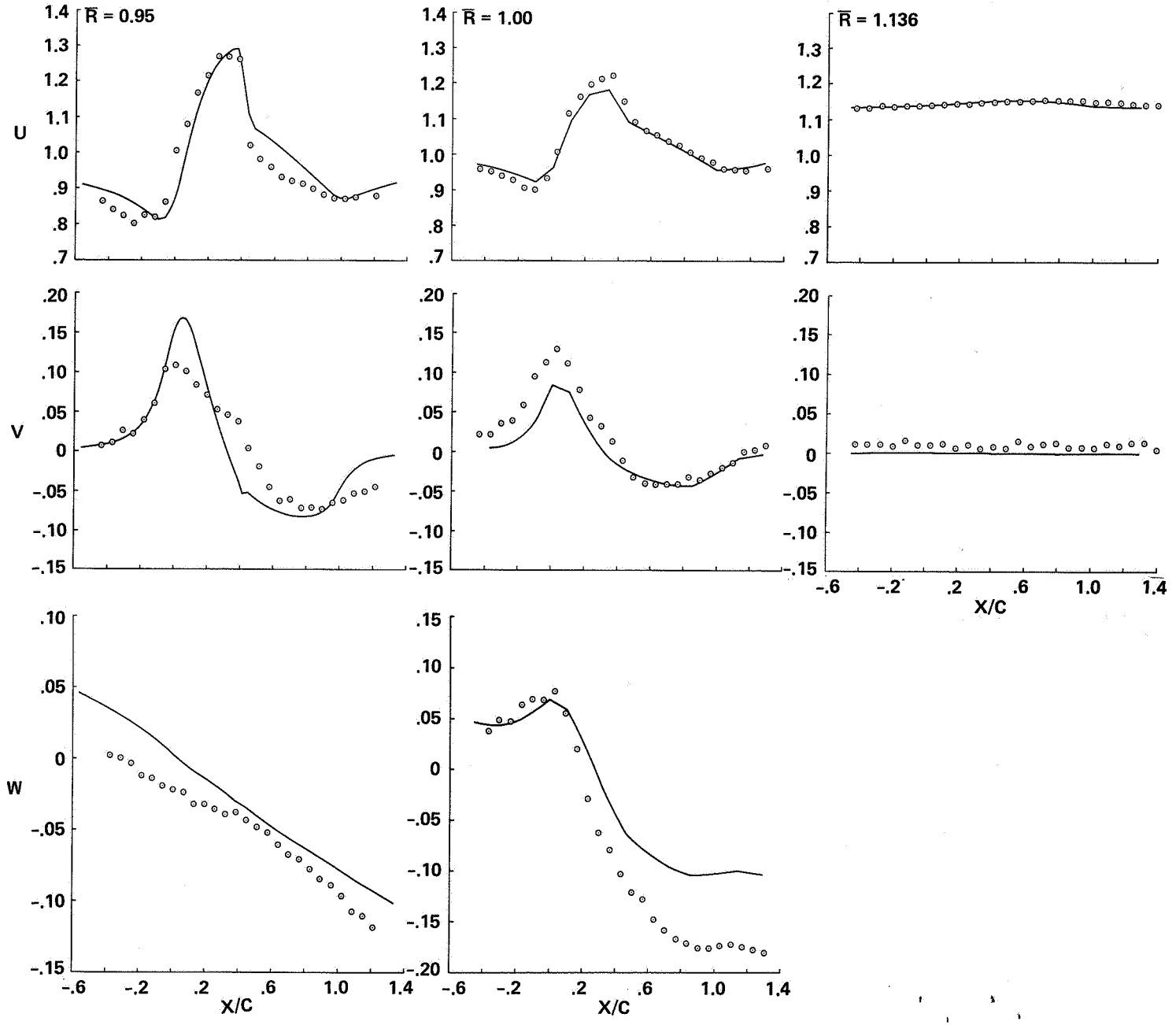

Figure 30.- Computed and measured velocity component comparisons: M_{tip} = 0.88, Y/C = 0.1505.

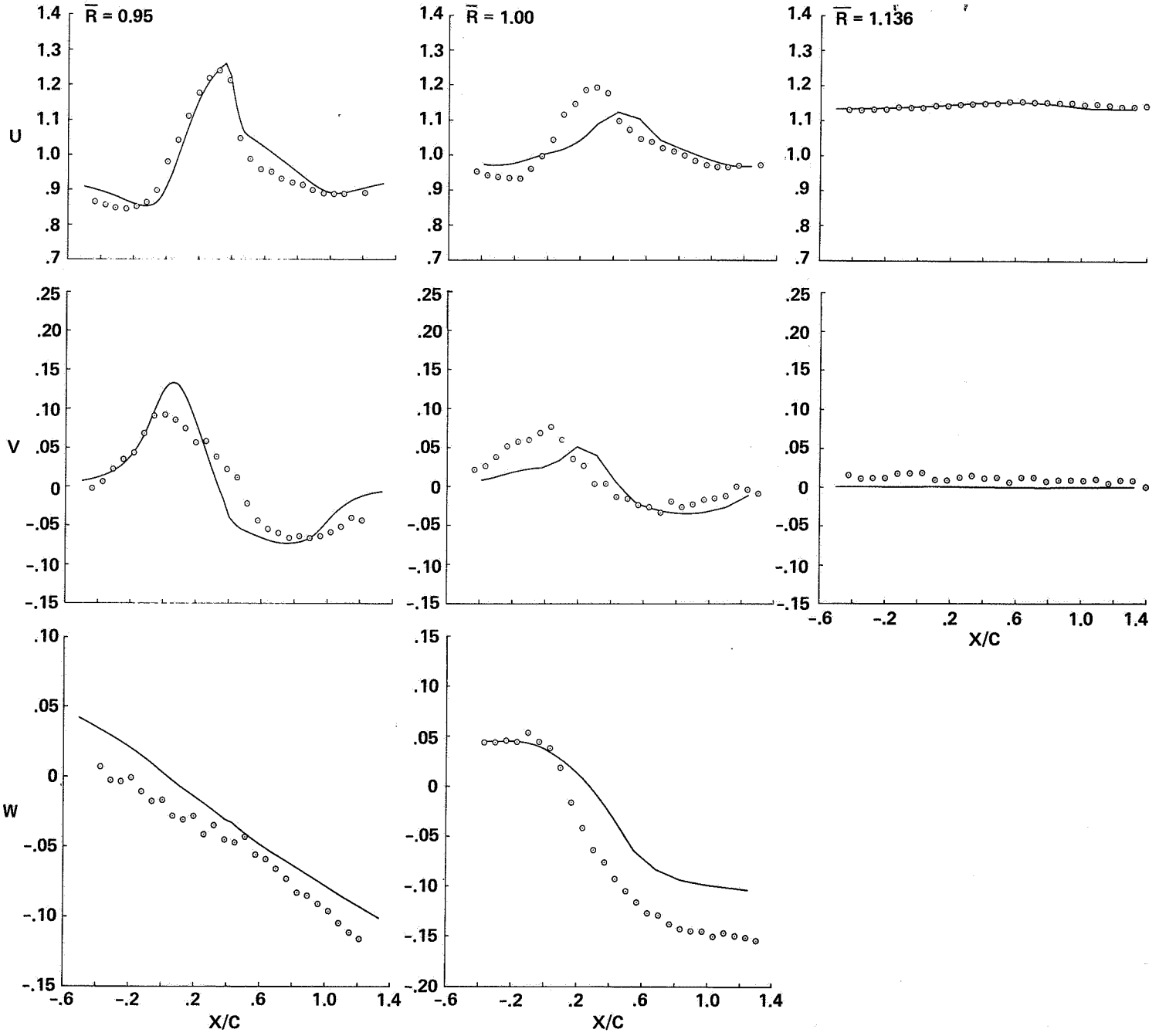

Figure 31.- Computed and measured velocity component comparisons: M_{tip} = 0.88, Y/C = 0.2172.

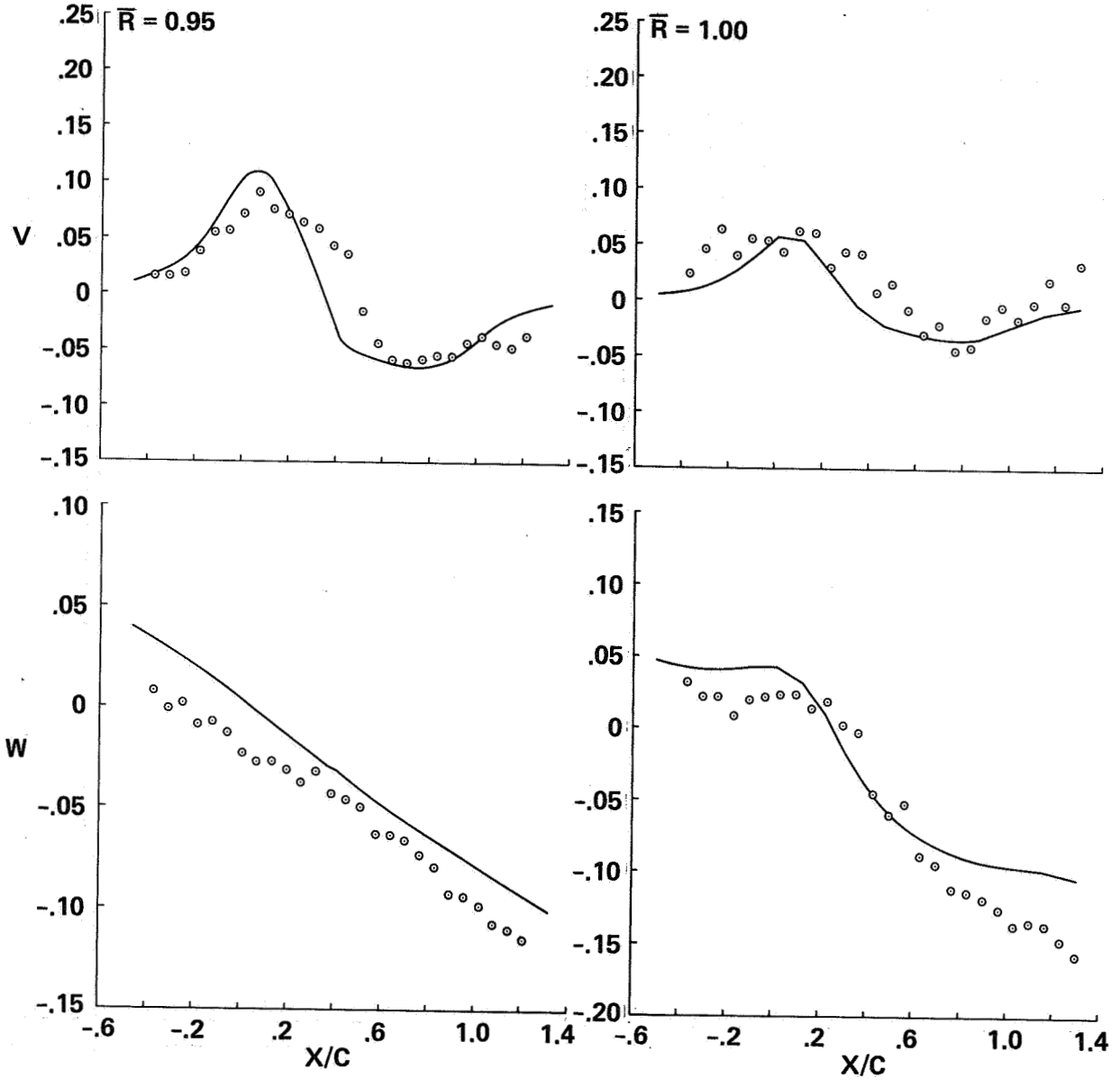

Figure 32.- Computed and measured velocity component comparisons: M_{tip} = 0.88, Y/C = 0.2838.

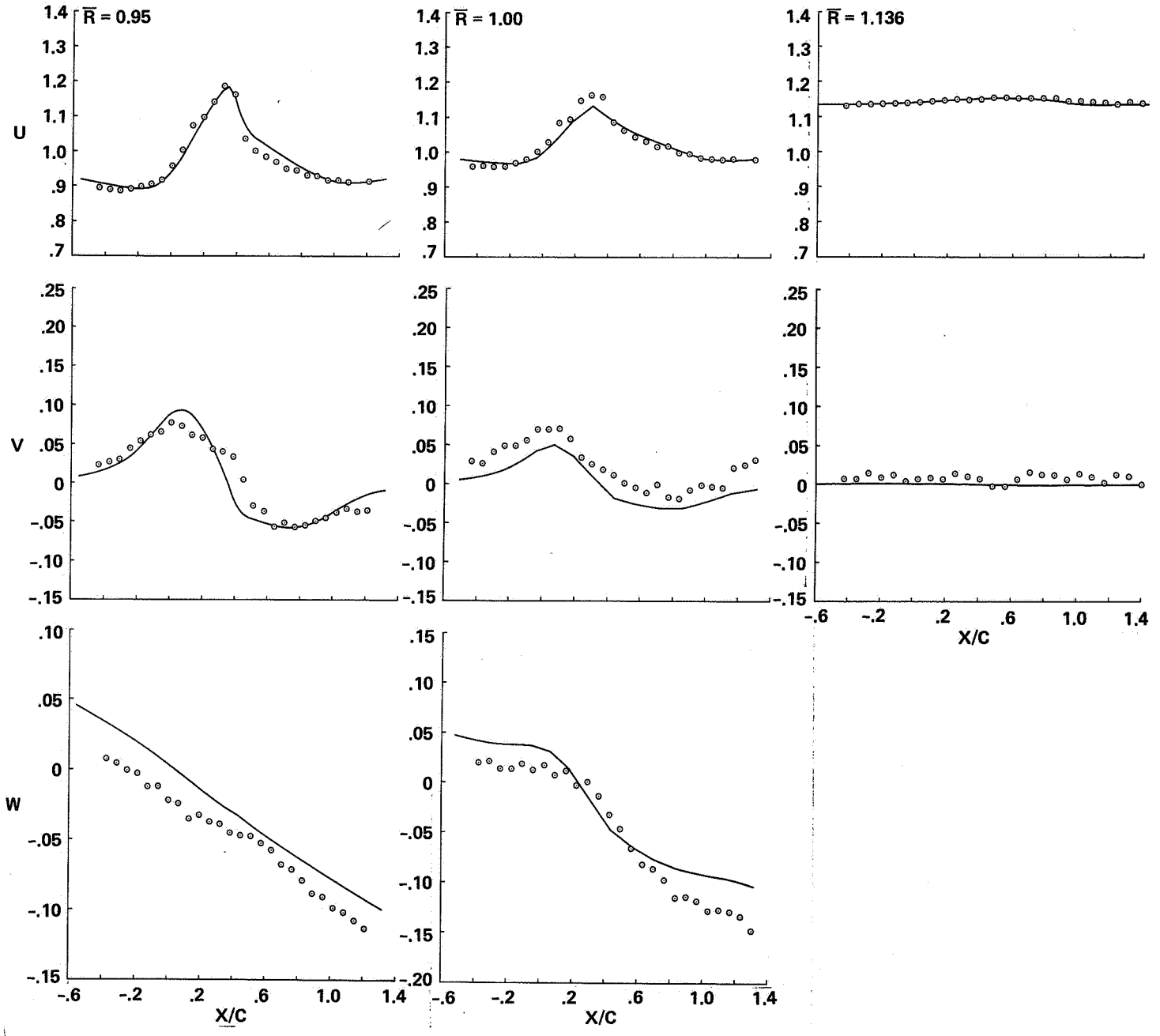

Figure 33.- Computed and measured velocity component comparisons: M_{tip} = 0.88, Y/C = 0.3505.

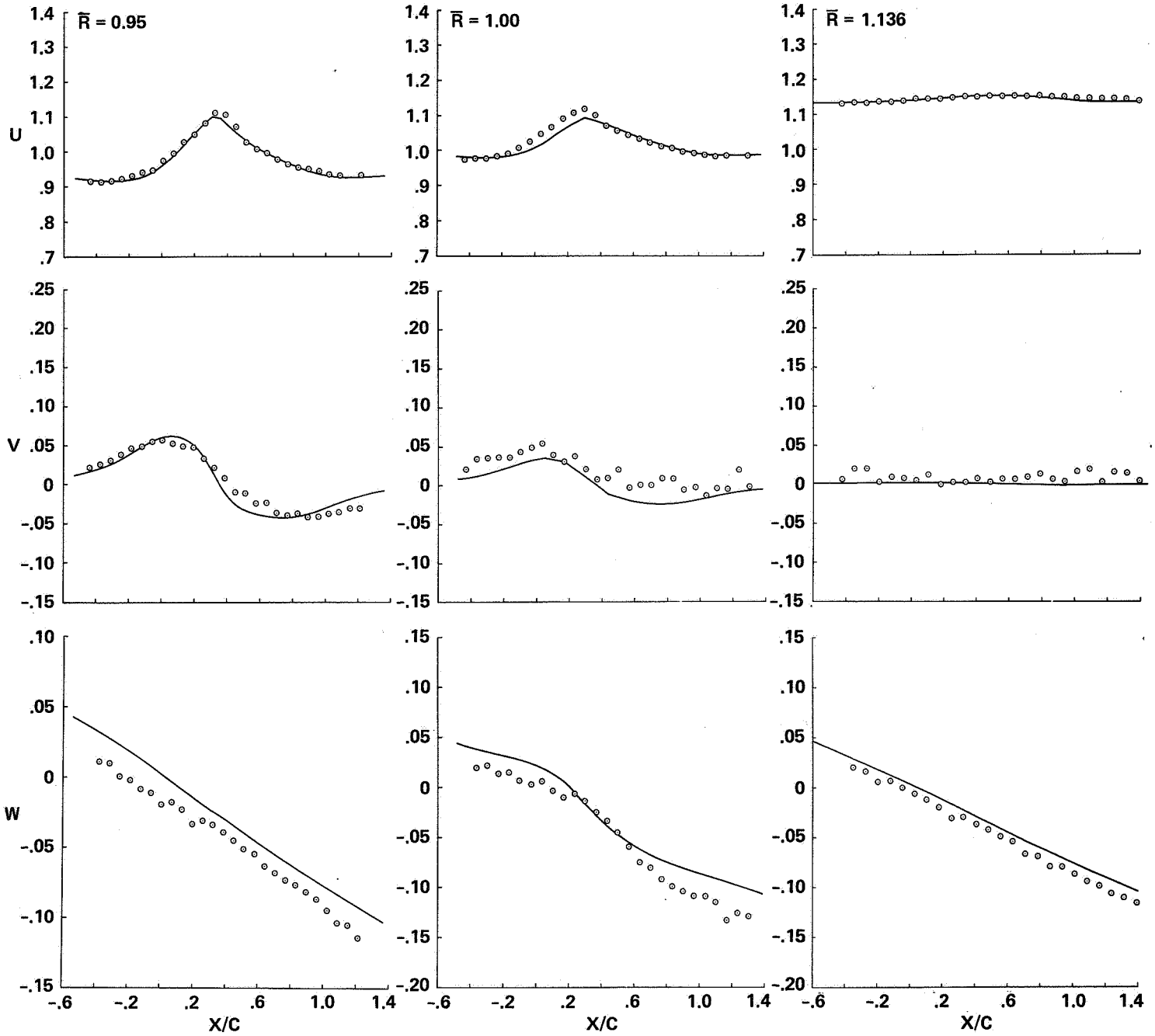

Figure 34.- Computed and measured velocity component comparisons: M_{tip} = 0.88, Y/C = 0.5172.

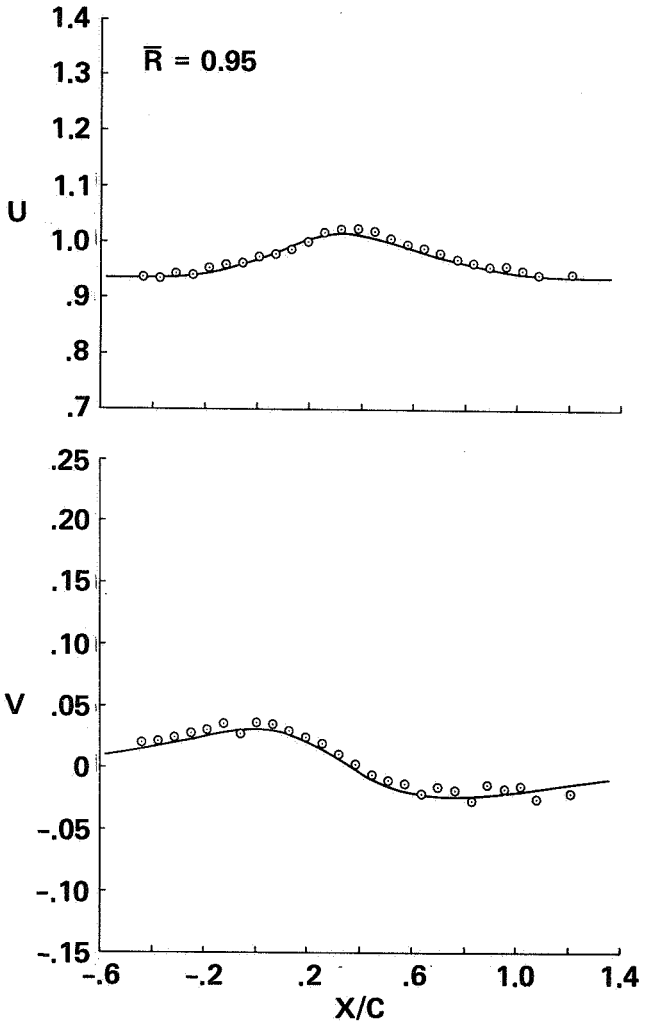

Figure 35.- Computed and measured velocity component comparisons: M_{tip} = 0.88, Y/C = 0.8505.

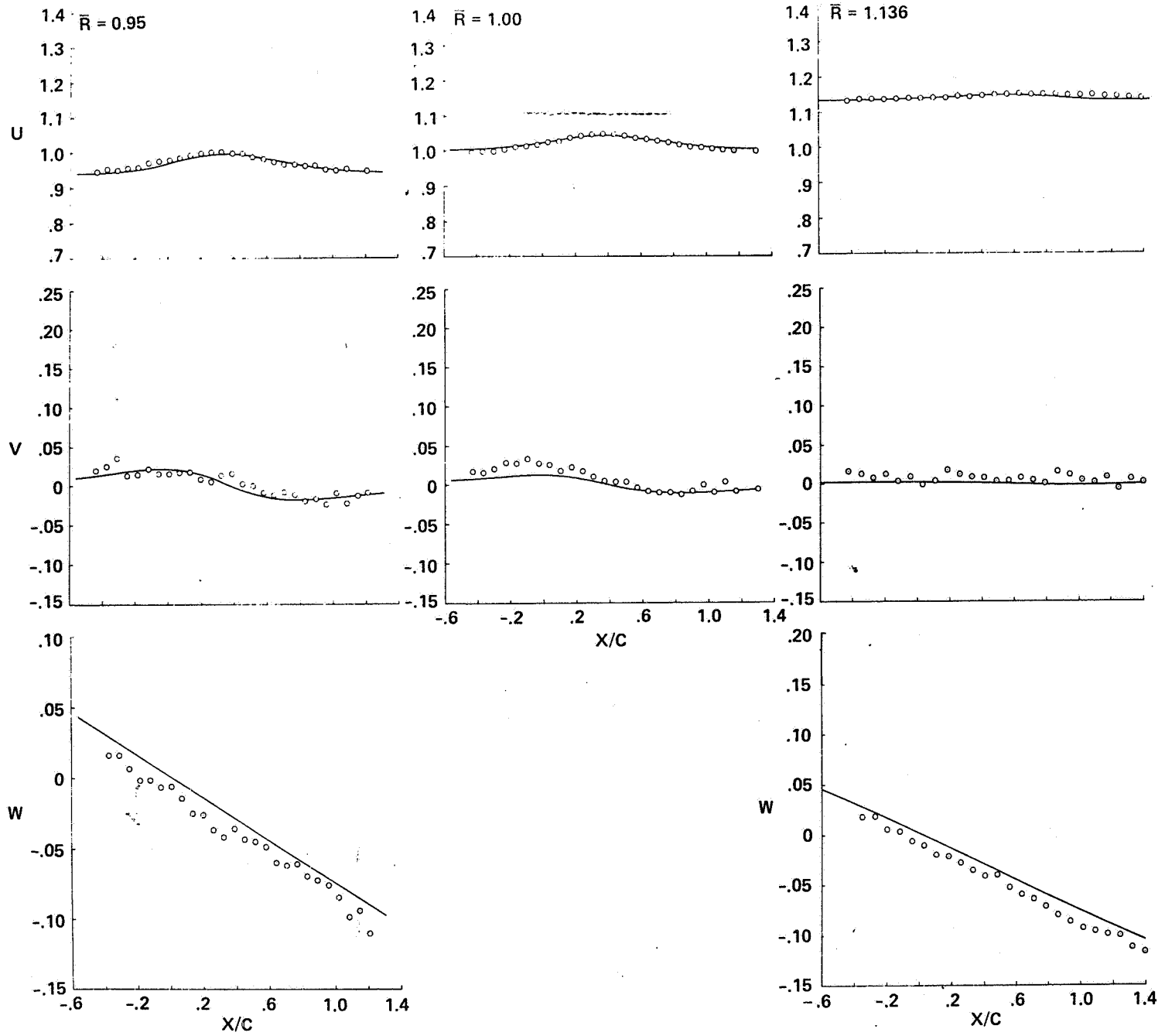

Figure 36.- Computed and measured velocity component comparisons: M_{tip} = 0.88, Y/C = 1.0172.

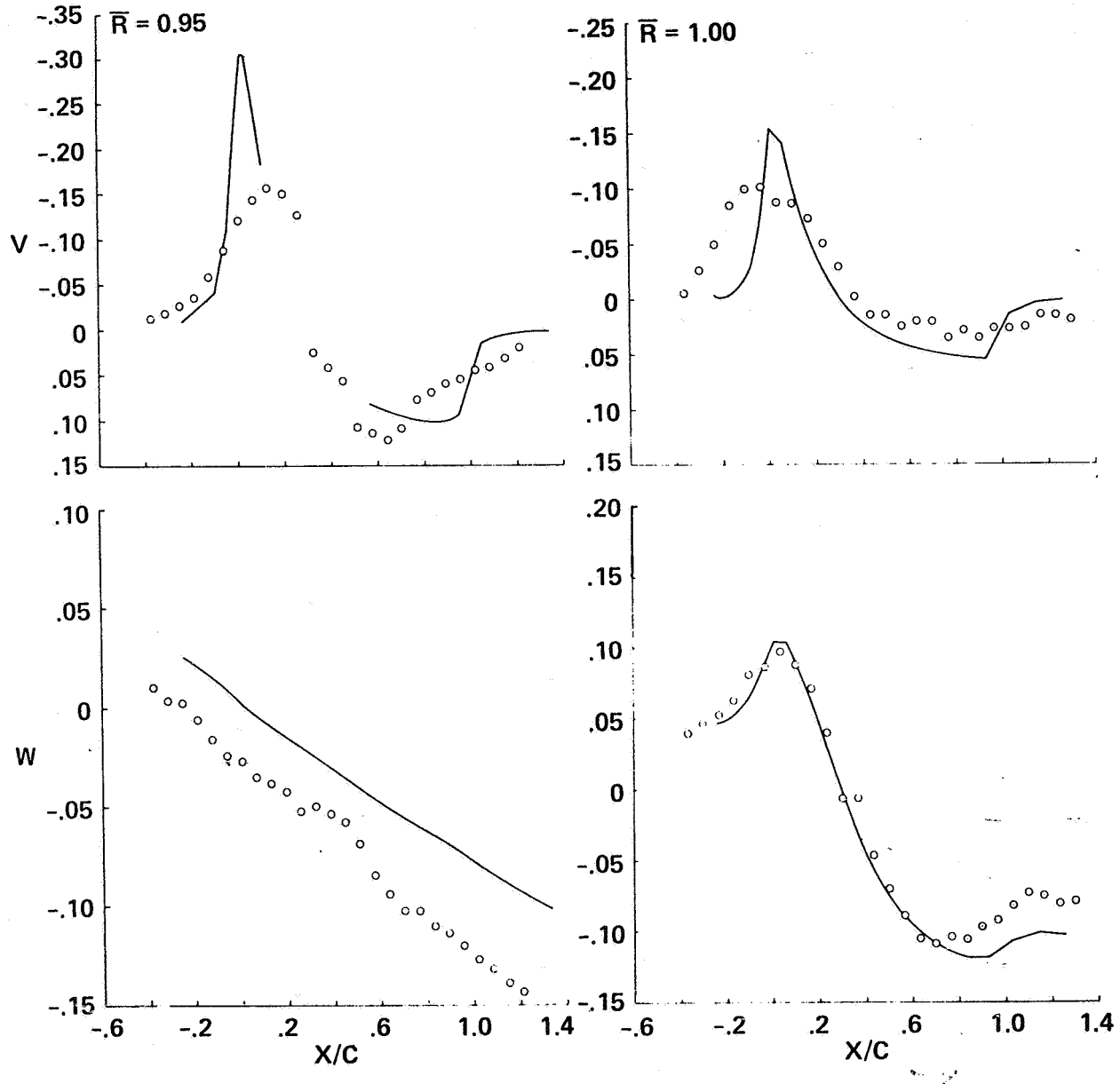

Figure 37.- Computed and measured velocity component comparisons: M_{tip} = 0.88, Y/C = -0.0495.

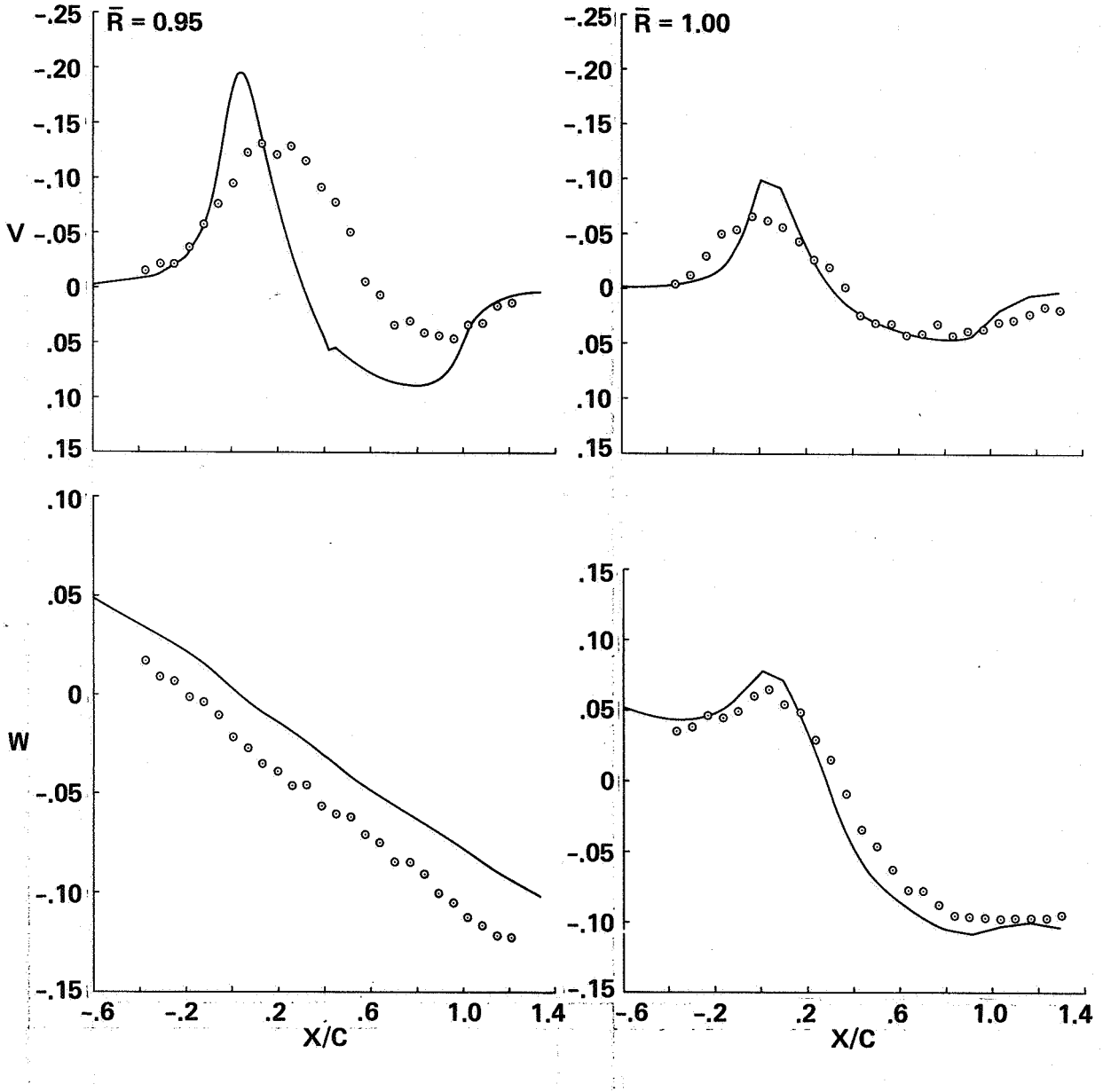

Figure 38.- Computed and measured velocity component comparisons: M_{tip} = 0.88, Y/C = -0.1162.

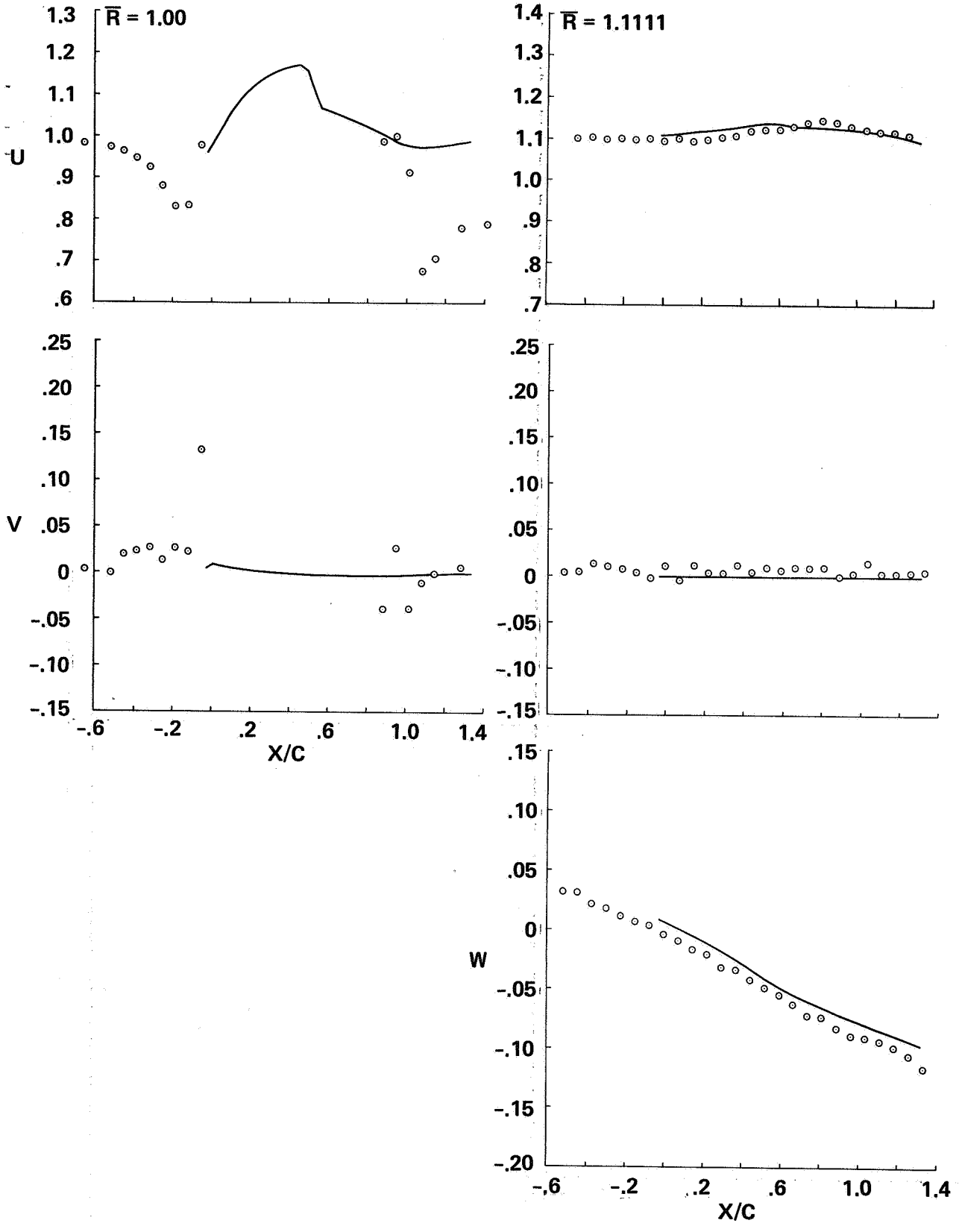

Figure 39.- Computed and measured velocity component comparisons: M_{tip} = 0.90, Y/C = 0.0172.

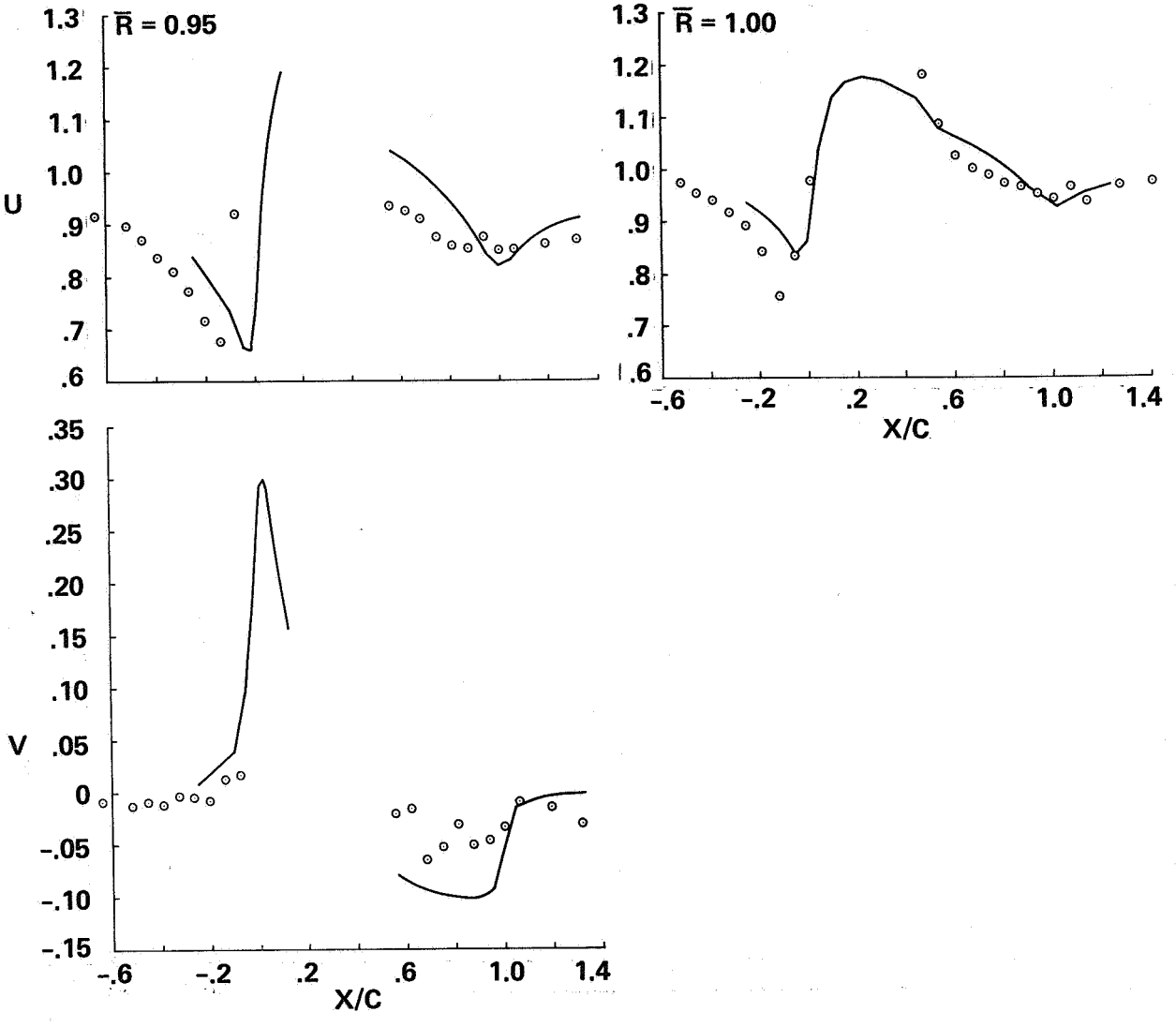

Figure 40.- Computed and measured velocity component comparisons: M_{tip} = 0.90, Y/C = 0.0505.

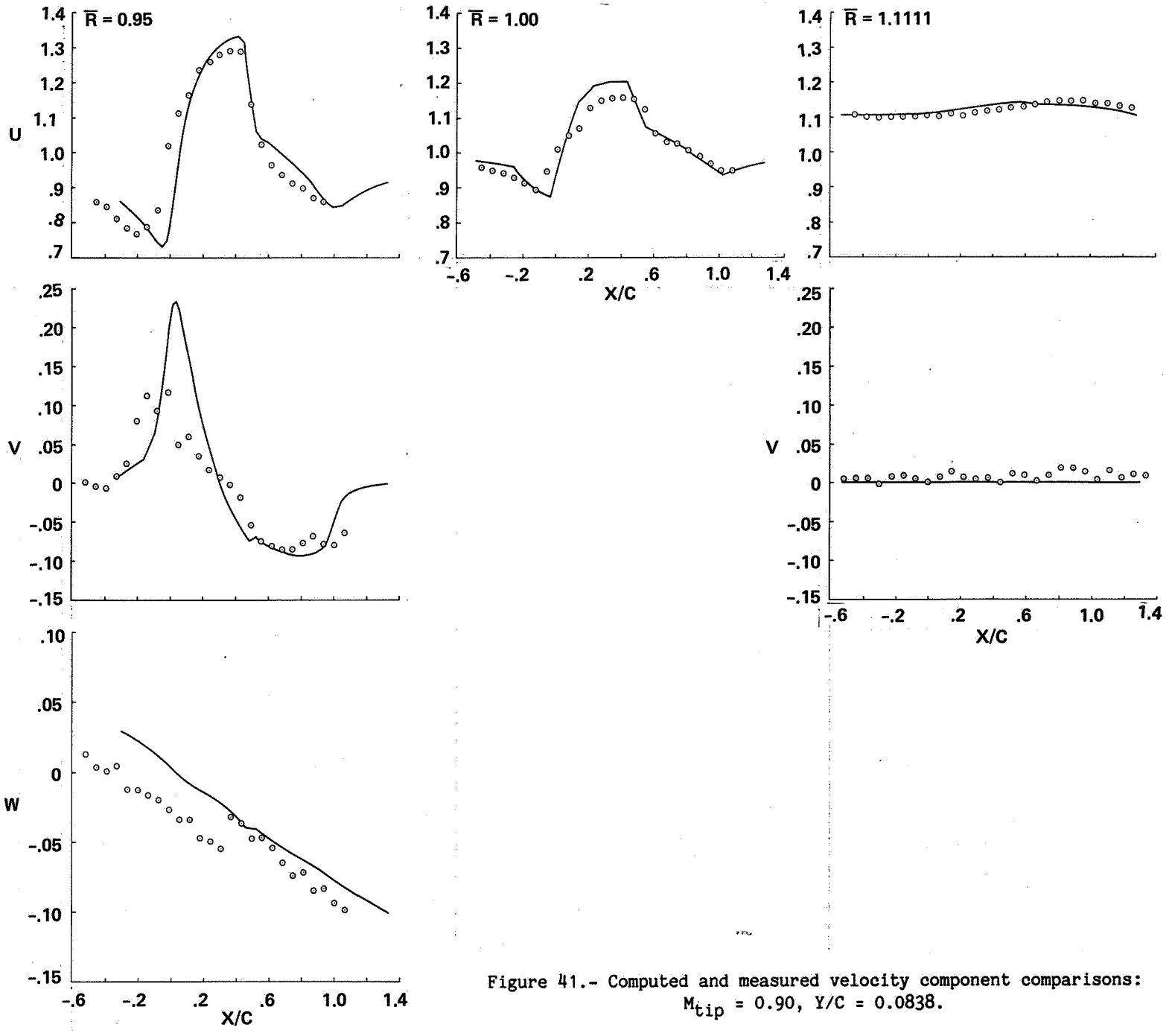

Figure 41.- Computed and measured velocity component comparisons: M_{tip} = 0.90, Y/C = 0.0838.

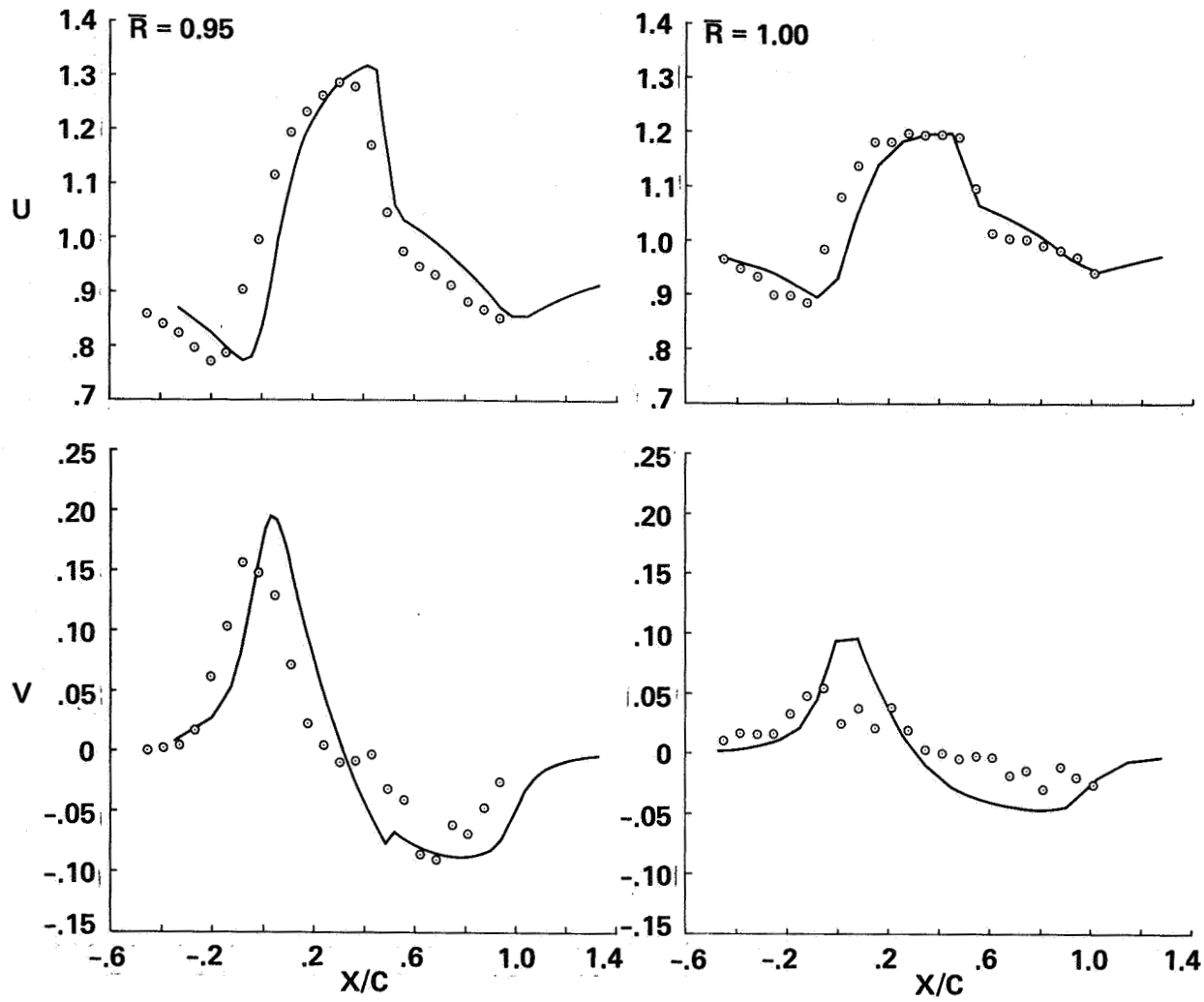

Figure 42.- Computed and measured velocity component comparisons: M_{tip} = 0.90, Y/C = 0.1172.

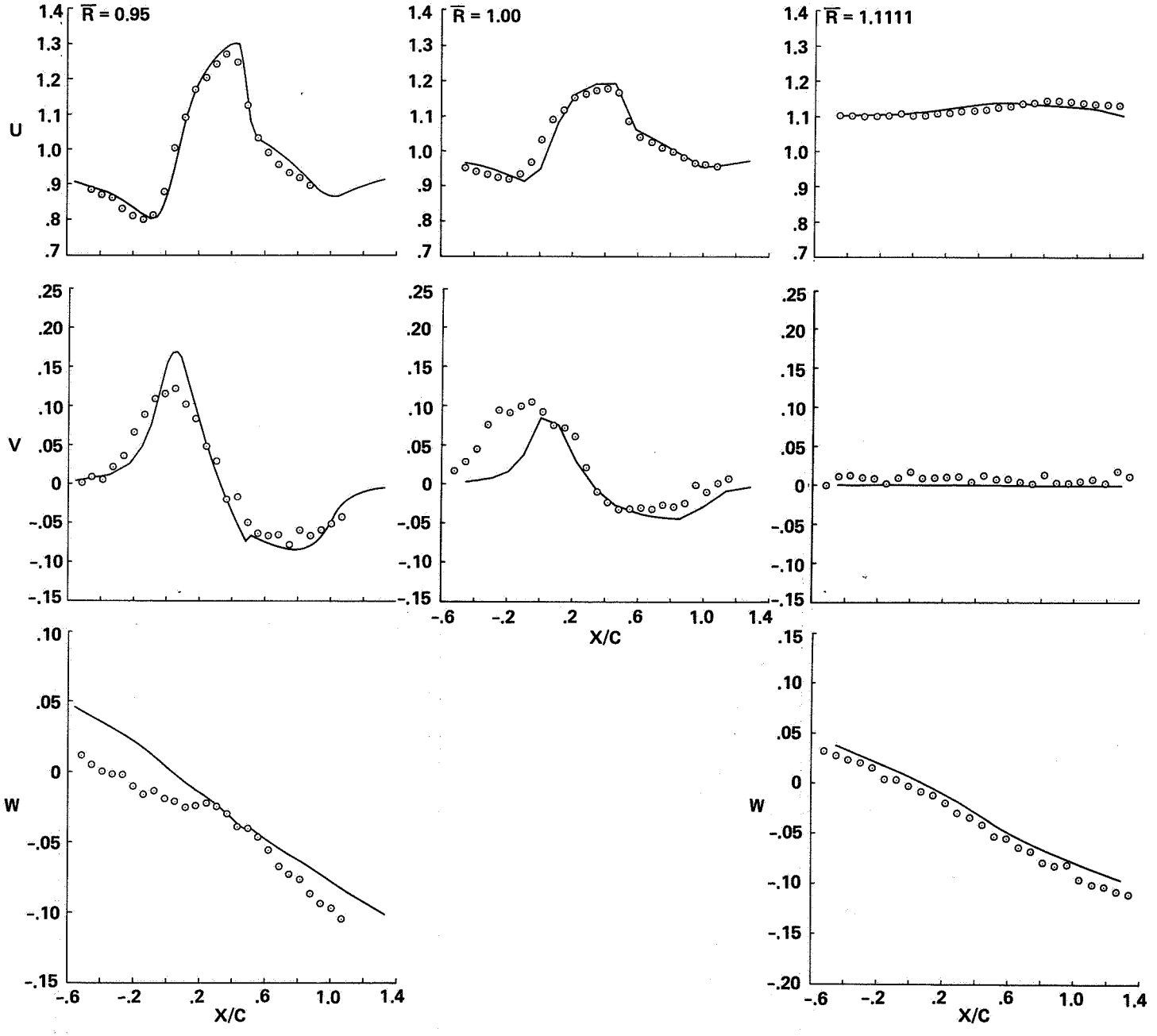

Figure 43.- Computed and measured velocity component comparisons:
M_{tip} = 0.90, Y/C = 0.1505.

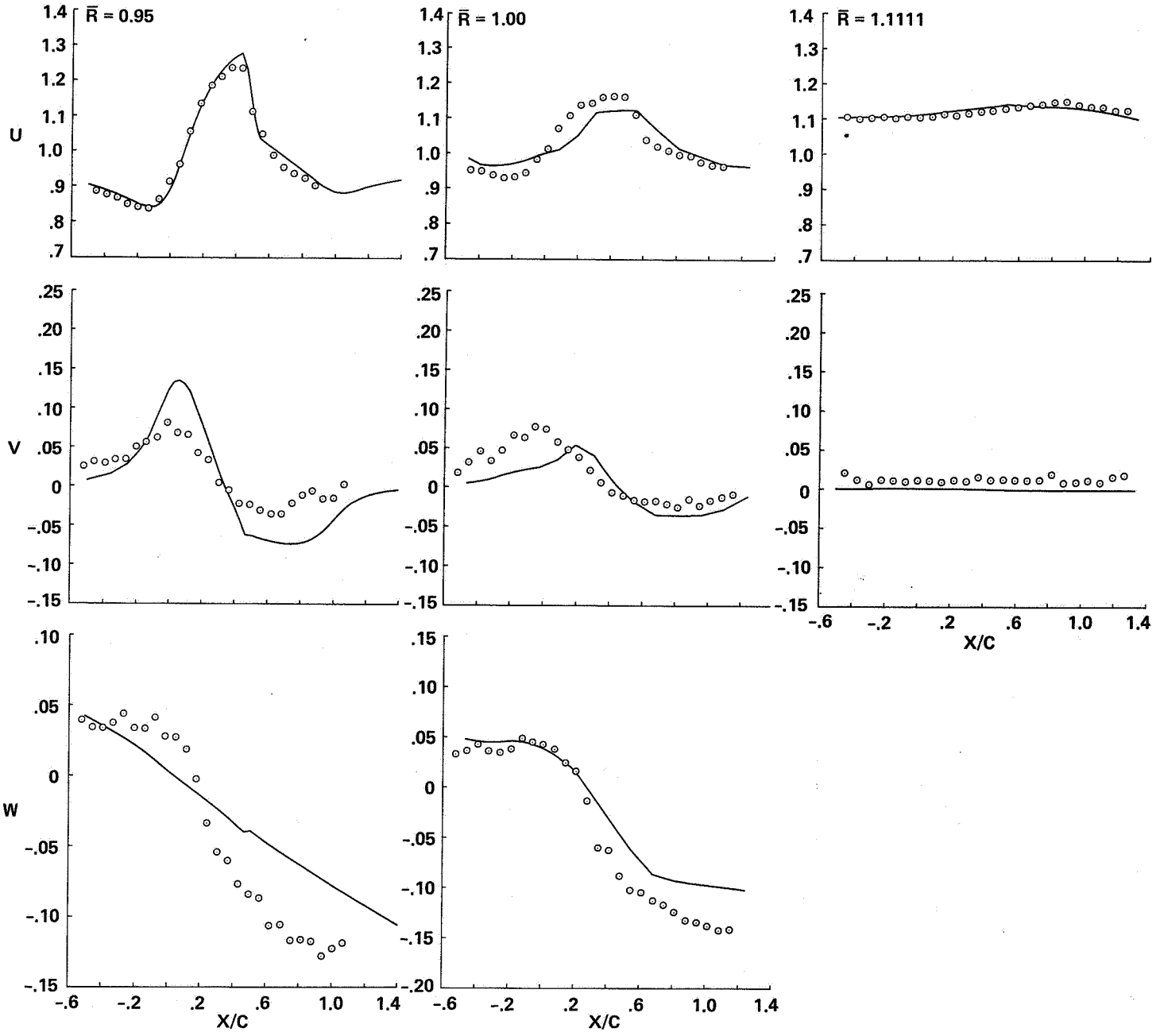

Figure 44.- Computed and measured velocity component comparisons: M_{tip} = 0.90, Y/C = 0.2172.

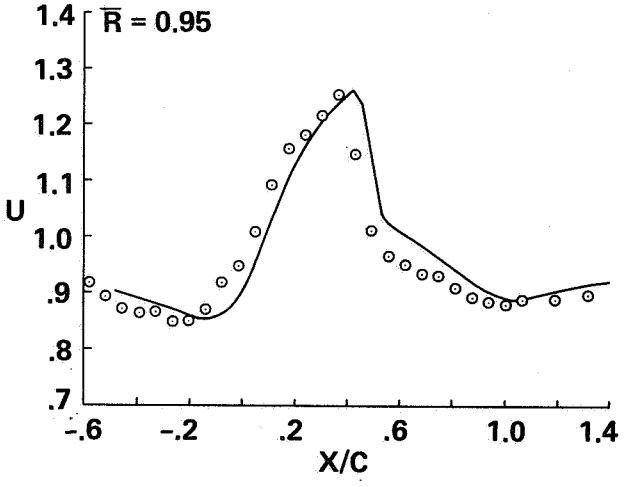

Figure 45.- Computed and measured velocity component comparisons: M_{tip} = 0.90, Y/C = 0.2505.

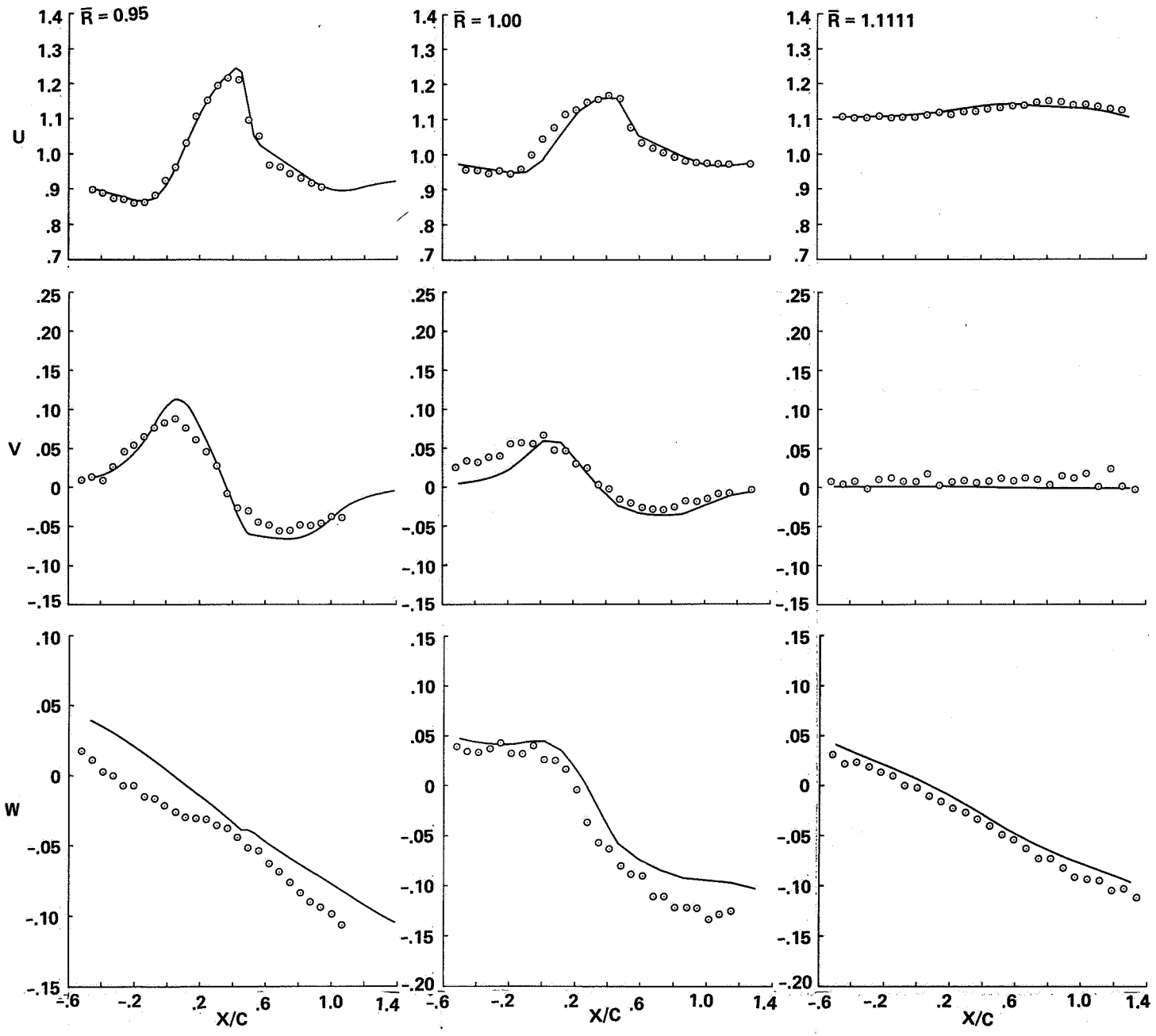

Figure 46.- Computed and measured velocity component comparisons: M_{tip} = 0.90, Y/C = 0.2838.

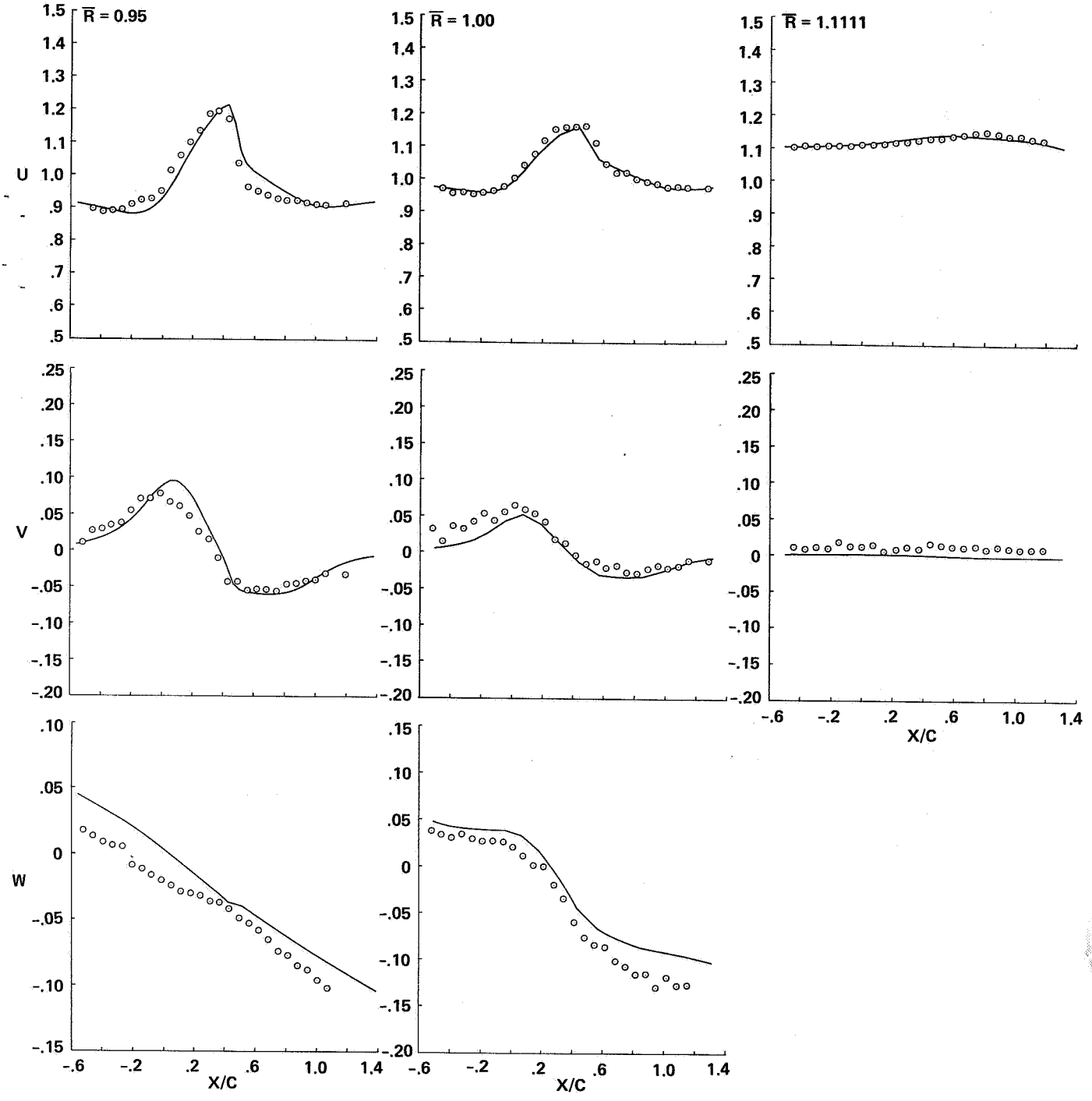

Figure 47.- Computed and measured velocity component comparisons: M_{tip} = 0.90, Y/C = 0.3505.

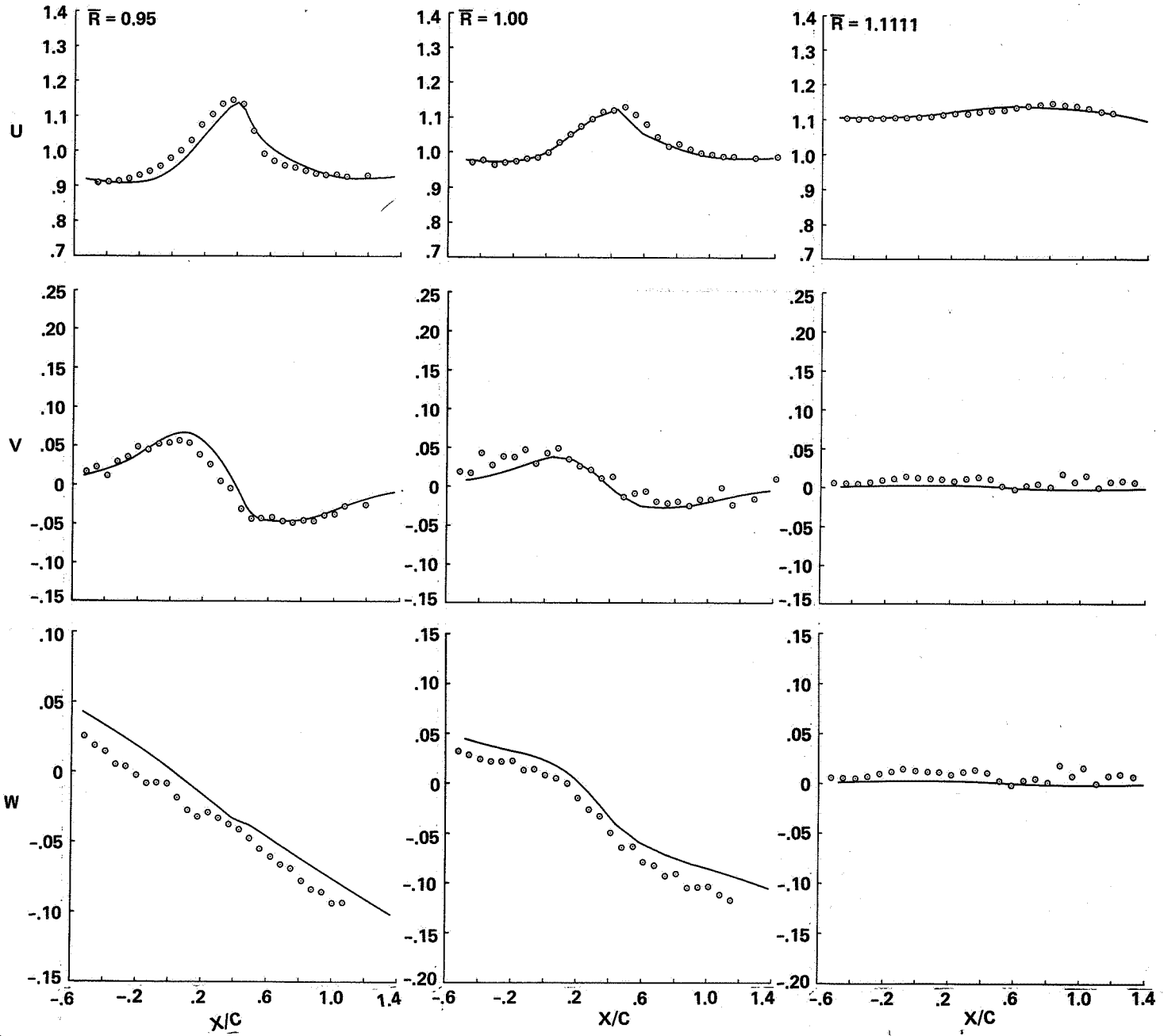

Figure 48.- Computed and measured velocity component comparisons: M_{tip} = 0.90, Y/C = 0.5172.

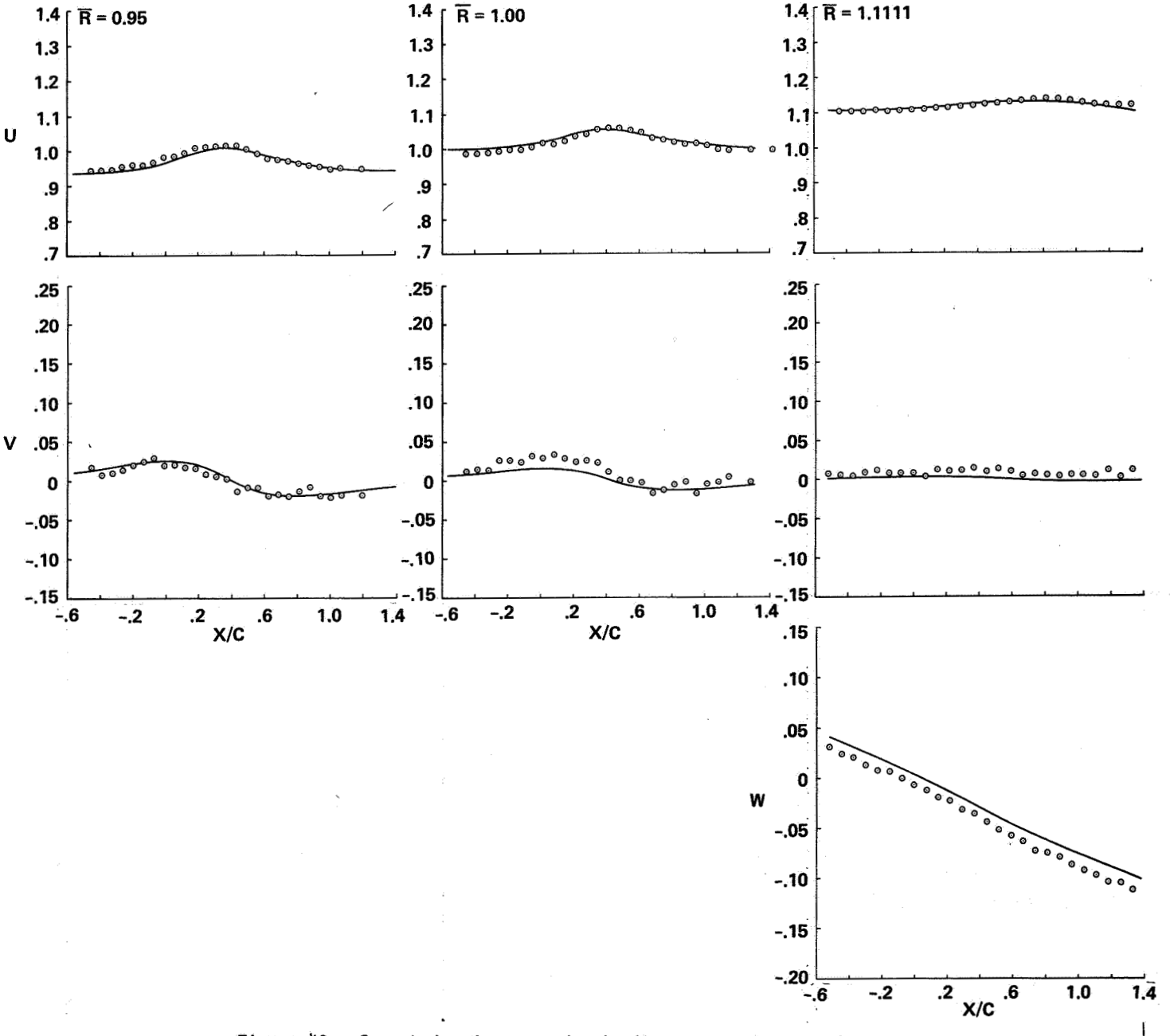

Figure 49.- Computed and measured velocity component comparisons:
M_{tip} = 0.90, Y/C = 1.0172.

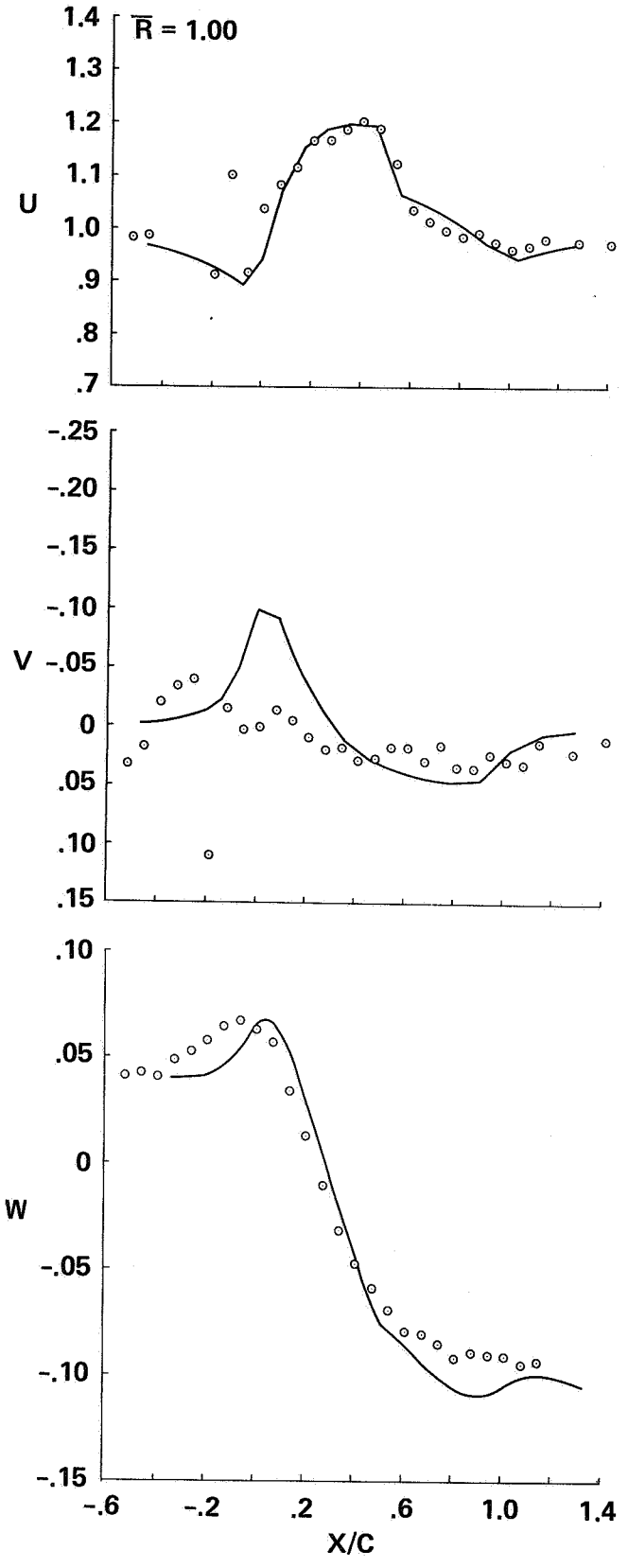

Figure 50.- Computed and measured velocity component comparisons: M_{tip} = 0.90, Y/C = -0.1162.

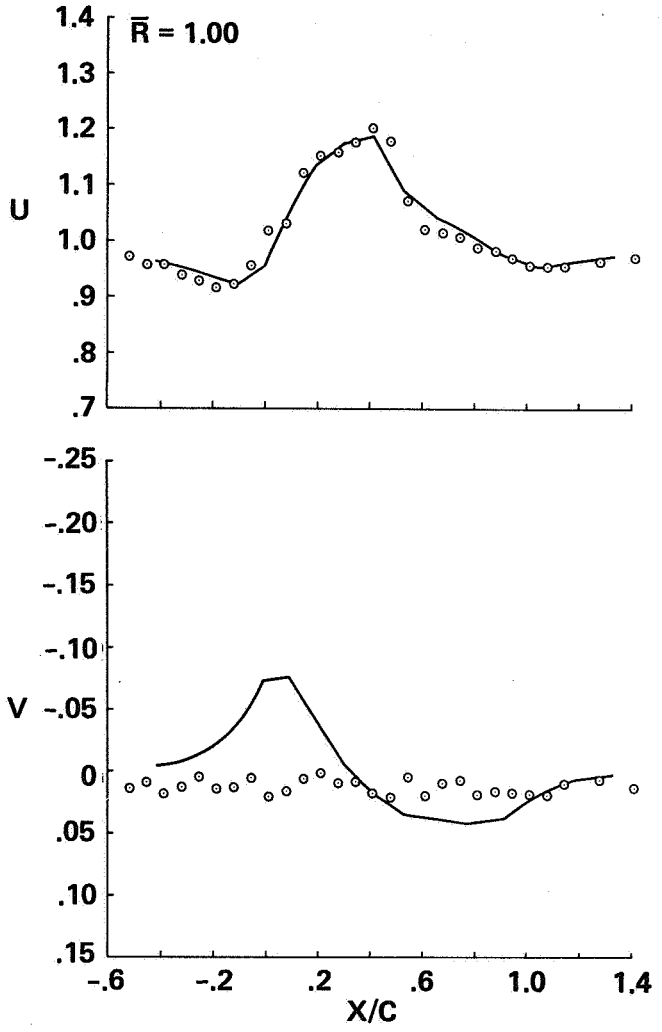

Figure 51.- Computed and measured velocity component comparisons: M_{tip} = 0.90, Y/C = -0.1828.

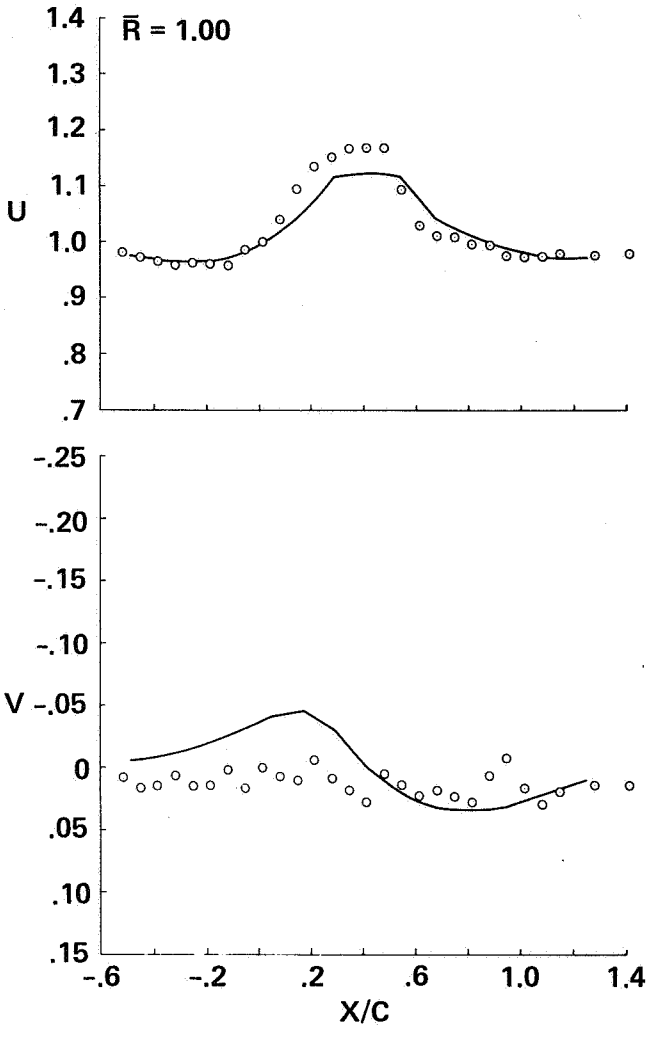

Figure 52.- Computed and measured velocity component comparisons: M_{tip} = 0.90, Y/C = -0.3162.

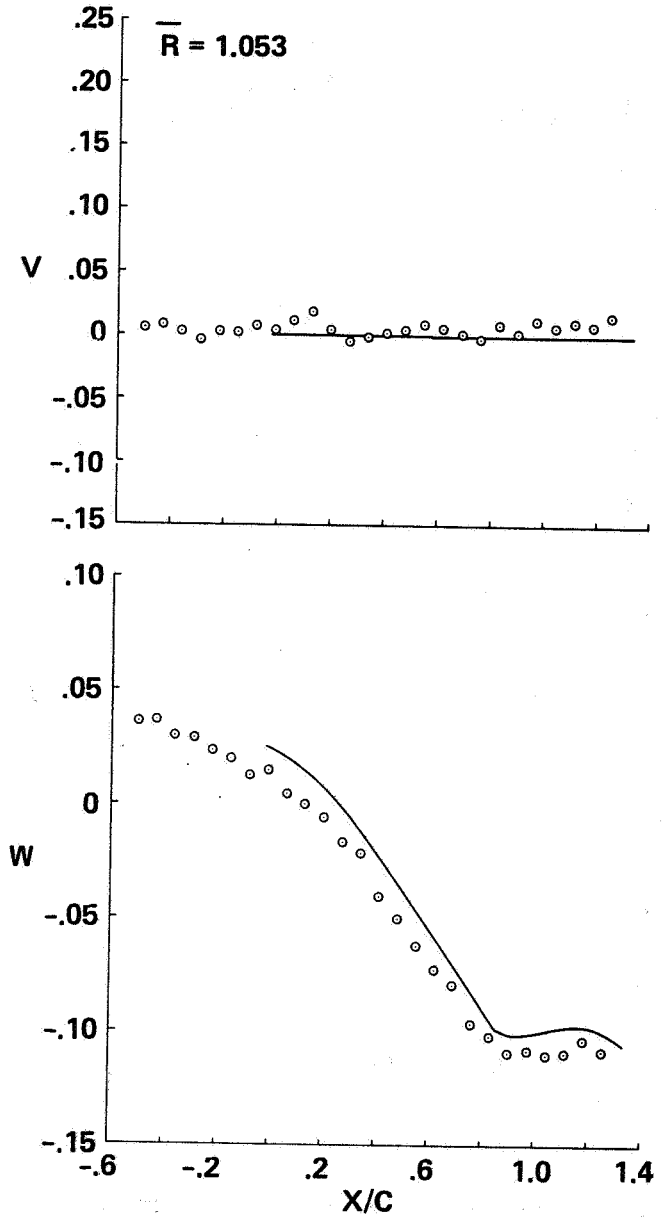

Figure 53.- Computed and measured velocity component comparisons: M_{tip} = 0.95, Y/C = 0.0172.

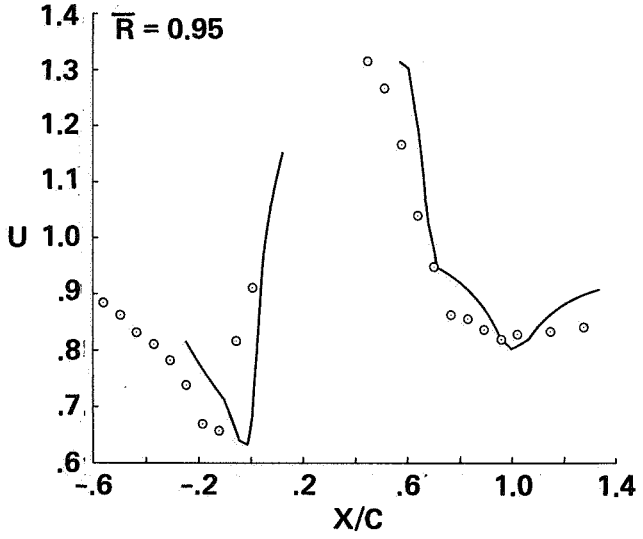

Figure 54.- Computed and measured velocity component comparisons: M_{tip} = 0.95, Y/C = 0.0505.

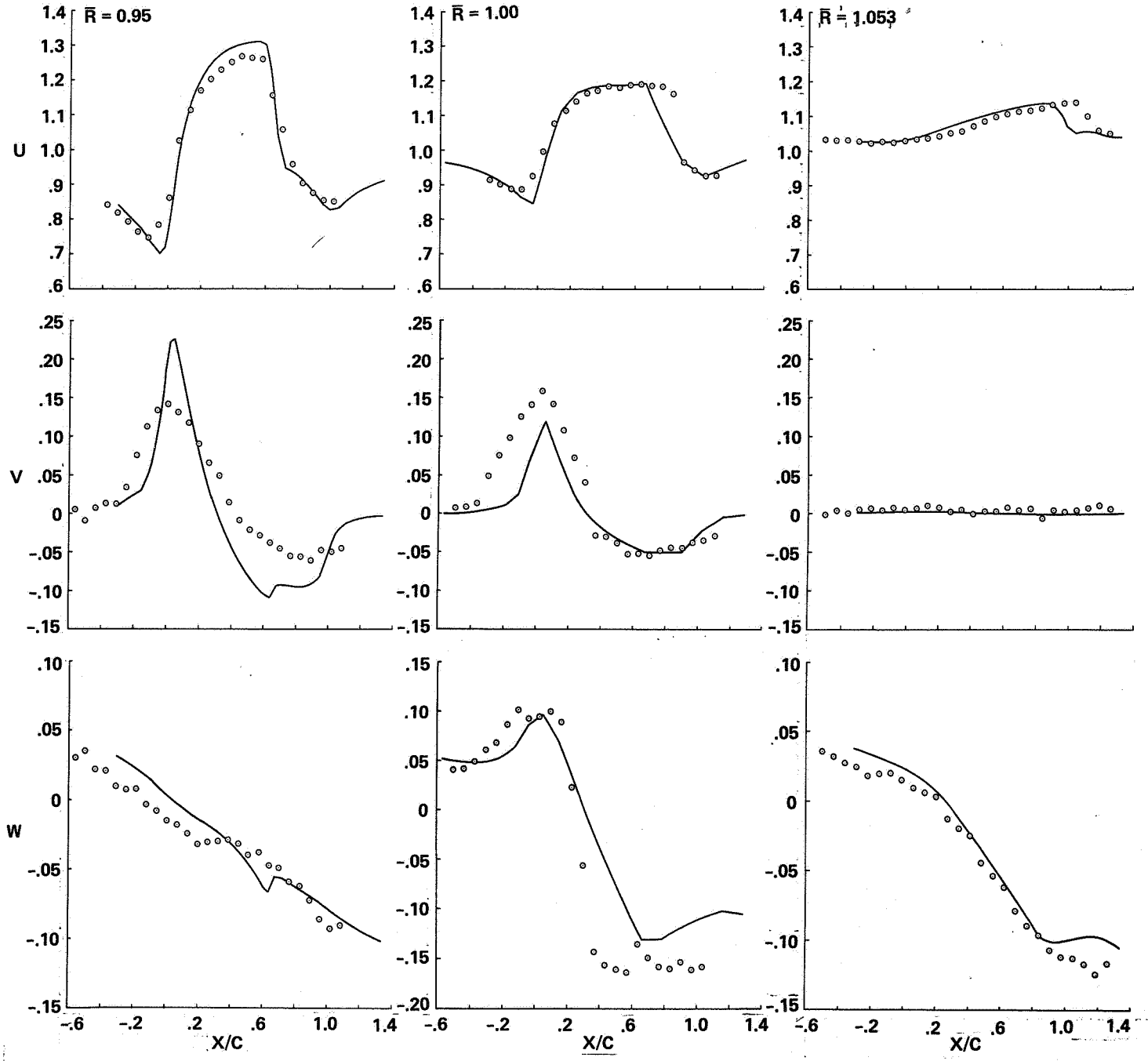

Figure 55.- Computed and measured velocity component comparisons: M_{tip} = 0.95, Y/C = 0.0838.

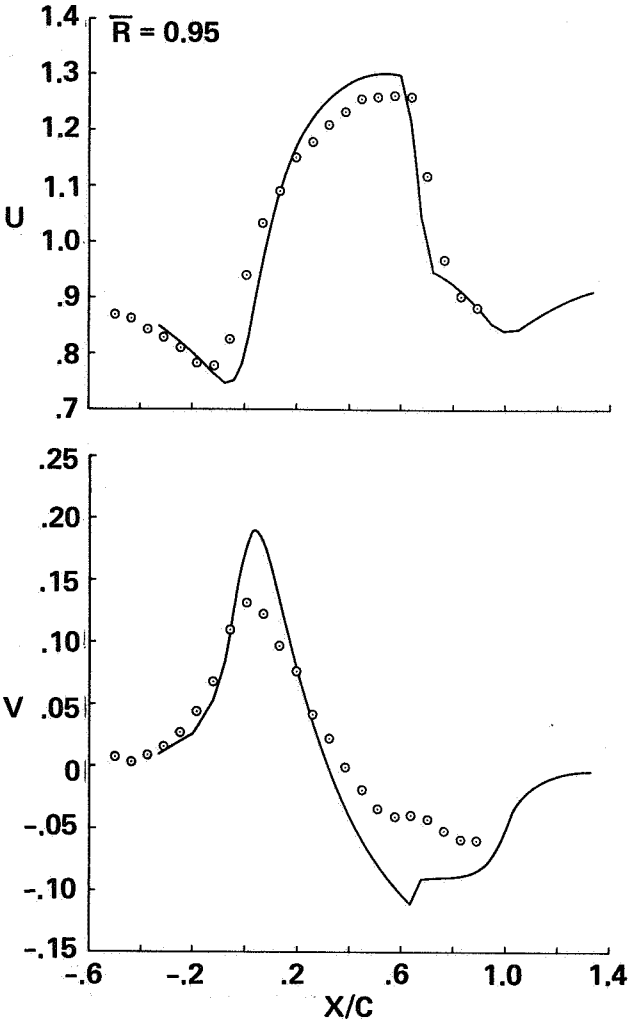

Figure 56.- Computed and measured velocity component comparisons: M_{tip} = 0.95, Y/C = 0.1172.

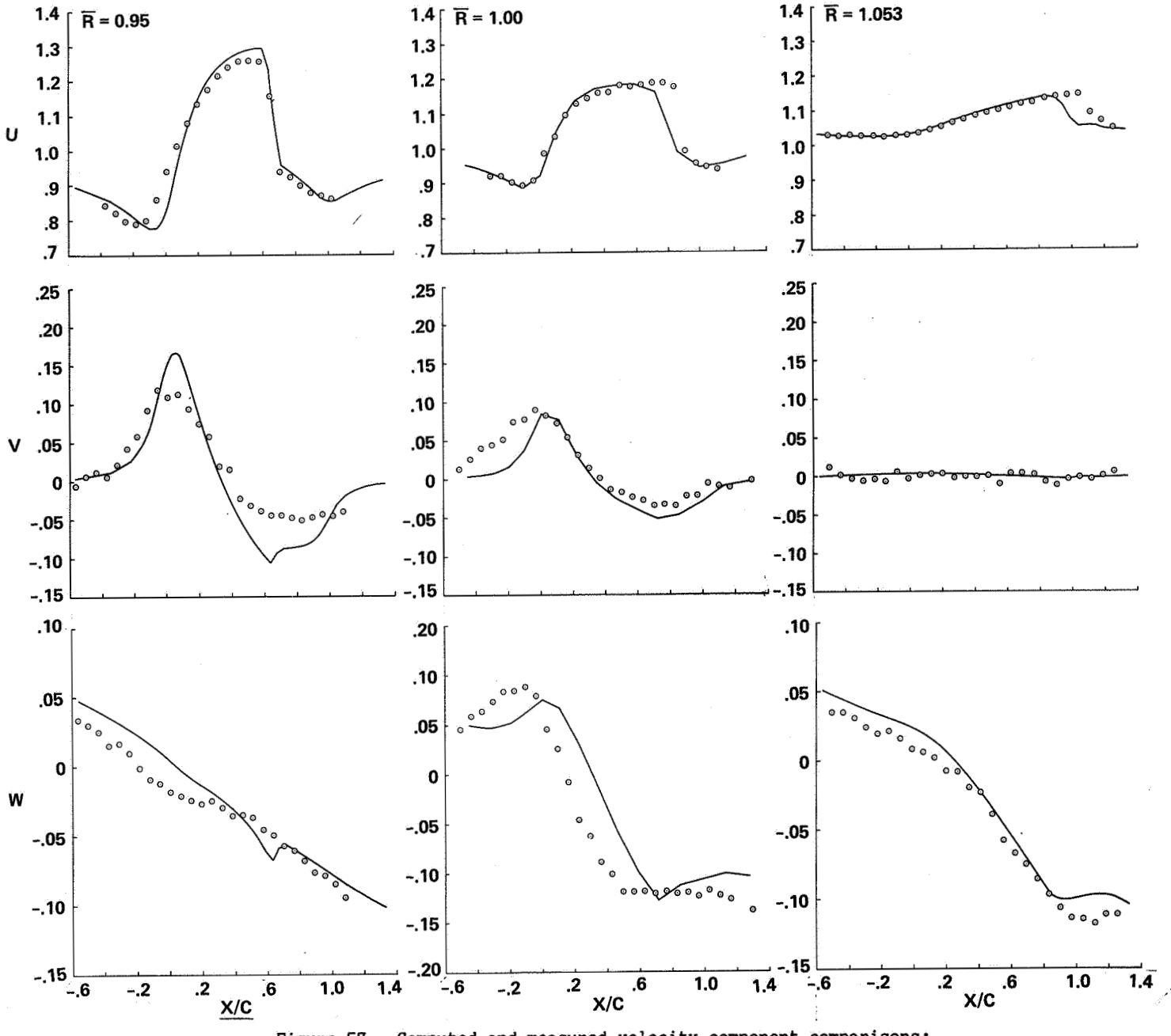

Figure 57.- Computed and measured velocity component comparisons: M_{tip} = 0.95, Y/C = 0.1505.

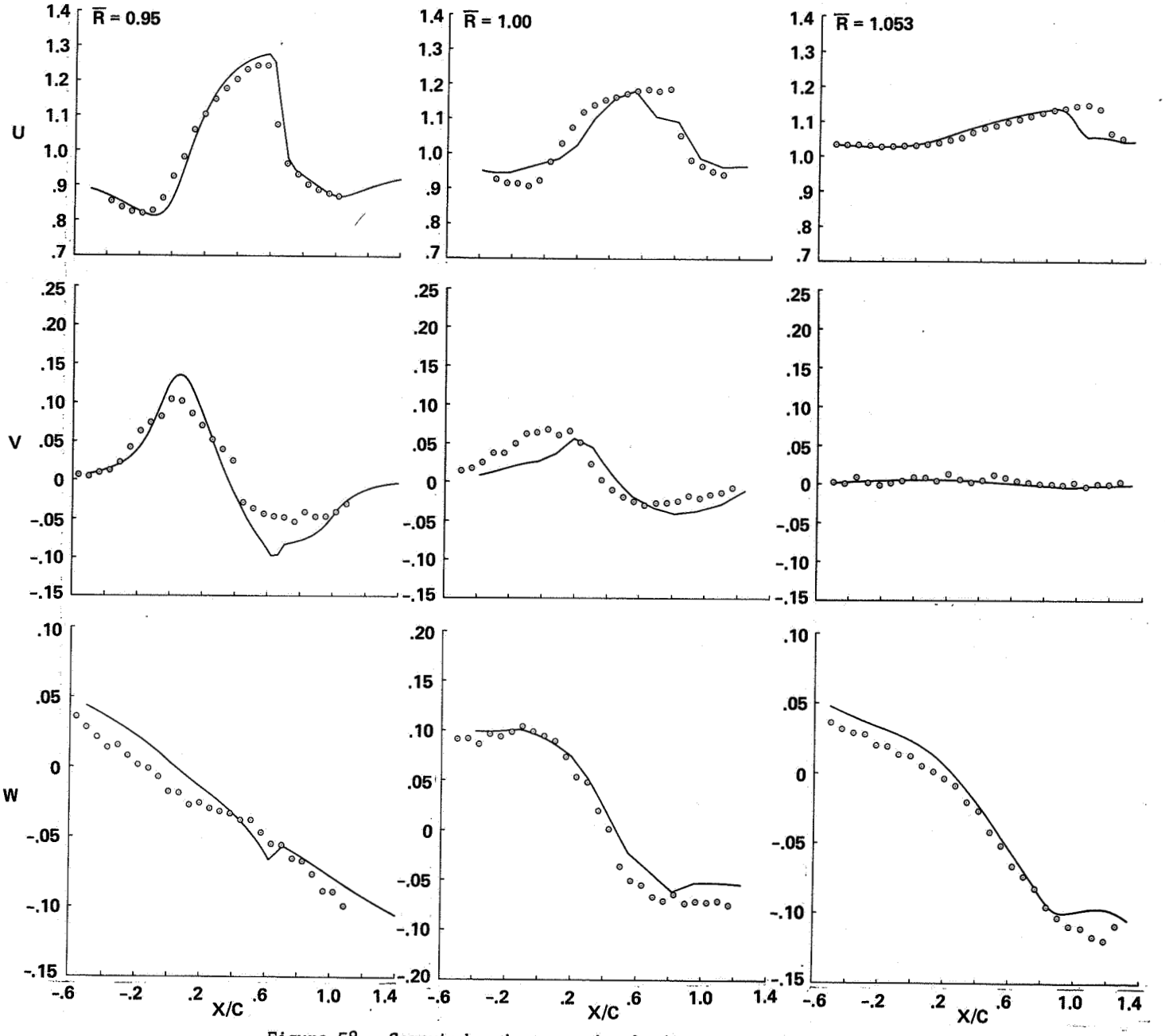

Figure 58.- Computed and measured velocity component comparisons: M_{tip} = 0.95, Y/C = 0.2172.

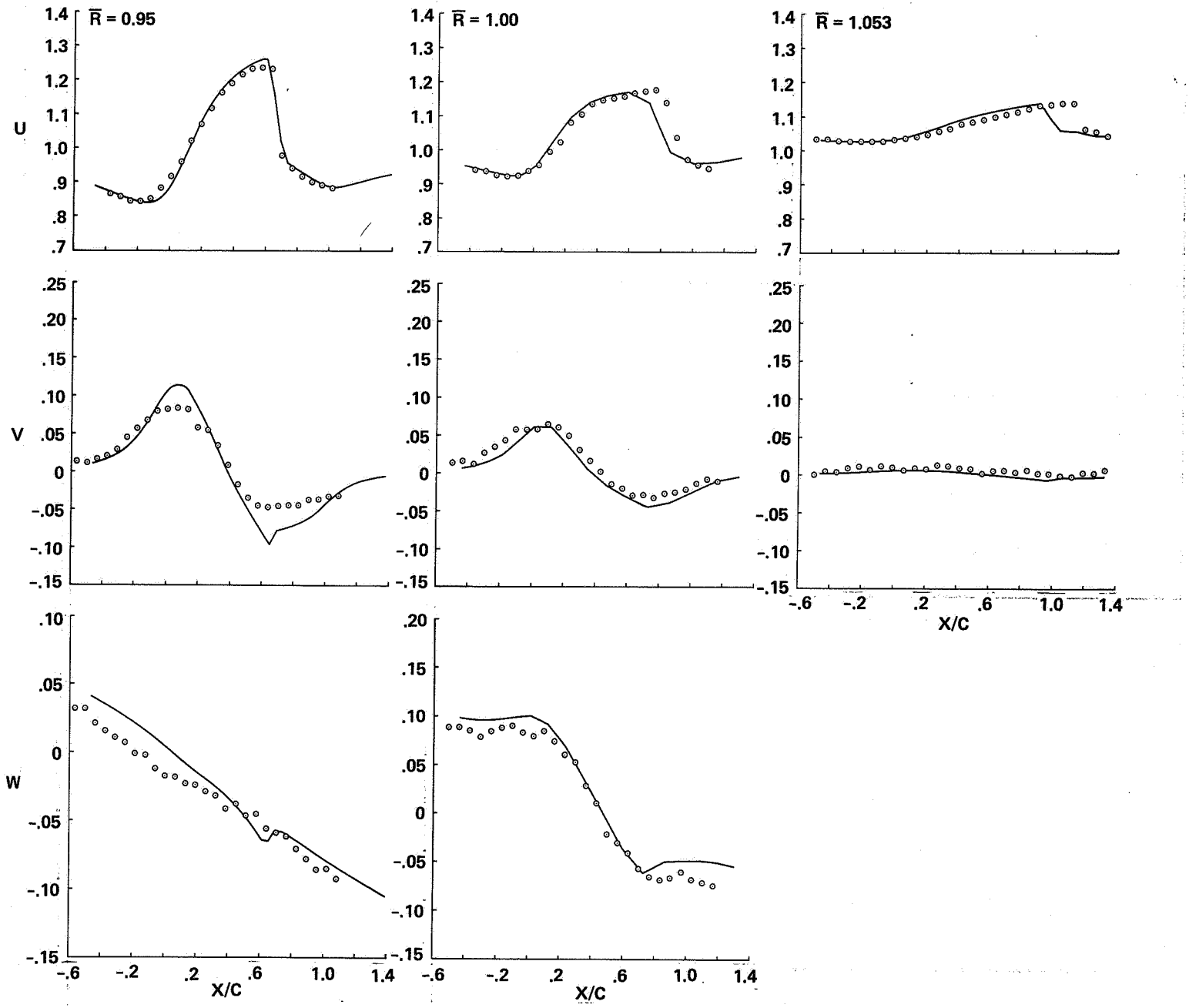

Figure 59.- Computed and measured velocity component comparisons: M_{tip} = 0.95, Y/C = 0.2838.

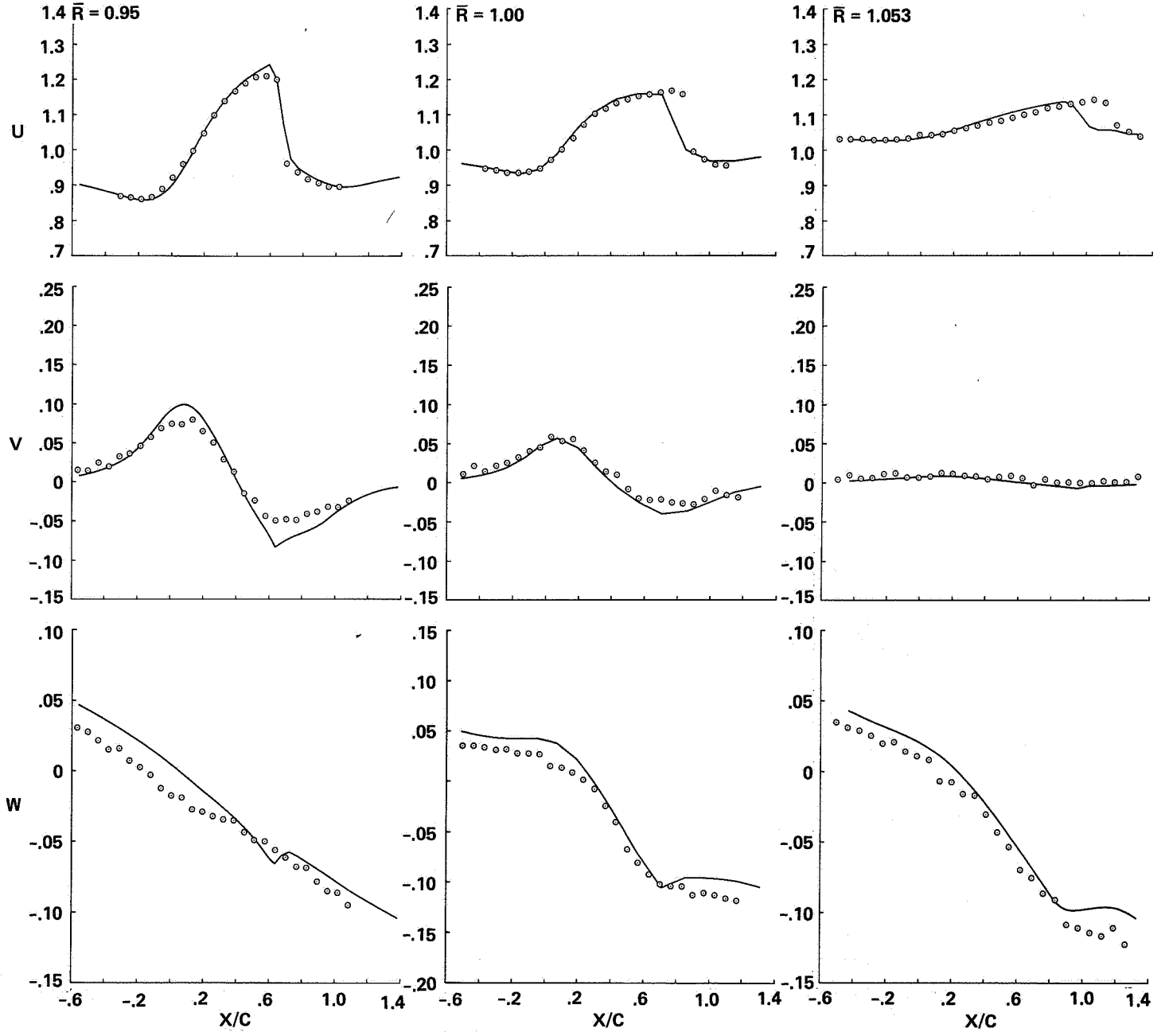

Figure 60.- Computed and measured velocity component comparisons: M_{tip} = 0.95, Y/C = 0.3505.

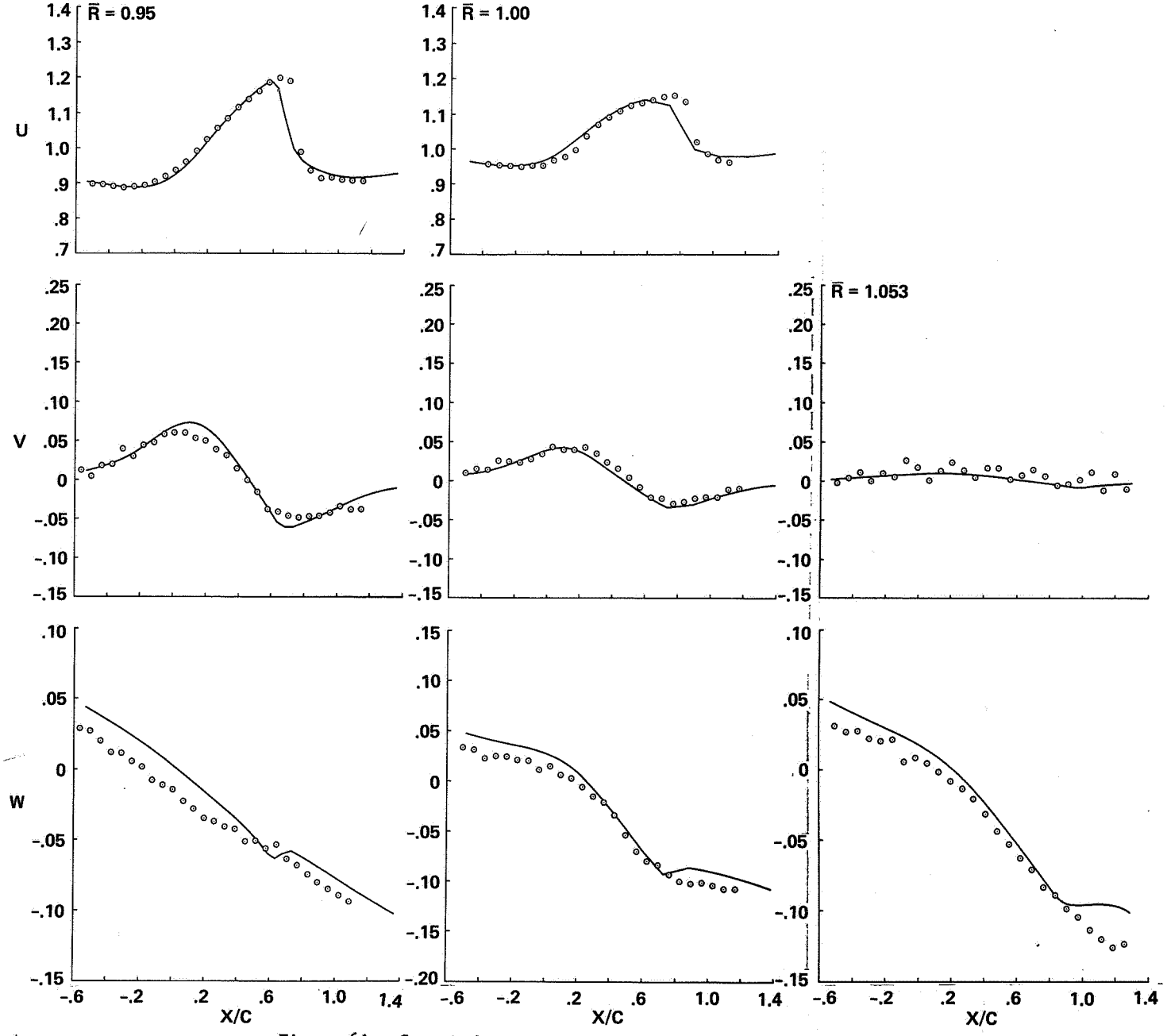

Figure 61.- Computed and measured velocity component comparisons: M_{tip} = 0.95, Y/C = 0.5172.

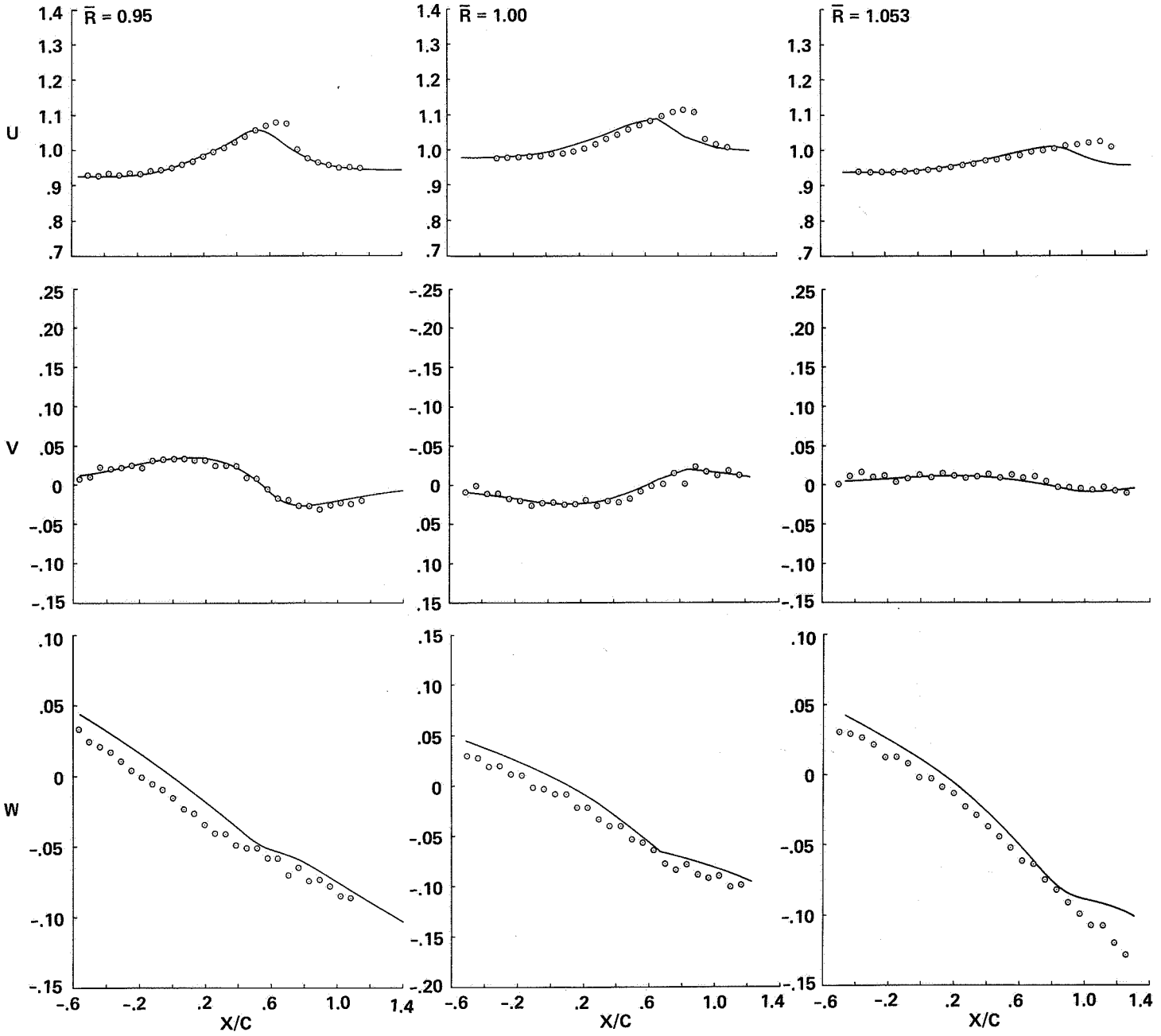

Figure 62.- Computed and measured velocity component comparisons: M_{tip} = 0.95, Y/C = 1.0172.

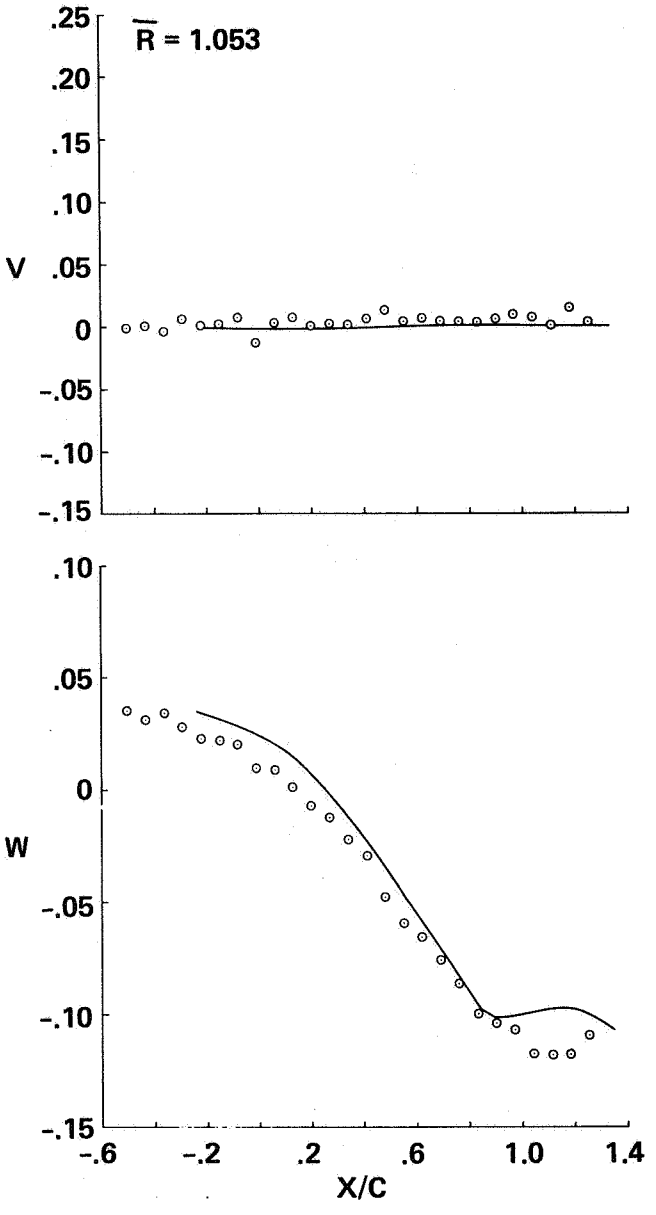

Figure 63.- Computed and measured velocity component comparisons: M_{tip} = 0.95, Y/C = -0.0495.

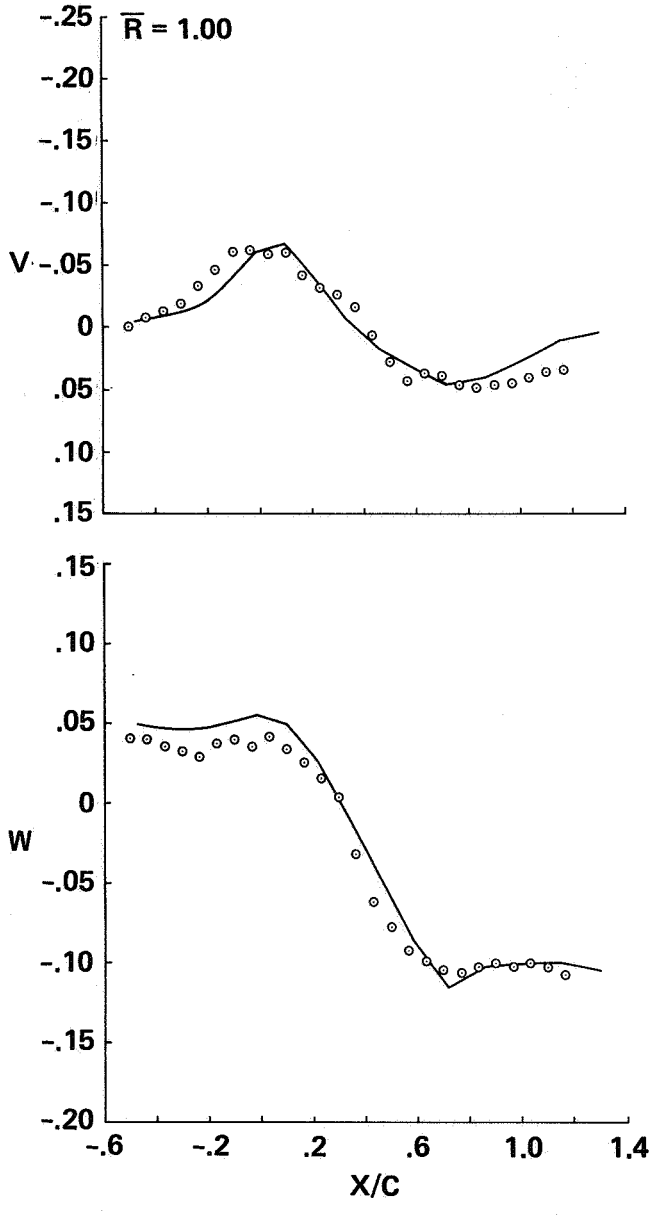

Figure 64.- Computed and measured velocity component comparisons: M_{tip} = 0.95, Y/C = -0.2495.

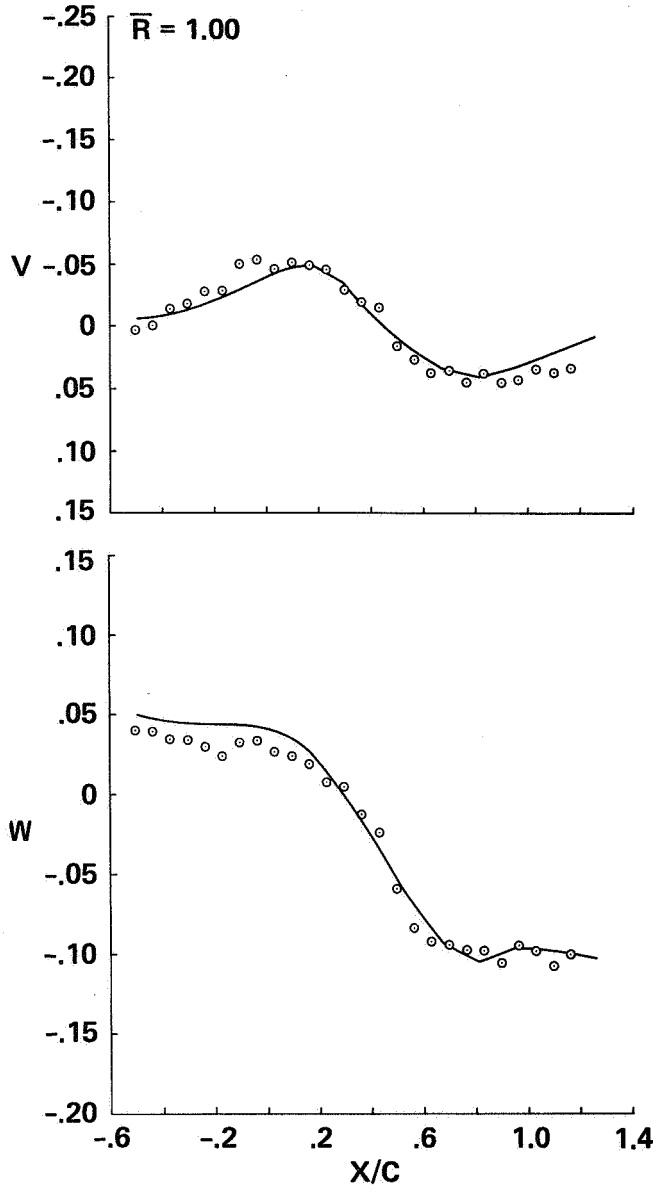

Figure 65.- Computed and measured velocity component comparisons: M_{tip} = 0.95, Y/C = -0.3162.

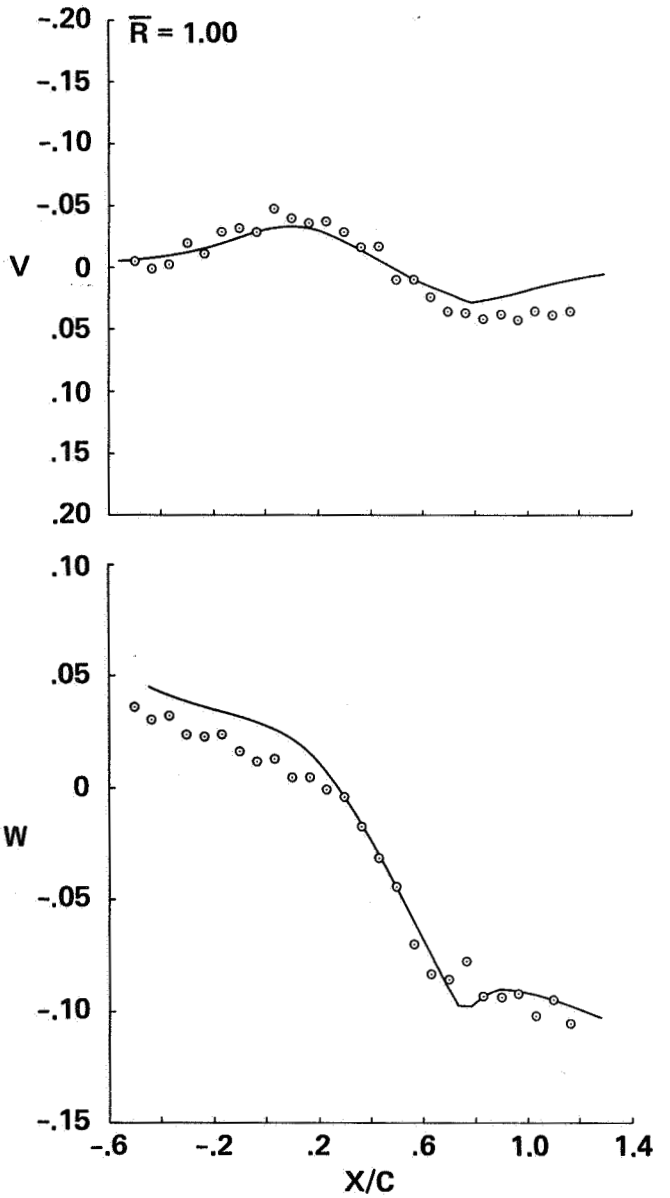

Figue 66.- Computed and measured velocity component comparisons: M_{tip} = 0.95, Y/C = -0.4828.

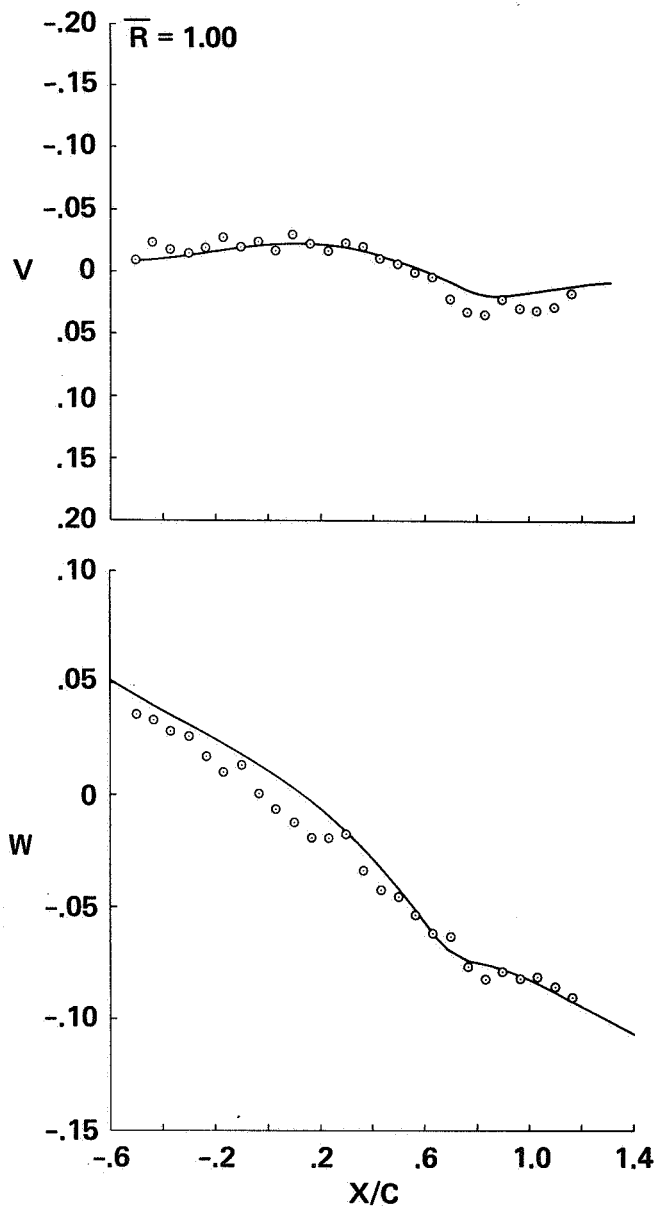

Figure 67.- Computed and measured velocity component comparisons: M_{tip} = 0.95, Y/C = -0.9828.

1. Report No.	2. Government Accession No.	3. Recipient's Catalog No.
NASA TM 86697		

4. Title and Subtitle	5. Report Date
COMPARISON OF CALCULATED AND MEASURED VELOCITIES NEAR THE TIP OF A MODEL ROTOR BLADE AT TRANSONIC SPEEDS.	August 1985
	6. Performing Organization Code
7. Author(s)	8. Performing Organization Report No.
Michael E. Tauber, F. Kevin Owen,* Ronald G. Langhi,+ and Grant E. Palmer	85158
	10. Work Unit No.
9. Performing Organization Name and Address	11. Contract or Grant No.
NASA Ames Research Center, Moffett Field, CA. *Complere, Inc., Palo Alto, CA. +Informatics General Corp., Palo Alto, CA.	
	13. Type of Report and Period Covered
12. Sponsoring Agency Name and Address	Technical Memorandum
National Aeronautics and Space Administration Washington, DC, 20546	14. Sponsoring Agency Code 505-42-11

15. Supplementary Notes

Point of Contact: Michael E. Tauber, Ames Research Center, Moffett Field, CA. Mail Stop: 229-4, (415) 694-5372 or FTS 448-5372

16. Abstract

The ability of the ROT22 code to predict accurately the transonic flow field in the crucial region around and beyond the tip of a high-speed rotor blade was assessed. The computations were compared with extensive laser velocimetry measurements made at zero advance ratio and tip Mach numbers of 0.85, 0.88, 0.90, and 0.95. The comparison between theory and experiment was made using 300 scans for the three orthogonal velocity components covering a volume having a height of over one blade chord, a width of nearly two chords, and a length ranging from about 1 to 1.6 chords, depending on the tip speeds. The good agreement between the calculated and measured velocities established the ability of the code to predict the off-blade flow field at high tip speeds. This supplements previous comparisons where surface pressures were shown to be well-predicted on two different tips at advance ratios to 0.45, especially at the critical 90° azimuth blade position. These results demonstrate that the ROT22 code can be used with confidence to predict the important tip region flow field including the occurrence, strength, and location of shock waves causing high drag and noise.

17. Key Words (Suggested by Author(s))	18. Distribution Statement
Transonic Flow Field ROT 22 Code Tip Velocities	Unlimited Subject category: 05

19. Security Classif. (of this report)	20. Security Classif. (of this page)	21. No. of Pages	22. Price*
Uncl	Uncl.	69	A05

*For sale by the National Technical Information Service, Springfield, Virginia 22161